STUDIES ON THE BEHAVIOR OF NICKEL-BASE SUPERALLOYS AT HIGH TEMPERATURES

INGARD KVERNES AND PER KOFSTAD

CENTRAL INSTITUTE FOR INDUSTRIAL RESEARCH
BLINDERN, OSLO, NORWAY

FOREWORD

This report was prepared by The Central Institute for Industrial Research, Oslo, Norway, under Contract No. F61052-67-C-0057. The contract was initiated under Project 7312, "Metals Surface Deterioration and Protection," Task No. 731202, "Metal Surface Deterioration." The report covers work conducted from 1 November 1967 to 31 October 1969. The work was administered by the Air Force Materials Laboratory, Air Force Systems Command, Wright-Patterson Air Force Base, with Mr. J. Jay Crosby as program monitor.

Dr. I. Kvernes served as principal investigator for the work and Dr. P. Kofstad as consultant. A number of other staff members of the Institute have participated in the various phases of the work. Mr. Chr. J. Simensen performed the electron diffraction and microscope studies, Mr. T.A. Dahlstrom the thermogravimetric measurements, Mr. S. E. Ness the electron microprobe studies, Mrs. K. Martinsen and Mrs. T.L. Rolfsen the X-ray diffraction measurements, and Miss G. Kunze and Mrs. M. Espeland the metallographic work.

This technical report has been reviewed and is approved.

J Perlmutter

F. PERLMUTTER
Chief, Metals Branch
Metals and Ceramics Division
Air Force Materials Laboratory

ABSTRACT

The work covers the investigation of the oxidation behavior of nickel-chromium-aluminum base alloys at high temperatures.

Part I. The oxidation of ternary nickel-chromium-aluminum alloys containing different chromium/aluminum ratiors has been investigated in the temperature range 800-1200°C in pure oxygen or air. The investigation included thermogravimetric measurements of oxidation rates and generally the oxidation rate decreased faster with time than that for an ideal parabolic behavior. The oxidation however in some cases can be described as parabolic over parts of the reaction period. The major reaction products were NiO, Cr_2O_3, α-Al_2O_3, $NiAl_2O_4$, and $Ni(CrAl)_2O_4$. The Ni-9Cr-6Al alloy displayed the best oxidation resistance. The oxidation mechanism of the alloys is discussed.

Part II. The oxidation of Ni-9Cr-5Al with alloy additions of 2 w/o (weight percent) titanium and of 2 w/0 titanium +0.1 w/o samarium were investigated in the temperature range 800-1300°C in flowing air (1 liter/min) and oxygen at a pressure of 1 atm. The major reaction products were NiO, Cr_2O_3, α-Al_2O_3, spinel, and TiO_2. The titanium-addition had a deleterious effect on the oxidation resistance of the Ni-9Cr-5Al base alloy.

Part III. The oxidation behavior of two nickel-chromium and three nickel-chromium-aluminum alloys with small additions of manganese (0.2-1.2%) was investigated in the temperature range 800-1200°C. The manganese-additions produced no significant changes in the reaction behavior of the alloys.

Part IV. Oxidation of three nickel-chromium-aluminum alloys and two nickel-chromium-aluminum-niobium-manganese-silicon alloys with small additions of yttrium (0.005-1.5%) has been studied in the temperature range 800-1200°C. The effects of yttrium-additions less than 0.1% were difficult to analyze and evaluate, but larger additions had a marked effect on the microstructures and detailed reaction characteristics of the alloys. Yttrium was enriched at the grain boundaries of the alloys probably as a nickel-yttrium intermetallic compound. A preferential oxidation of grain boundaries next to the alloy surface was shown with increased oxide adherence. The increased oxide adherence is attributed to a "key-on" effect due to the irregularity in the interface between the oxide and alloy.

CONTENTS

CONTENTS - cont.

PART III - INFLUENCE OF MANGANESE-ADDITIONS ON HIGH TEMPERATURE OXIDATION OF SOME NICKEL-CHROMIUM AND NICKEL-CHROMIUM-ALUMINIUM BASE ALLOYS

PART IV - EFFECTS OF YTTRIUM ADDITIONS ON THE OXIDATION BEHAVIOUR OF NICKEL-CHROMIUM-ALUMINIUM BASE ALLOYS AT HIGH TEMPERATURES

LIST OF TABLES

LIST OF ILLUSTRATIONS

LIST OF ILLUSTRATIONS (continued)

LIST OF ILLUSTRATIONS (continued)

LIST OF ILLUSTRATIONS (continued)

LIST OF ILLUSTRATIONS (continued)

LIST OF ILLUSTRATIONS (continued)

PART I - THE HIGH TEMPERATURE OXIDATION OF SOME NICKEL-CHROMIUM-ALUMINIUM ALLOYS CONTAINING DIFFERENT CHROMIUM/ALUMINIUM RATIO.

1. INTRODUCTION

Many studies have been made on nickel-chromium base alloys to determine the use of these alloys as high temperature materials in oxidizing atmospheres.[1-5] Aluminium additions to high temperature alloys generally impart good oxidation resistance, but systematic studies on the effect of aluminium addition to nickel-chromium alloys have only been reported in a few cases.[6-8] Ignatov and Shamgunova[6] studied the kinetics of the thermal oxidation of Ni-20Cr* alloys with addition of 1, 4.2, 7.2, and 10 % aluminium between 600 and 1000 °C in 1 atm. air. They reported that additions of aluminium to Ni-20Cr increase the oxidation resistance.

Gulbransen and Andrew[7] studied oxidation of Ni-20Cr with addition of 4 % aluminium. They reported that the addition of aluminium to nickel-chromium alloys does not yield any appreciable improvement in the oxidation resistance.

This paper presents studies on oxidation of 6 different nickel-chromium-aluminium alloys with different chromium/aluminium ratio. An objective of the work is to determine if the chromium-content may be reduced and still retain a good oxidation behaviour. The oxidizing atmosphere was oxygen or air at 1 atm., but in one case the oxidation was also studied as a function of the oxygen pressure. The reaction behaviour was studied at temperatures from 800 to 1300 °C and for reaction periods up to 100 hours.

* The compositions of the alloys are in the following given in weight percent.

2. MATERIALS AND METHODS

2.1 Materials.

The nickel-chromium-aluminium alloys were prepared in argon atmosphere (pressure 0.5 atm.) in an induction furnace and cast in an alumina crucible. The chemical analysis of the alloys are given in Table I.

2.1.1 Specimen Preparation. All specimens used in these studies were machined by means of the spark errosion method to rectangular oxidation test specimens. The test specimens had a thickness ranging from 0.4 to 0.6 mm and a total area of about 2.3 cm^2. Prior to oxidation test the specimens were washed in acetone and annealed in high vacuum ($< 10^{-5}$ torr) for 1 hr at 1000 °C.

2.2 Methods.

2.2.1 Thermogravimetric Measurements of Oxidation. Rates of oxidation were measured thermogravimetrically with a Cahn automatic recording balance firmly mounted above a vertical furnace. The complete furnace assembly consisted of two separate high vacuum systems, which were connected to the reaction and heating element chambers, respectively. An alumina (recrystallized) tube was used as a reaction chamber. The reaction temperature was measured with Pt-5 % Rh/Pt-20 % Rh thermocouples located next to the specimens. The specimens were suspended in a Pt-10 % Rh wire or in sintered alumina fibers.

The specimens were introduced at room temperature and the system was evacuated to 10^{-5} torr. After establishing the desired temperature and gas pressure, the specimens were lowered into the reaction zone and suspended on the balance.

2.2.2 Identification of the Reaction Products. The methods for characterizing the reaction products formed during the oxidation were metallographic techniques (Reichert MeF Microscope), X-ray diffraction (FeCRD-3d) techniques and electron probe micro-analysis (Cambridge X-ray Scanning Microanalyser Mark II A), electron diffraction and electron microscope techniques (Jem 7).

TABLE I

CHEMICAL ANALYSIS

Alloy No.	Ni w/o	Cr w/o	Al w/o	Ti w/o	Sm w/o	Mn w/o	Y w/o	Nb w/o	Si w/o	Oxidizing atm. (1 atm.)
2	Bal.	14.4	6.4							Oxygen
3*	Bal.	9.3	5.8							Air, oxygen
4	Bal.	8.2	2.5							Air
5	Bal.	7.1	9.1							Oxygen
6	Bal.	3.8	6.0							Air
7	Bal.	8.5	4.7	2						
8	Bal.	8.6	5.3	2	0.1**					
9	Bal.	8.5				0.4				
10	Bal.	4.8				0.2				
11	Bal.	8.5	6.0			1.1				
12	Bal.	5.6	5.5			1.2				
13	Bal.	5.7	5.2			0.2				
14	Bal.	9.0	5.4				0.005[v]			
15	Bal.	2.6	6.4				0.3[ov]			
16	Bal.	8.6	5.6			1.2	1.5[ov]	4.5	0.45	
17	Bal.	8.7	6.3				0.7[v]			
20	Bal.	8.0	6.2			1.4	0.1[v]	3.2	0.5	

*) Alloy No. 3 was prepared in two batches. The chromium content was 0.6 % less in the batch used for thin film studies and kinetic measurements at low pressures.
**) Not analyzed.
v) Analyzed by spectrographic methods.
o) Analyzed by neutron activation analysis.

Light microscopy permitted an evaluation of the reaction zone, an estimate of the number of the surface oxide phases in the scale, and the nature of the internal oxidation zones. The metallographic cross sections of the specimens were prepared as follows: the cross section of the specimen was first ground with various grades of SiC-paper, then polished with diamond paste and finally with alumina. The specimens were usually etched to reveal clearly the different reaction products and microstructure resulting during the oxidation process. A solution of 10 ml HNO_3 + 0.3 ml Vogel's Sparbeige + 100 ml cons. HCl + 100 ml dest H_2O or 150 ml CH_3COOH + 100 ml cons HNO_3 + 360 ml cons. HCl + 30 ml cons H_2SO_4 + 20-30 ml sat.sol. of $FeCl_3$ + 150 ml dest H_2O was used as etchant.

In the electron probe analysis the surface was made conductive by evaporating a thin carbon film. The microanalyser was run with 20 kV acceleration potential. Calibrations of the element concentration were established, using pure standards. For the absorption corrections the method by Philibert[9] was used.

The oxide layers were examined in bright field, dark field and selected area diffraction in order to determine the composition of each layer. The different polycrystalline oxides were identified by their diffraction pattern. The distance d_{hkl} between the rational (hkl) planes was determined by the equation

$$d_{hkl} = 2L/x_{hkl}$$

where x_{hkl} = the distance between the $\overline{hkl}$ and the hkl spots on the film;

L = the apparatus constant.

L was determined in a standard way[10]. Structural characterization of oxide phases was determined by means of an electron microscope analysis method described by Hirsch et al.[10] and Gjönnes and Simensen.[14]

The oxide films were stripped from the surface by scoring the surface into small grids and etching in a solution of 4% bromine in methanol. The oxide films were washed, dried and placed immediately in the microscope.

3. EXPERIMENTAL RESULTS

3.1 Oxidation in 1 atm. air or oxygen.

3.1.1 Reaction Rate Measurements. The nickel-chromium-aluminium alloys listed in Table 1 were studied in the temperature range of 800-1300 °C. Alloys No. 2, 3 and 5 were studied in oxygen and alloys No. 3, 4, and 6 were studied in air.

Results of thermogravimetric studies are presented in Fig. 1-6. The weight change of the specimens are given in mg/cm^2. The surface area was taken as the geometrical surface area of the unoxidized specimens. The results are presented in both linear (mg/cm^2 versus time) and parabolic (mg^2/cm^4 versus time) plots.

From the linear plots is seen that in most cases the oxidation rates decrease with time, showing that the oxide scales have protective properties. The corresonding parabolic plots, however, illustrate that only in a few cases can the oxidation be described as parabolic over the whole time period studied. The oxidation usually decreases faster with time than that for an ideal parabolic behaviour. But the oxidation can be approximated as parabolic over parts of the reaction periods.

Further examination of the results show that the oxidation exhibits usually an irregular temperature dependence in that the oxidation generally goes through a maximum in the temperature range 900-1300 °C. This behaviour reflects change in the oxidation mechanism with temperature. It may be noted that the oxidation kinetics for alloy No. 3 oxidized in pure oxygen exhibit a regular temperature dependence compared to that in air.

For comparative purposes the oxidation of Ni-19.5Cr, Ni-8.8Cr and Ni-6Al[7] was studied in 1 atm. oxygen and at 800, 1000, and 1200 °C. The oxidation is approximately parabolic, but it tends to deviate from such behaviour with increasing temperature. The relative oxidation rates of the nickel-chromium-aluminium, nickel-chromium, and nickel-aluminium alloys are illustrated in Fig. 7 which shows linear plots of the oxidation of the alloys in 1 atm. oxygen at 1000 °C and 1200 °C.

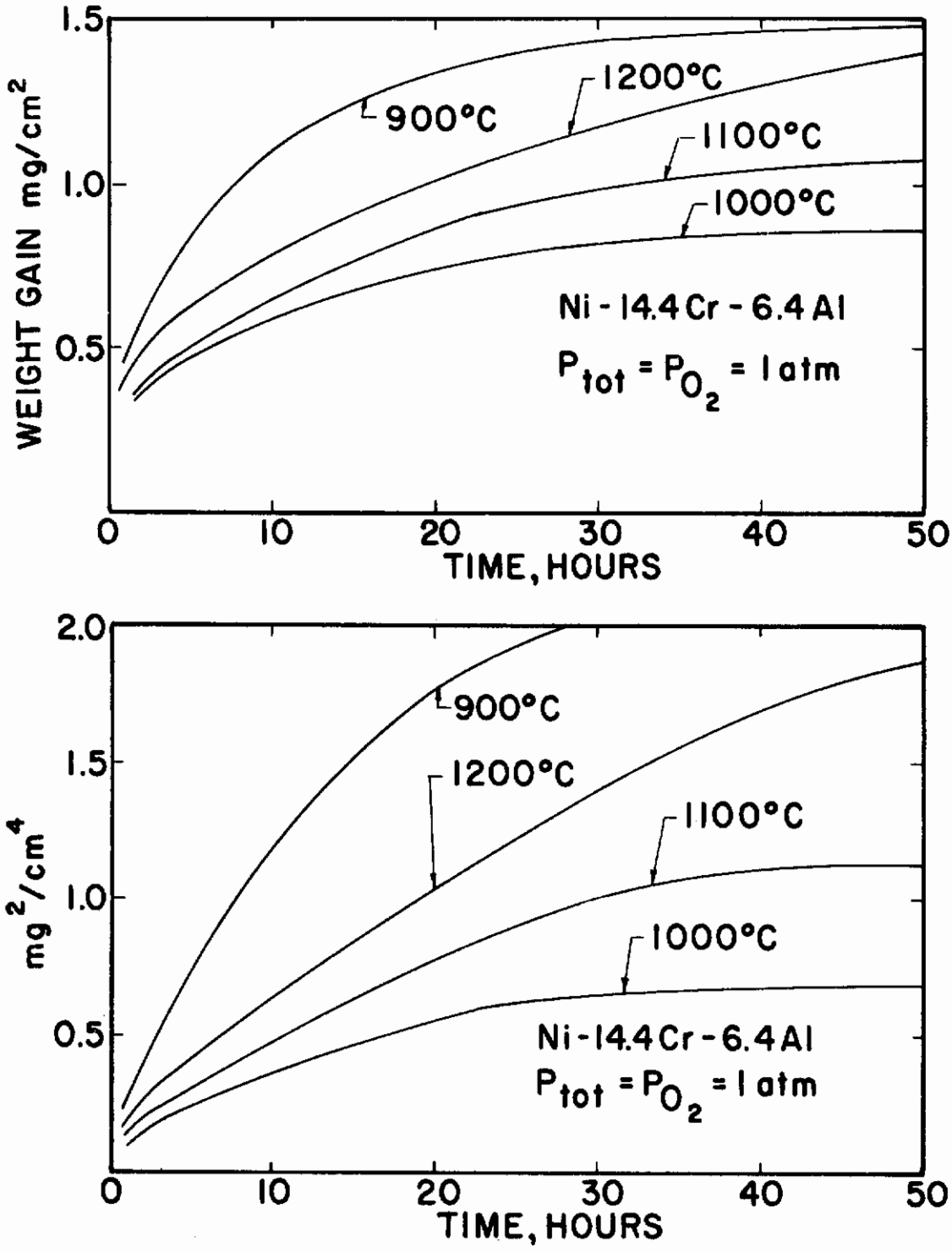

Fig. 1. Oxidation of alloy No. 2 (Ni-14.4Cr-6.4Al). Linear and parabolic plots.

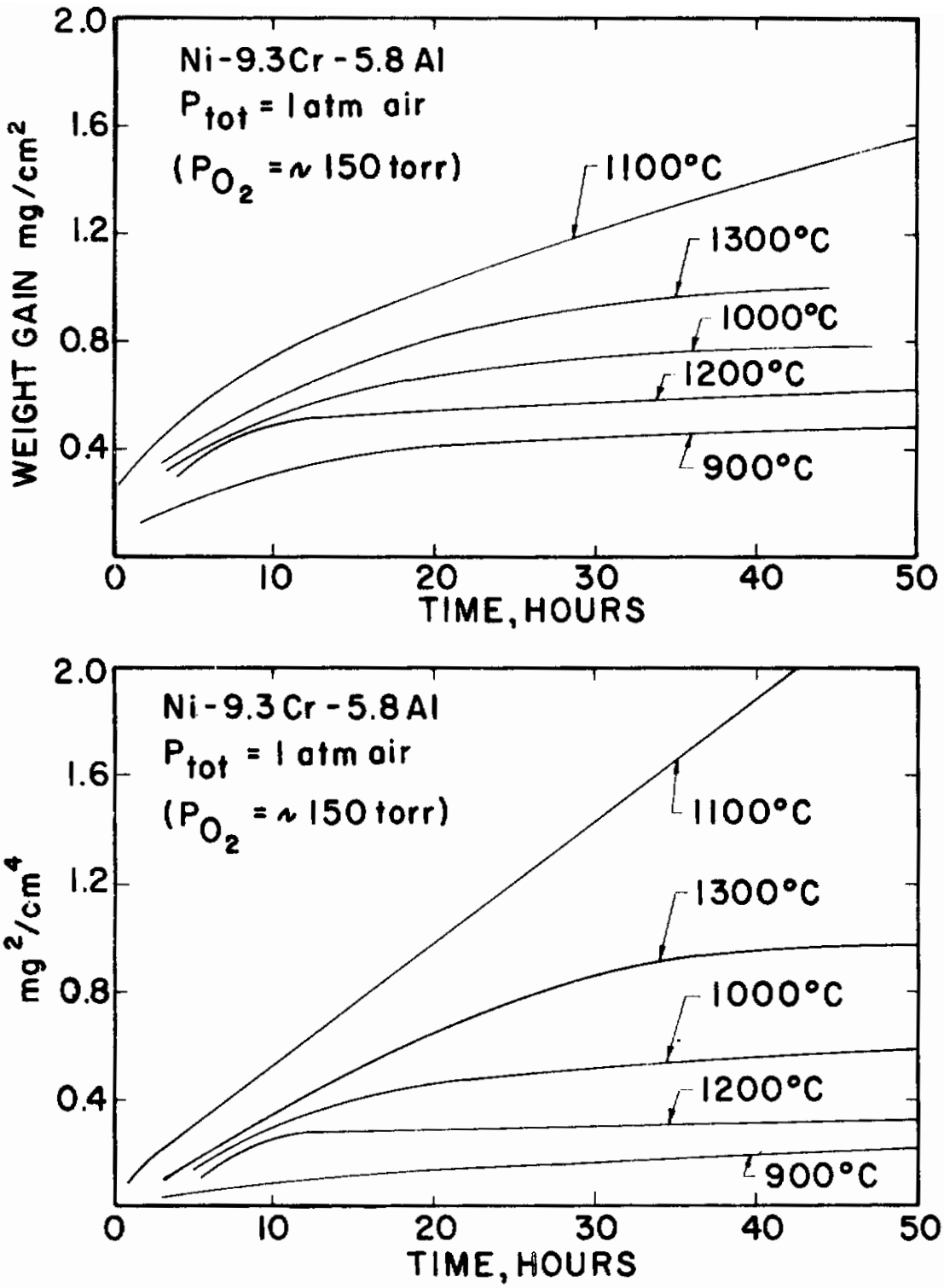

Fig. 2. Oxidation of alloy No. 3 (Ni-9.3Cr-5.8Al). Linear and parabolic plots.

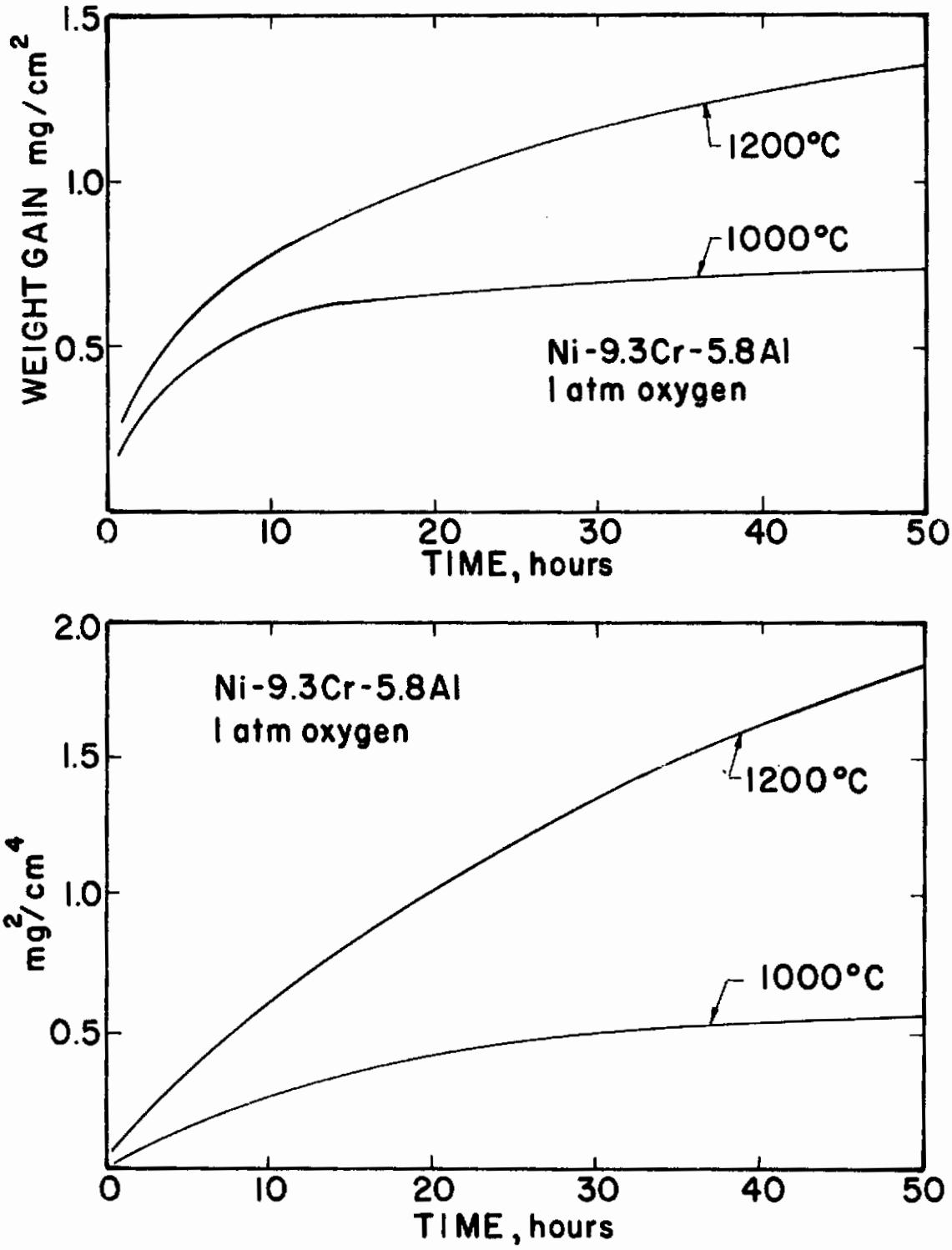

Fig. 3. Effect of temperature on oxidation of alloy No. 3 (Ni-9.3Cr-5.8Al) at an oxygen pressure of 1 atm. Linear and parabolic plots.

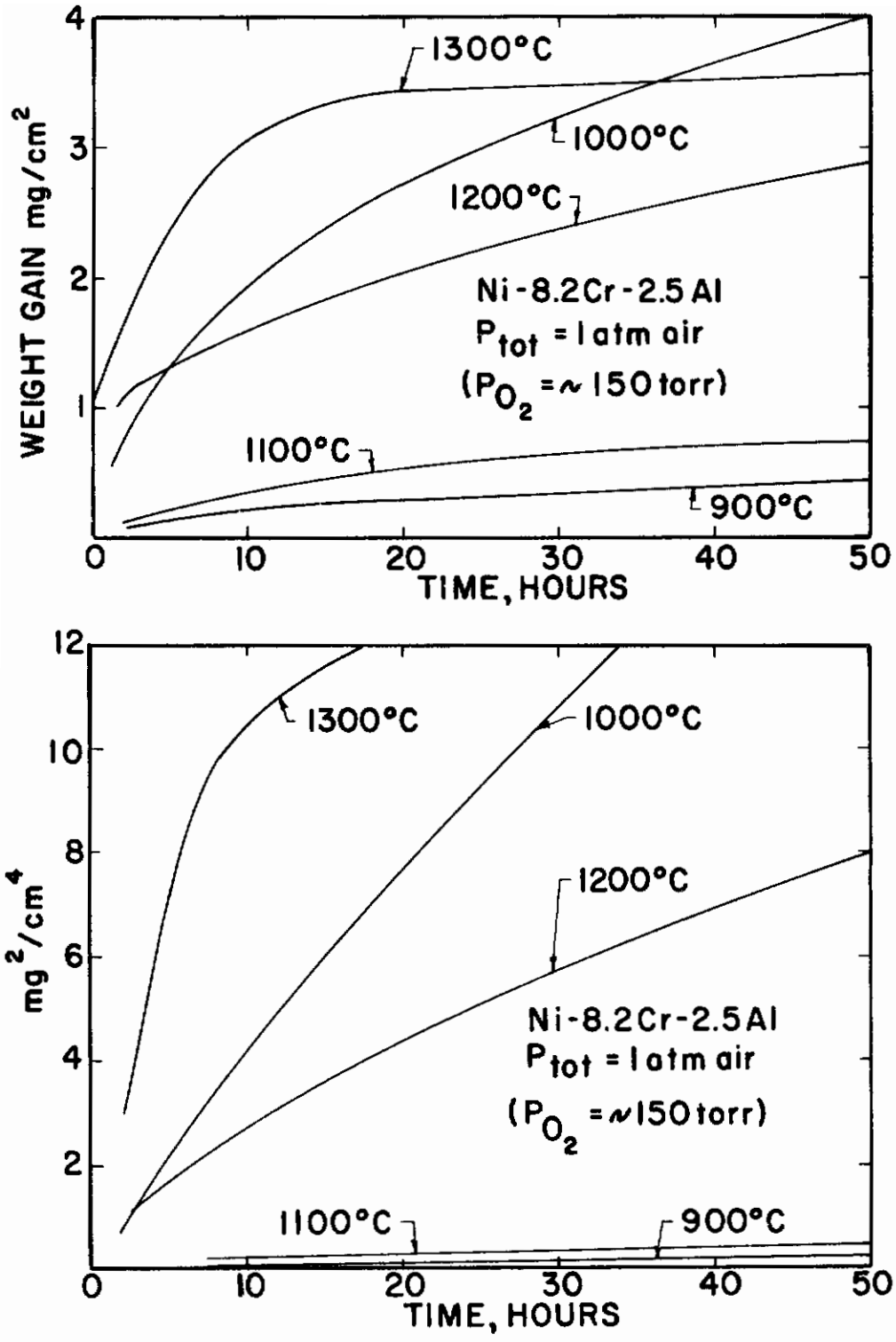

Fig. 4. Oxidation of alloy No. 4 (Ni-8.2Cr-2.5Al). Linear and parabolic plots.

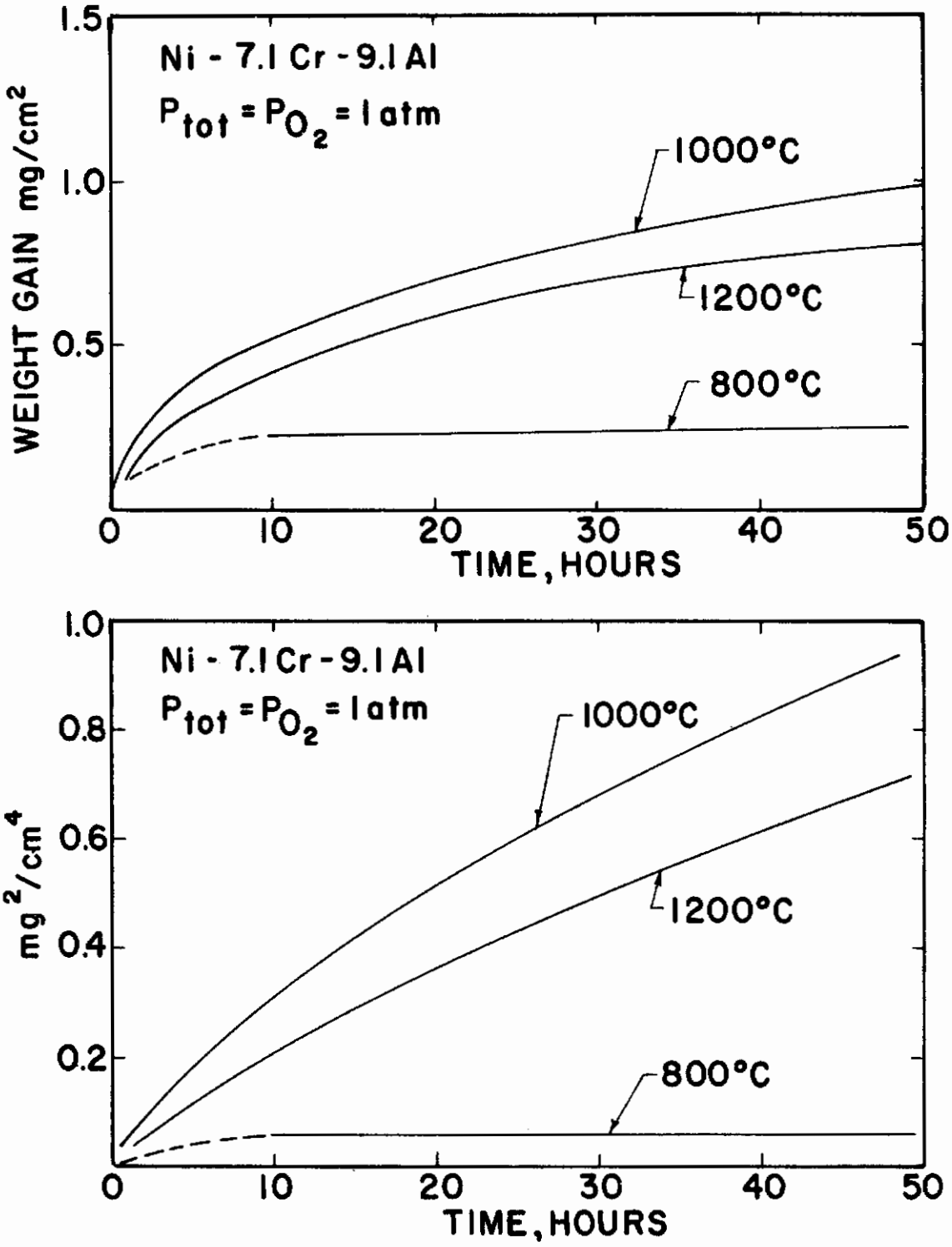

Fig. 5. Oxidation of alloy No. 5 (Ni-7.1Cr-9.1Al). Linear and parabolic plots.

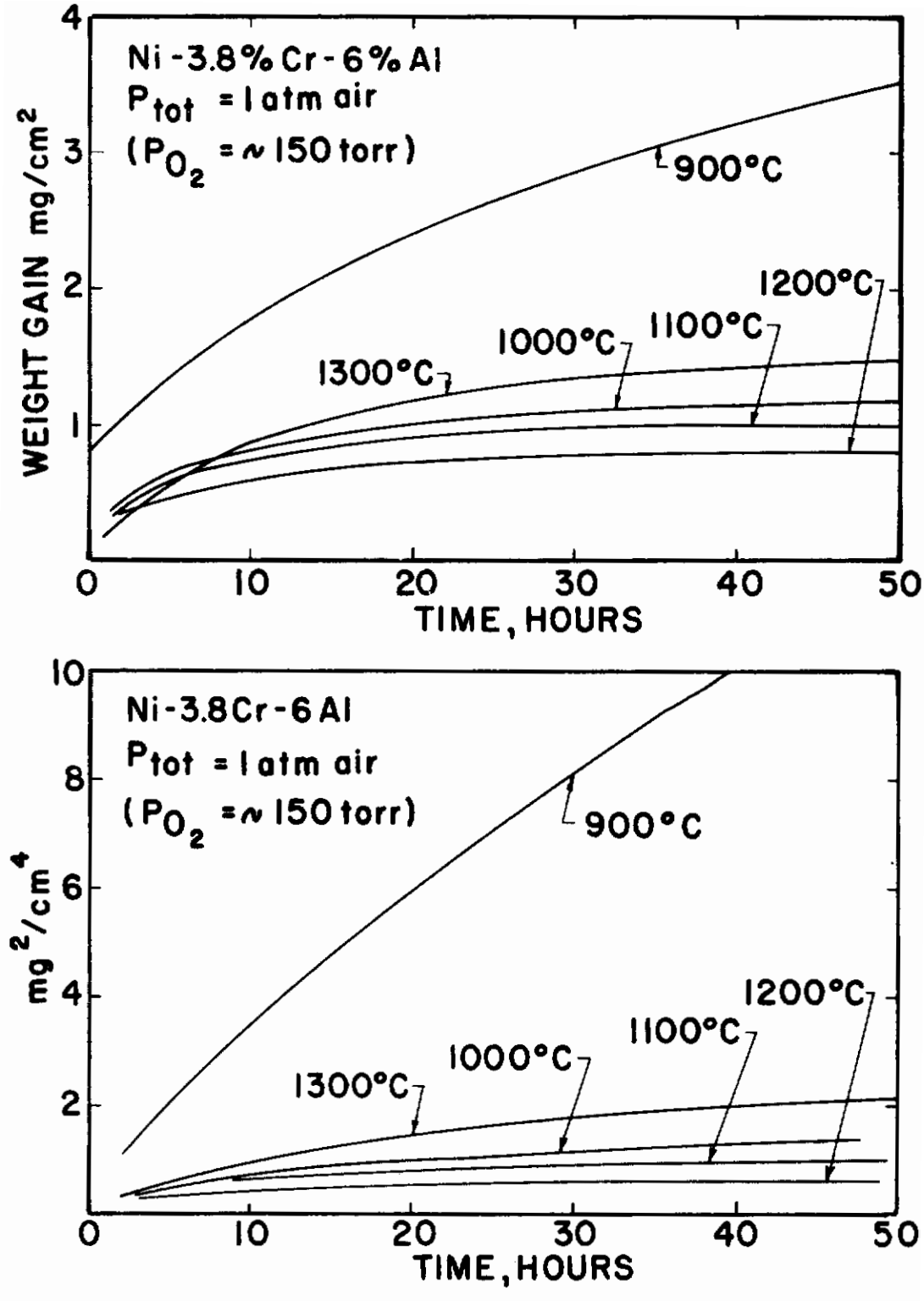

Fig. 6. Oxidation of alloy No. 6 (Ni-3.8Cr-6Al). Linear and parabolic plots.

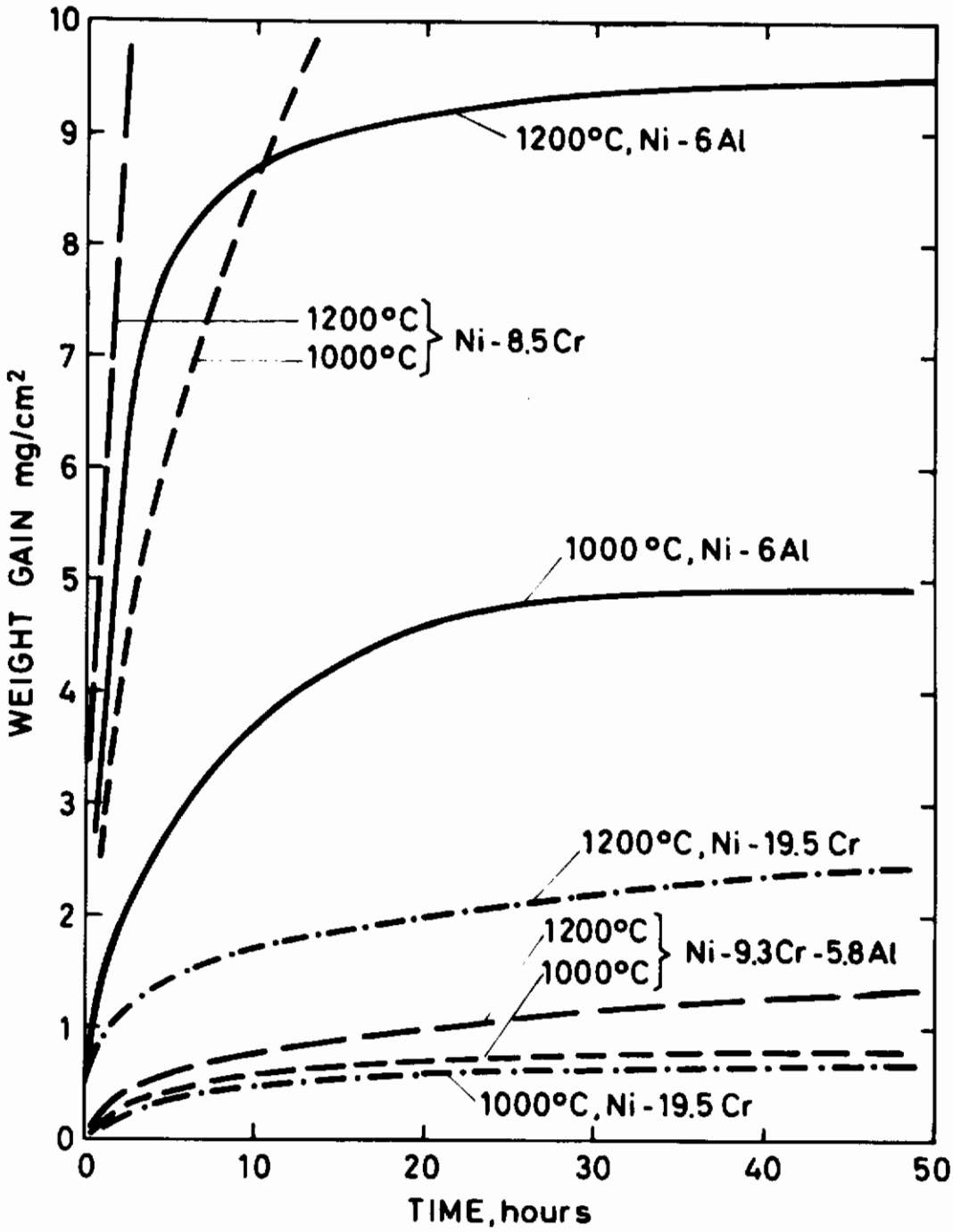

Fig. 7. Comparison of oxidation of Nickel-Chromium, Nickel-Aluminium, and Nickel-Chromium-Aluminium alloys reacted at 1000 and 1200 °C in oxygen at 1 atm. pressure.

3.1.2 Studies on Reacted Specimens. Reacted specimens were examined by means of metallographic techniques, X-ray diffraction and electron probe microanalyses as described above.

In most cases the surface scales could be described as single or double-layered. In addition, internal oxidation zones were observed in some cases. The major reaction products on the ternary alloys after about 50 hrs. reaction time were NiO, Cr_2O_3, and α-Al_2O_3. After short reaction periods (about 10 min.) $NiAl_2O_4$ and $Ni(Al,Cr)_2O_4$ could also be identified.

Alloy No. 2 (Ni-14Cr-6Al). Fig. 8 shows a metallographic cross section of this alloy reacted for ~48 hrs. in air at 1000 °C. The oxide scale on this alloy specimen was loosely adherent and partly spalled off during cooling in the furnace. X-ray diffraction studies directly on the surface of the reacted specimens show that the surface oxide mainly consists of NiO at 900 °C and of α-Al_2O_3 at higher temperatures. At 1200 °C the α-Al_2O_3 layer partly spalled off during cooling.

Alloy No. 3 (Ni-9Cr-6Al). Figs. 9a, b, and c show metallographic cross sections of this alloy reacted for 50 hrs. in air at 900, 1100, and 1200 °C, respectively.

In the X-ray diffraction studies on the surface only α-Al_2O_3 could be identified and the amount of α-Al_2O_3 increases with increasing temperature. The preferential oxidation of aluminium was further illustrated by concentration profiles shown in Figs. 10a-c. Corresponding X-ray images of aluminium are shown in the same figures. They illustrate only a small enrichment of aluminium in the oxide scale at 900 °C and a porous α-Al_2O_3 layer at 1100 °C and a compact α-Al_2O_3 layer at 1200 °C. The concentration profiles of aluminium show a similar behaviour. At 1200 °C the aluminium concentration increases to a high sharp peak in the oxide scale. The concentration profiles for chromium show a decrease in the oxide scale for specimens reacted at 900 and 1200 °C, but at 1100 °C the chromium shows a small increase.

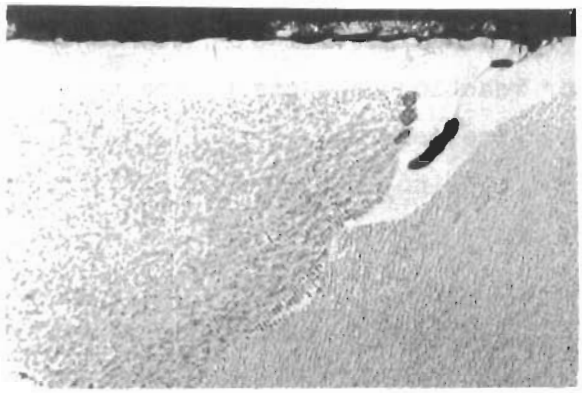

Fig. 8. Metallographic cross section of alloy No. 2 (Ni-14.4Cr-6.4Al) reacted in oxygen at 1 atm. pressure, etched. Reacted for ~ 48 hrs. at 1000 °C. 500 x.

a) Reacted at 900 °C. 500 x.

b) Reacted at 1100 °C. 500 x.

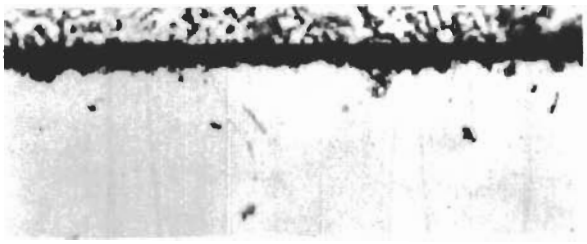

c) Reacted at 1200 °C. 500 x.

Fig. 9. Metallographic cross section of alloy No. 3 (Ni-9.3Cr-5.8Al) reacted for ~ 50 hrs. in air at 1 atm. pressure, unetched.

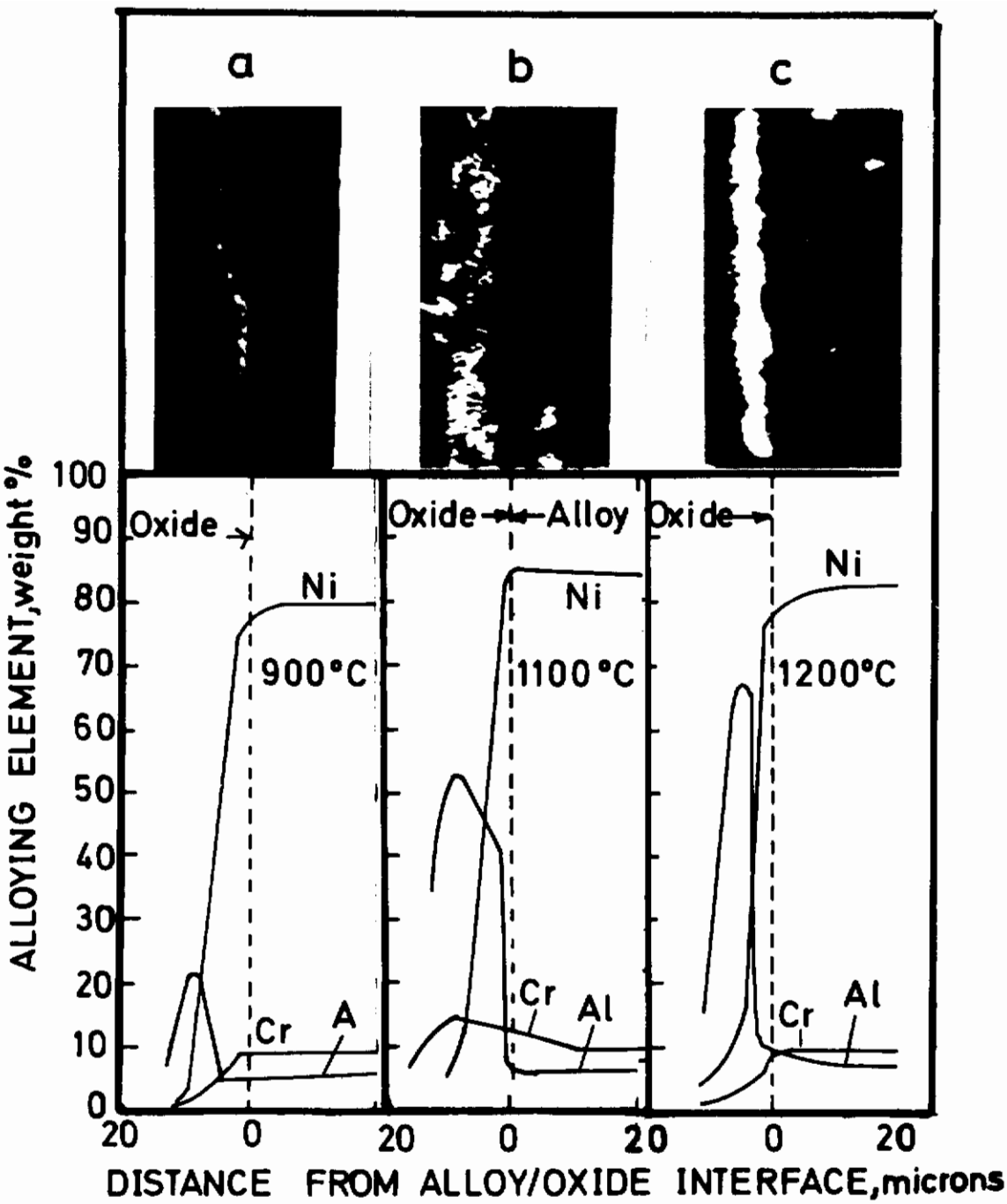

Fig. 10. Electron microprobe scans and aluminium X-ray images on metallographic cross-sections of alloy No. 3 (Ni-9.3Cr-5.8Al) specimens oxidized in 1 atm. air, (a) reacted at 900 °C, (b) reacted at 1100 °C, and (c) reacted at 1200 °C.

Alloy No. 4 (Ni-8Cr-3Al). The general features of the microstructure of reacted specimens of this alloy are shown in Fig. 11a and b. The specimens were reacted for about 50 hrs. in air at 900 and 1300 °C, respectively. The oxide scale formed at 900 °C consists of an outer layer which was identified as NiO and an internal oxidation zone of α-Al_2O_3 and Cr_2O_3. The matrix in this internal zone probably consists of nickel or NiO.

In going from 900 to 1300 °C, the oxidation mechanism changes. The thickness of the internal oxidation zone decreases and at 1300 °C it is absent. This latter feature is illustrated in Fig. 11b. At 1300 °C the oxide scale is triple-layered, consisting of an outer NiO-layer, an inner layer where α-Al_2O_3 predominates, and a middle zone where Cr_2O_3 seems to be the main reaction product. This clearly shows a tendency towards increasing selective oxidation of aluminium with increasing temperature. It may also be noted that the area between the NiO and Cr_2O_3 layer contains cavities.

The microprobe scans on the same alloy specimens are shown in Fig. 12a and b, respectively. The distribution of the elements illustrated by the concentration profiles confirm the above discussed results. In addition it may be noted that the oxygen concentration shows a maximum at the interface between the outer layer and the internal oxidation zone and then decreases rapidly in the internal oxidation zone.

Alloy No. 5 (Ni-7Cr-9Al). Fig. 13 refers to a specimen reacted at 1000 °C for 50 hrs. in oxygen at 1 atm. pressure and shows the general feature of the microstructure of this alloy. The precipitation free zone at the surface and on both sides of a grain boundary should be noted. The X-ray diffraction analysis shows α-Al_2O_3 to be the main oxide in the scale. Results obtained by microanalyses on oxidized specimens show a high concentration of aluminium in the oxide scale and in the grain boundaries. The precipitation free zones are enriched in chromium, and the nickel-concentration is approximately constant. These results are illustrated and confirmed in the X-ray images shown in Figs. 14 a-c.

Alloy No. 6 (Ni-4Cr-6Al). Examples of metallographic cross sections of reacted specimens are shown in Fig. 15 a and b which refer to specimens reacted for $\sim$ 50 hrs. at 900 and 1200 °C, respectively. At 900°C the oxide scale

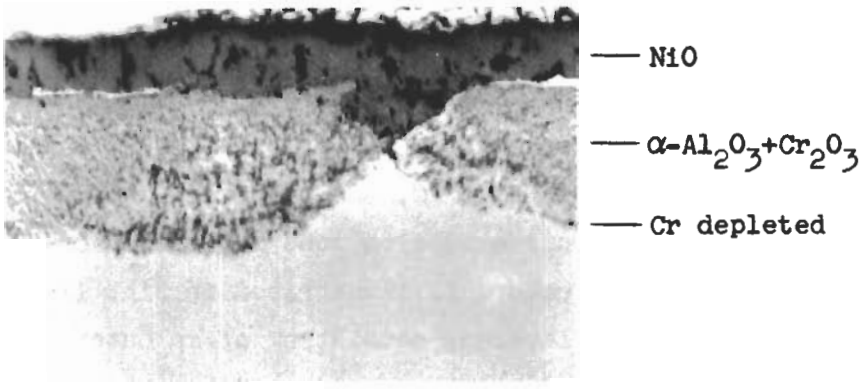

(a) Reacted at 900 °C. 500 x.

(b) Reacted at 1300 °C. 500 x.

Fig. 11. Metallographic cross section of alloy No. 4 (Ni-8.2Cr-2.5Al) reacted for ~ 50 hrs. in air at 1 atm. pressure, unetched.

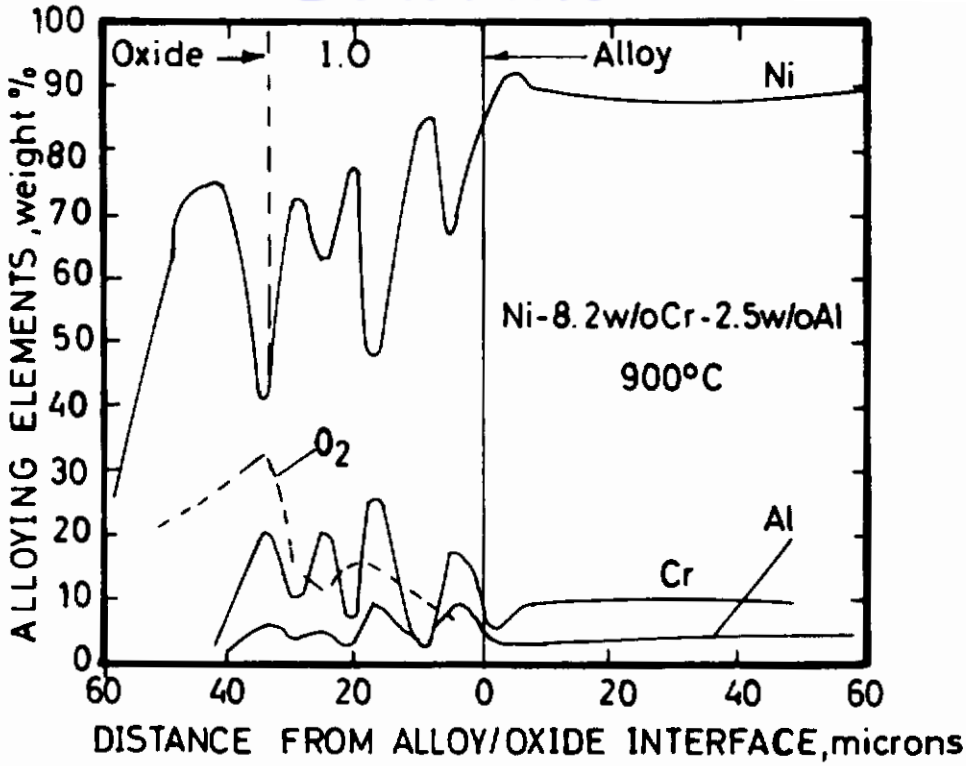

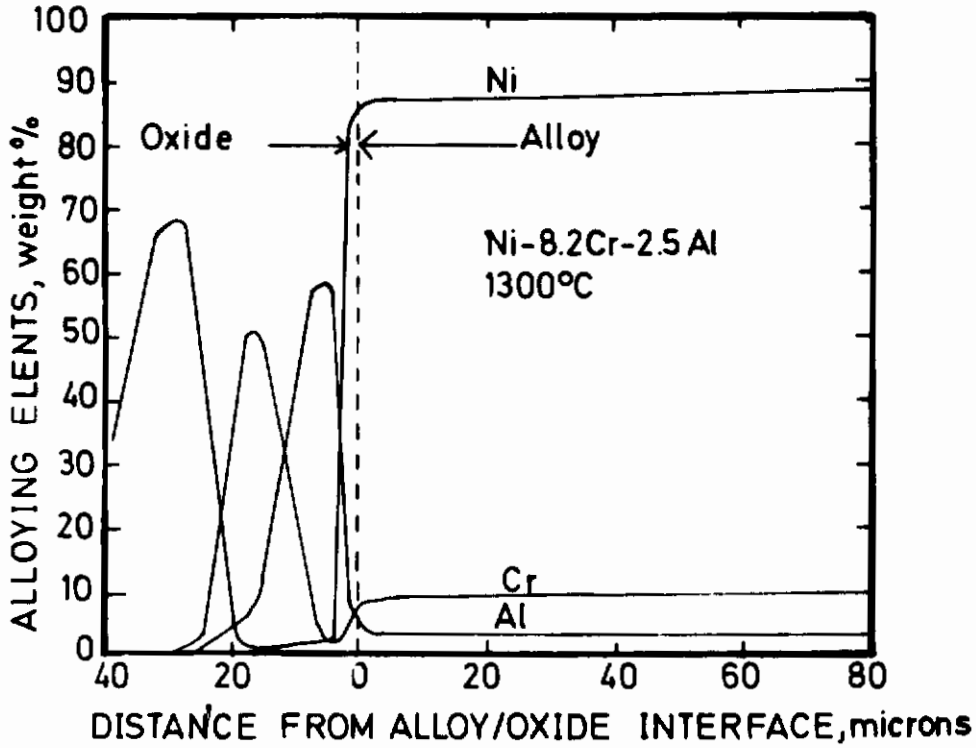

Fig. 12. Results of microprobe scans on metallographic cross section of alloy No. 4 (Ni-8.2Cr-2.5Al) reacted in air at 1 atm. pressure. (a) Reacted for ~ 50 hrs. at 900 °C, (b) reacted for ~ 50 hrs. at 1300 °C.

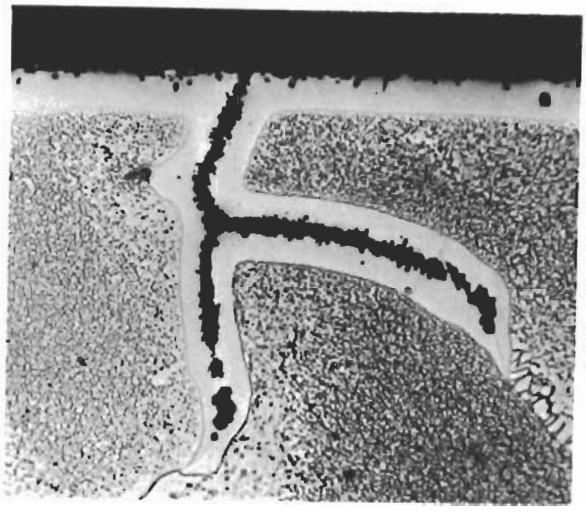

Fig. 13. Metallographic cross section of alloy No. 5 (Ni-7.1Cr-9.1Al) reacted at 1000 °C for ~ 50 hrs. in oxygen at 1 atm. pressure. 500 x.

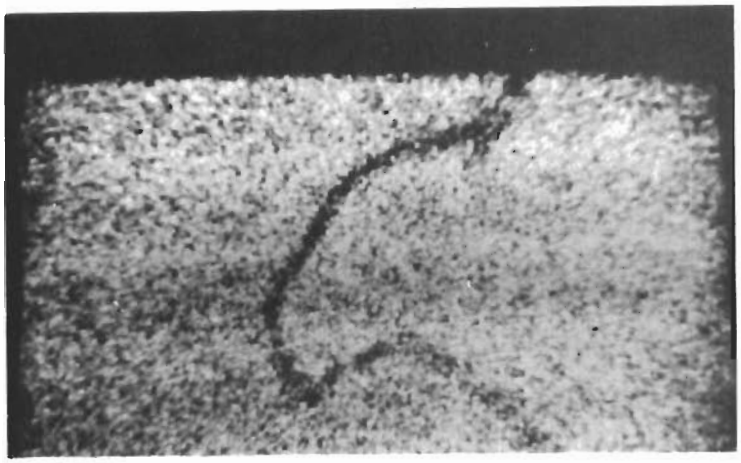

(a) X-ray image of Nickel. 500 x.

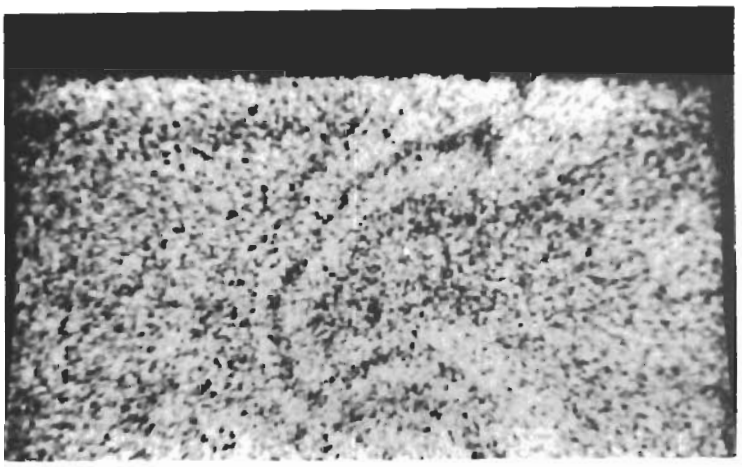

(b) X-ray image of Chromium. 500 x.

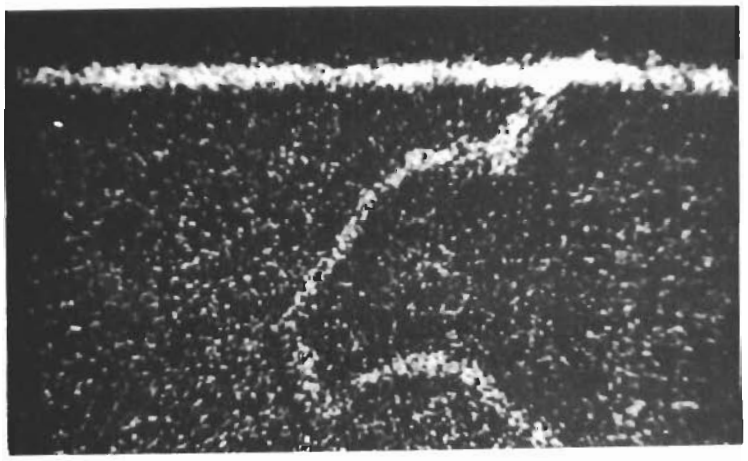

(c) X-ray image of Aluminium. 500 x.

Fig. 14. X-ray images of metallographic cross section of alloy No. 5 (Ni-7.1Cr-9.1Al) reacted at 1000 °C for ~ 50 hrs. in oxygen at 1 atm. pressure.

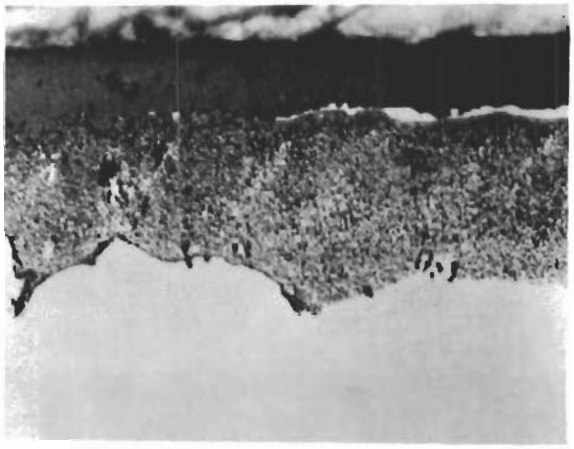

(a) Reacted at 900 °C. 500 x.

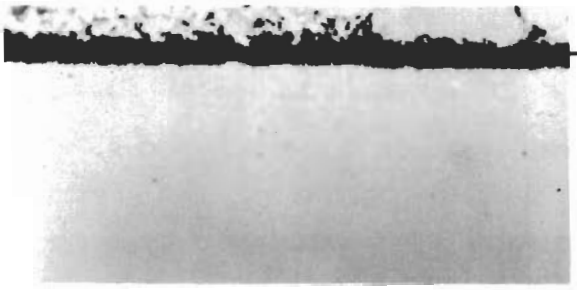

(b) Reacted at 1200 °C. 500 x.

Fig. 15. Metallographic cross section of alloy No. 6 (Ni-3.8Cr-6.0Al) reacted for ~50 hrs. in air at 1 atm. pressure.

consists of a compact outer oxide layer, identified as NiO, and an internal oxidation zone with α-Al_2O_3 and Cr_2O_3 as the main products. At higher temperature the oxidation mechanism differs from that at 900 °C. As shown in Fig. 15 b, the internal oxidation zone is absent, and the outer layer consists mainly of α-Al_2O_3. The concentration profiles shown in Fig. 16 illustrate the distribution of the elements in the oxide layers, and these results agree well with the results of the X-ray analyses.

3.2 Effect of Oxygen Pressure on the Oxidation of Alloy No. 3.

3.2.1 Reaction rate measurements. Oxidation of alloy No. 3 (Ni-8.7Cr-5.8Al) was also studied at oxygen pressures of 10 and 1 torr. Results of these studies are presented in Figs. 17-19.

Figs. 17 and 18 show parabolic plots of the oxidation at 10 and 1 torr, respectively. At 1 torr the oxidation is approximately parabolic at all temperatures, but at 10 torr marked deviations from this behaviour is observed.

Figs. 19 a and b show the oxidation at different oxygen pressures at 1000 and 1200 °C, respectively. The oxygen pressure dependence is most pronounced at 1200 °C.

3.2.2 Examination of reacted specimens. X-ray examinations of the oxide scales show that these consist of α-Al_2O_3, NiO, and Cr_2O_3, and the relative amounts of these vary with temperature and oxygen pressure.

After reaction at 10 torr O_2 it is found that NiO, Cr_2O_3, and α-Al_2O_3 are the main oxides at 1000 °C, while α-Al_2O_3 predominates at 1200 °C. Fig. 20 shows a metallographic cross section and X-ray images of the different elements of a specimen reacted at 1000 °C and 10 torr O_2. These data reveal an enrichment of aluminium and chromium in the oxide scale.

Fig. 21 shows the distribution of the different elements for specimens reacted at 1000 °C and at 1 atm., 10, and 1 torr O_2, respectively. At 1 atm. and 1 torr O_2 aluminium is markedly enriched in the scale, while at 10 torr nickel and chromium are enriched next to the surface and aluminium next to the alloy substrate.

At 1 torr O_2 α-Al_2O_3 is the main reaction product at both 1000 °C and 1200 °C.

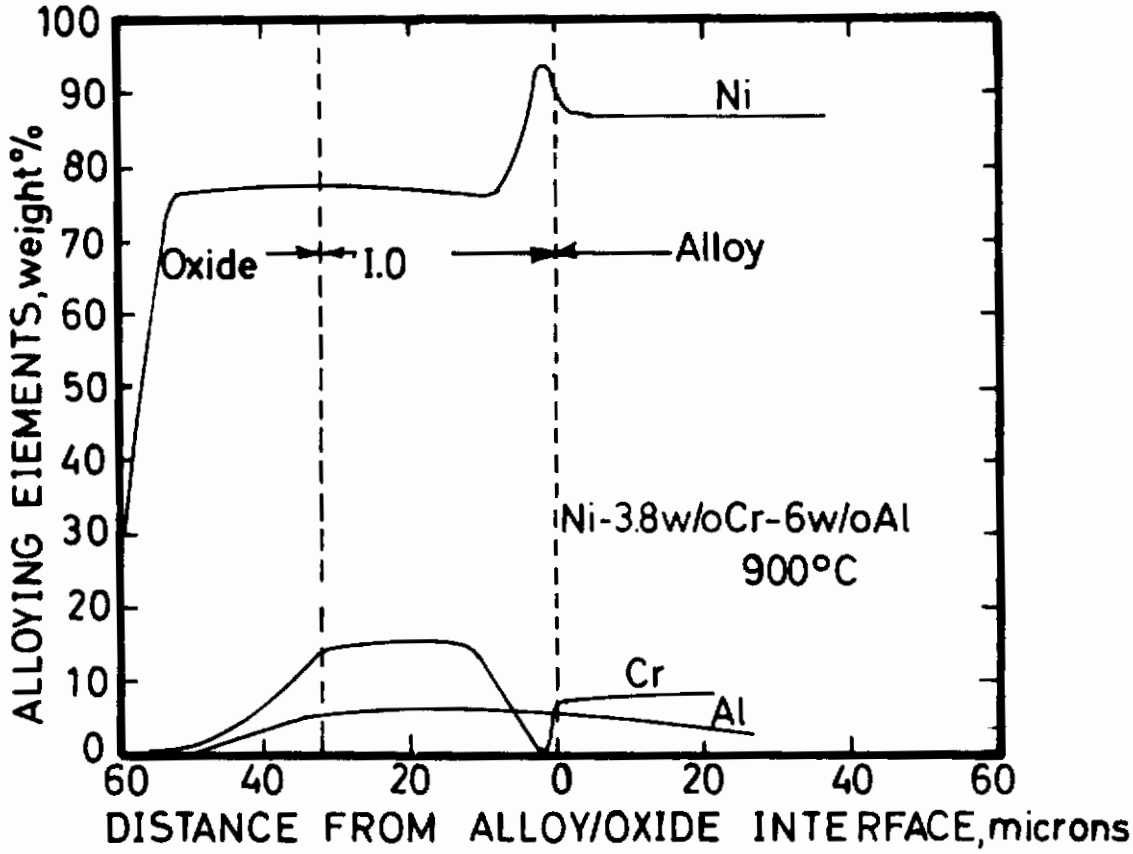

Fig. 16. Results of microprobe scans on metallographic cross section of alloy No. 6 (Ni-3.8Cr-6Al) specimen oxidized for ~ 50 hrs. at 900 °C and 1 atm. air.

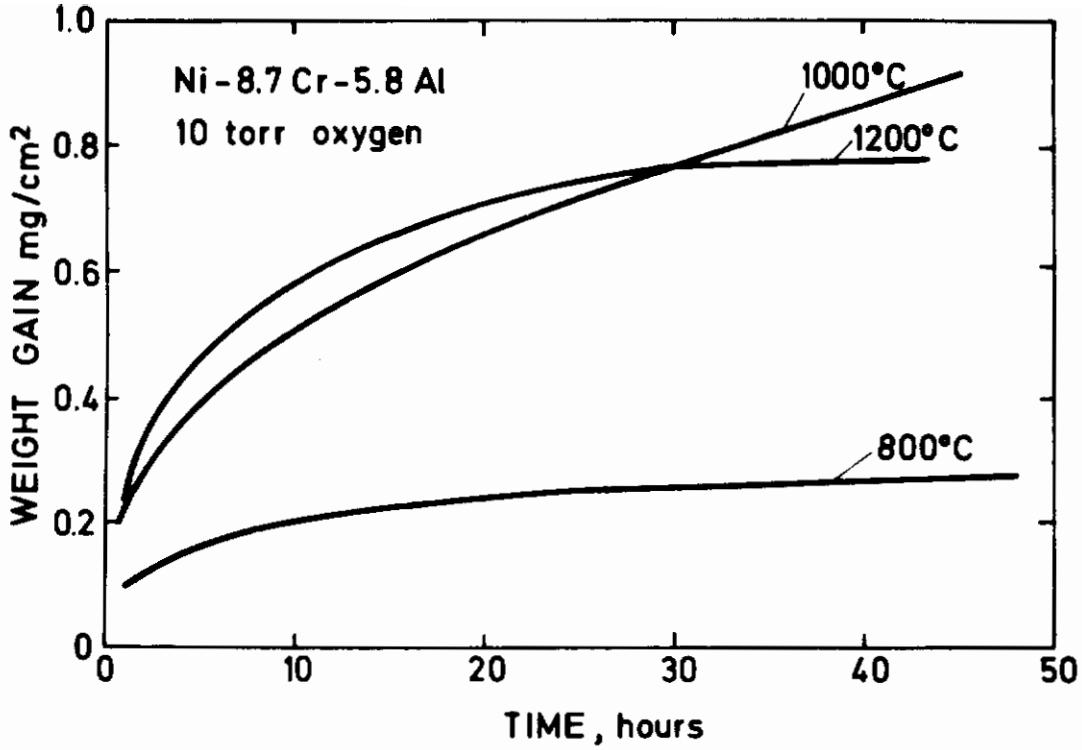

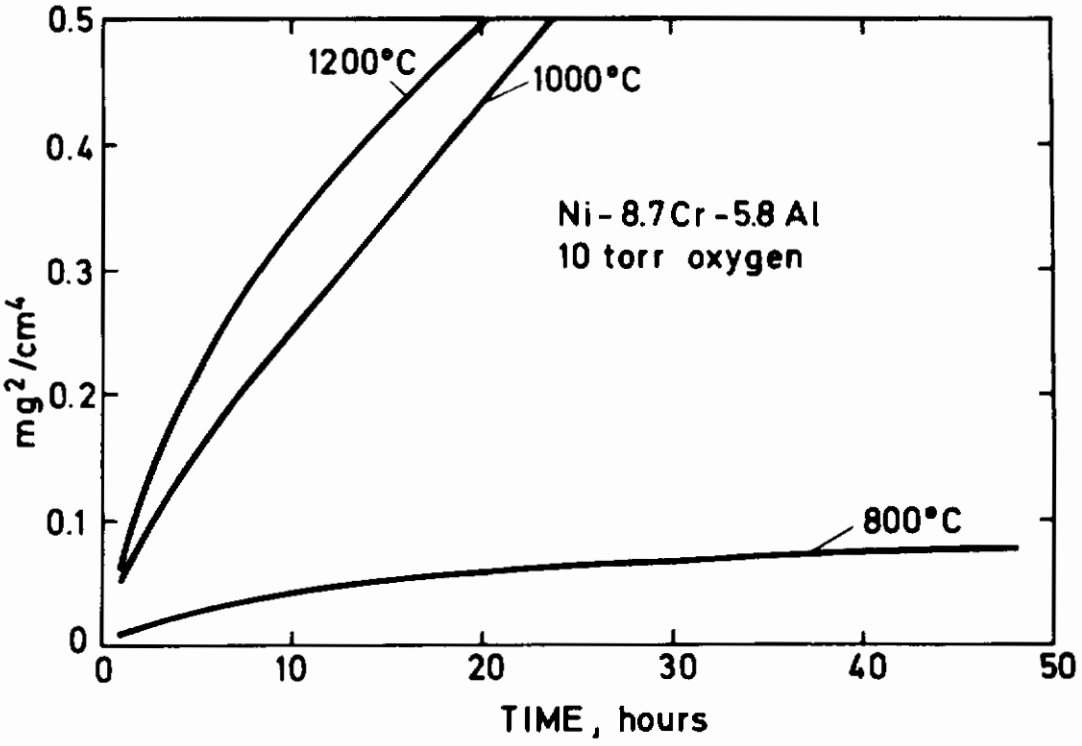

Fig. 17. Effect of temperature on oxidation of alloy No. 3 (Ni-8.7Cr-5.8Al) at an oxygen pressure of 10 torr. Linear and parabolic plots.

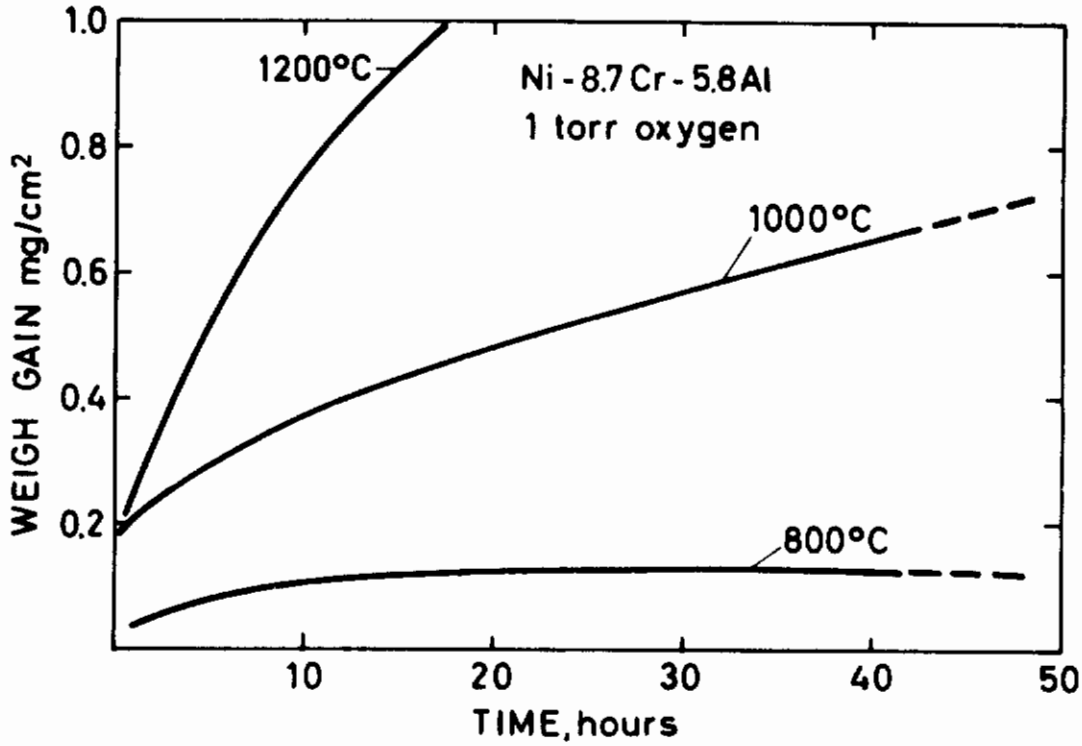

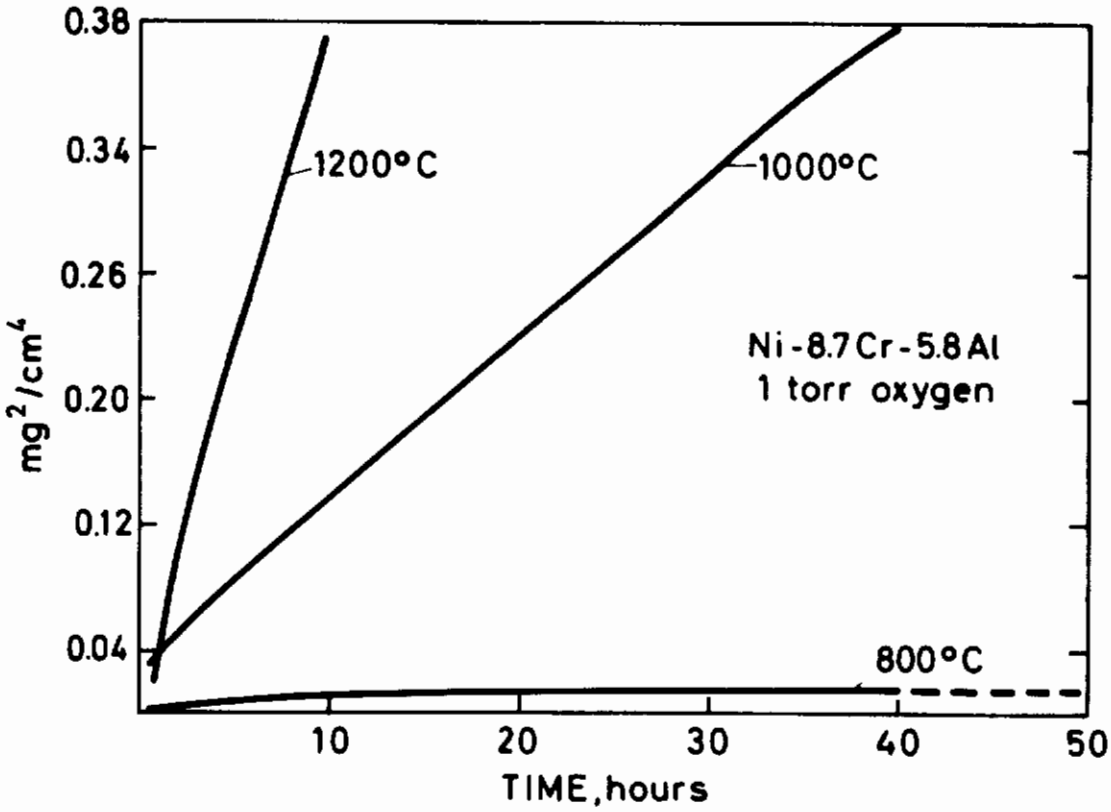

Fig. 18. Effect of temperature on oxidation of alloy No. 3 (Ni-8.7Cr-5.8Al) at an oxygen pressure of 1 torr. Linear and parabolic plots.

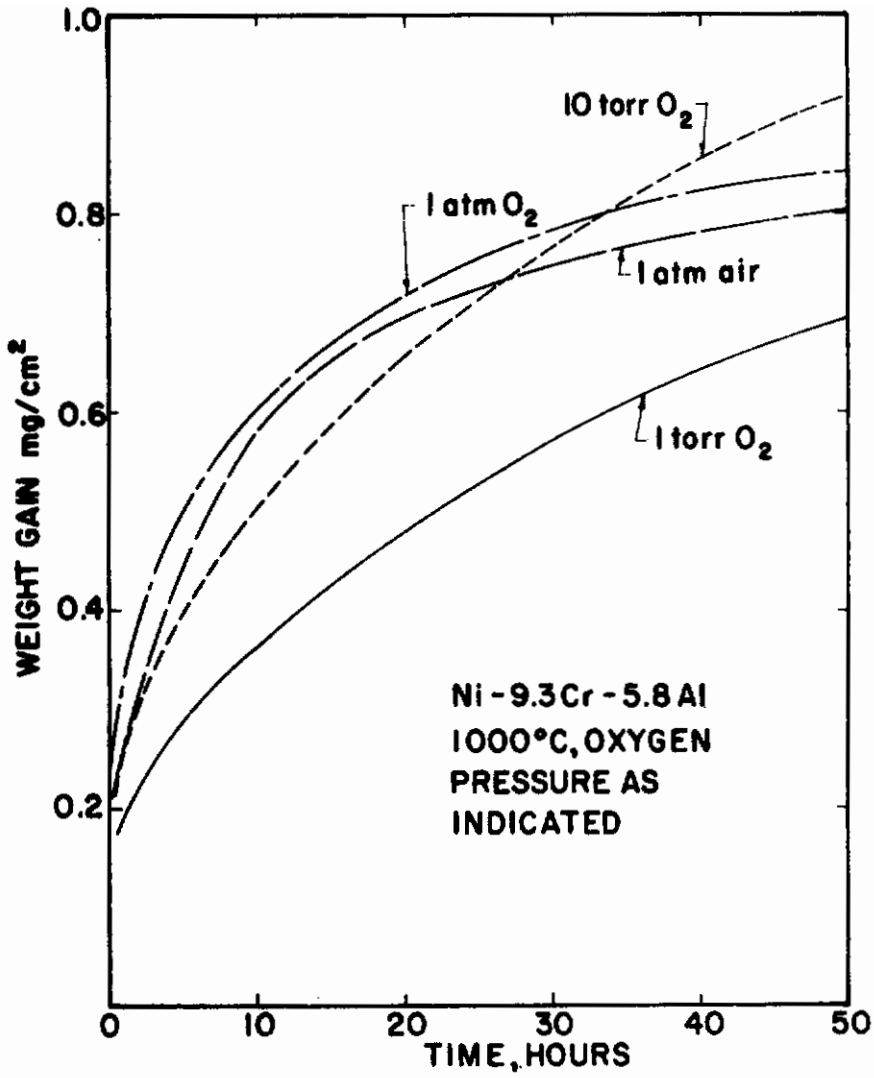

Fig. 19a. Effect of oxygen pressure on oxidation of alloy No. 3 (Ni-9.3Cr-6Al) reacted at 1000 °C.

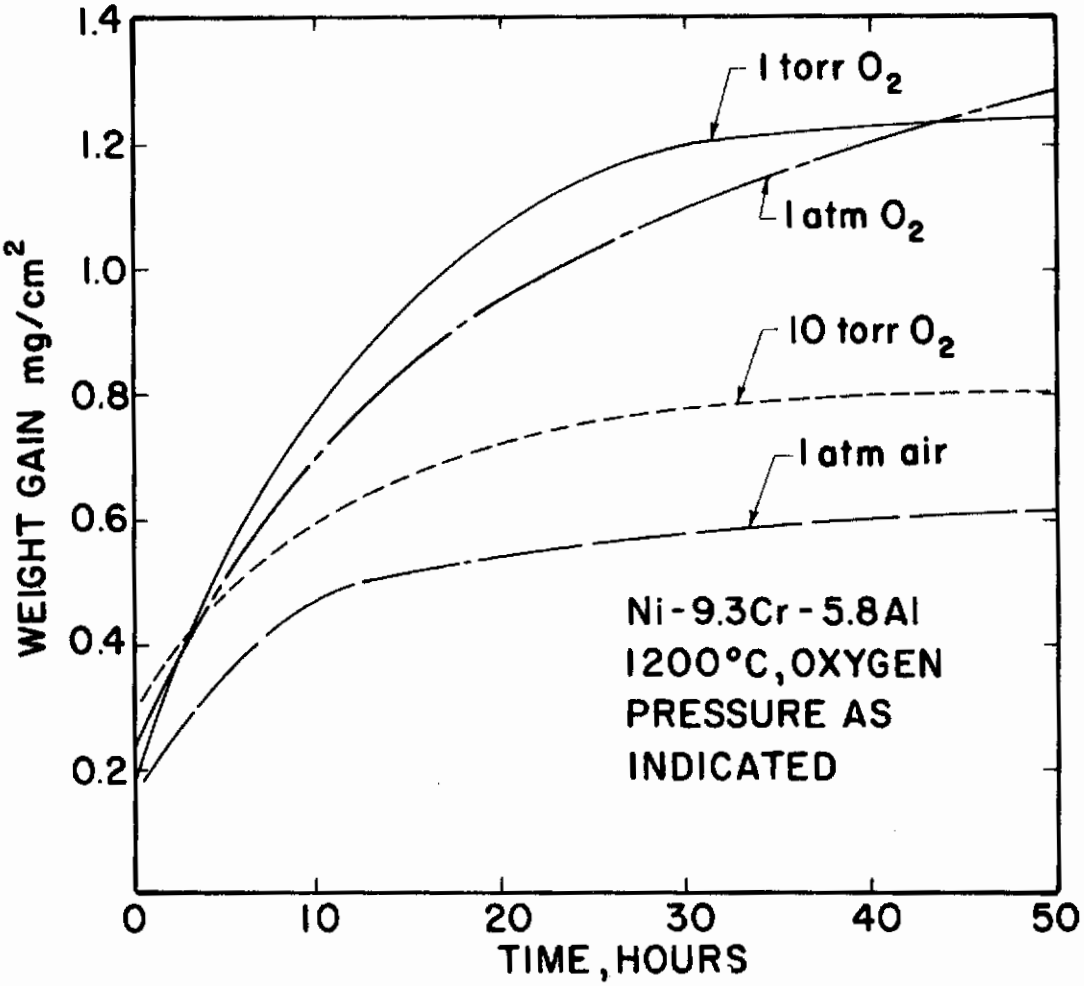

Fig. 19b. Effect of oxygen pressure on oxidation of alloy No. 3 (Ni-9.3Cr-6Al) reacted at 1200 °C.

(a)

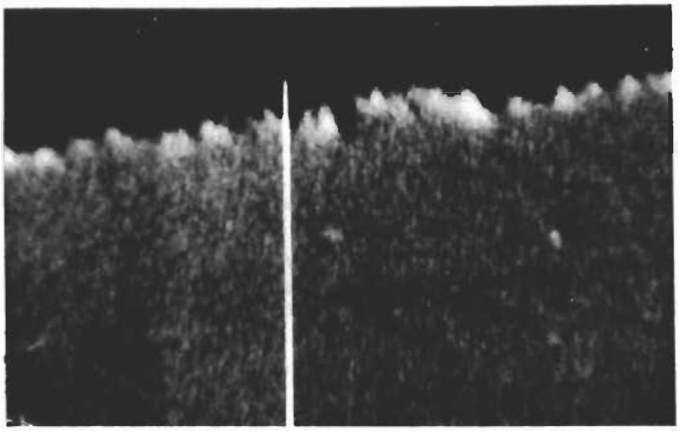

(b)

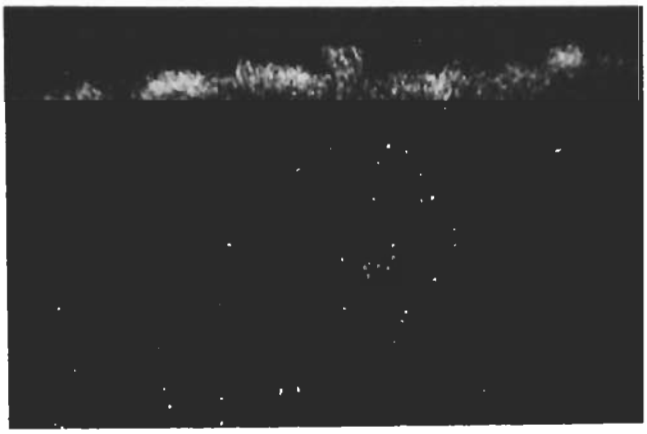

(d) Chromium

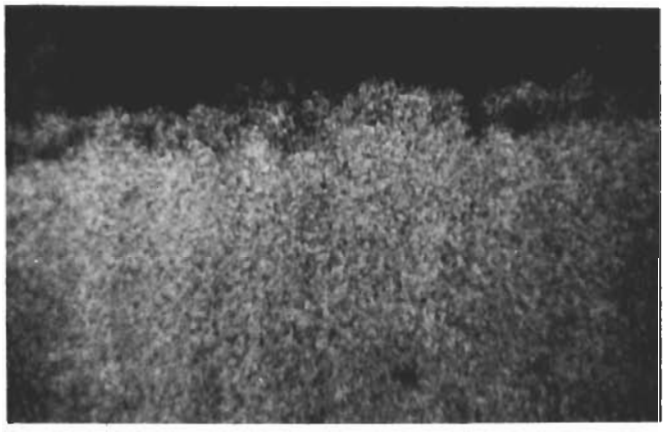

(c) Nickel

(e) Aluminium

Fig. 20. Light microscope (a), electron optical (b), and X-ray images (c-e) of metallographic cross sections of alloy No. 3 (Ni-8.7Cr-5.8Al) reacted for 45 hrs. at 1000 °C in 10 torr oxygen. 1000 x.

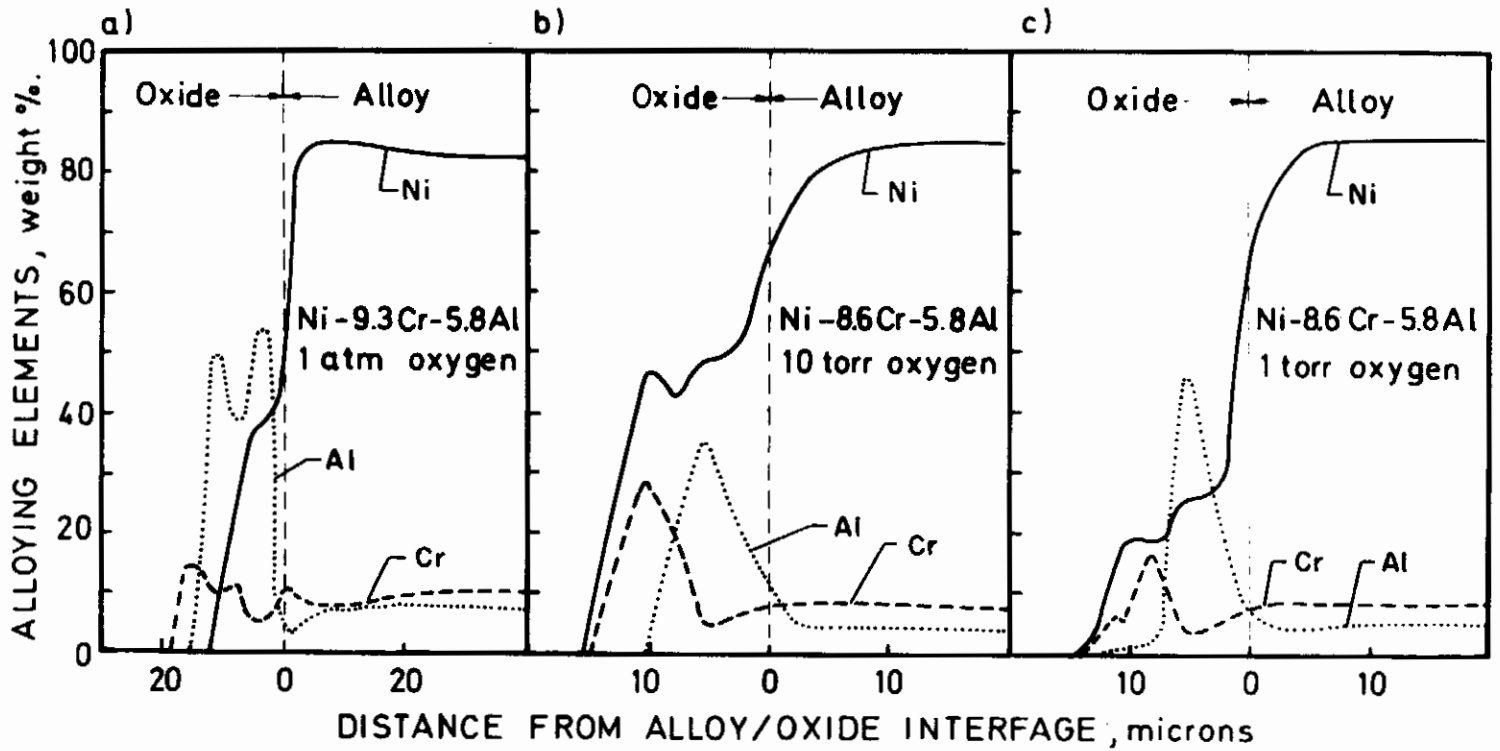

Fig. 21. Results of microprobe scans on metallographic cross sections of Nickel-Chromium-Aluminium specimen No. 3 (Ni-9.3Cr-5.8Al) reacted at 1000 °C and in pressures as indicated.

3.3 Studies of Thin Oxide Films.

The oxide films formed during initial oxidation (< 15 min) of alloy No. 3 (Ni-8.6Cr-5.8Al) was studied by means of electron diffraction and microscopy. The results reveal very heterogeneous oxide films both as regards the oxide composition and shapes of the crystals.

After reaction for 15 min. at 900 °C the oxide film consists of two main layers: an outer layer of NiO and an inner layer consisting of spinel $NiAl_2O_4$ (a = 8.04Å) and small amounts of γ-Al_2O_3. Regularly formed particles of Cr_2O_3 and rodlike particles of an unidentified tetragonal phase with lattice parameters a = 7.59Å and c = 2.82Å are observed next to the boundary between the outer and the inner layers. After reaction for 8-10 min. at 1200 °C the film may also be considered to consist of two main layers. The outer layer consists of NiO and traces of spinel crystallites (~ 400Å, lattice parameter ~8.25Å). Small cracks in the layer also contained Cr_2O_3 and α-Al_2O_3. The inner layer contains crystals of various shapes and sizes. The larger crystals had a tetragonal structure with axis a = 6.76Å and c = 6.95Å. This compound has not as yet been further identified.

4. DISCUSSION

The different nickel-chromium-aluminium alloys studied in this investigation have good or excellent oxidation resistance. Generally the alloy with the approximate composition Ni-9Cr-6Al shows the best oxidation characteristics. At 1000 °C its oxidation rate is of the same order as that of Nichrome, and at 1200 °C the rate is appreciably smaller.

The oxidation behaviour of the alloys is complex. The oxide scale may be single, double, or triple layered, and in cases appreciable internal oxidation takes place. The oxides formed in the oxidation comprise NiO, Cr_2O_3, Al_2O_3, and the spinels $NiAl_2O_4$ and $Ni(Cr,Al)_2O_4$. The relative amounts of these or whether they are present in the scales is a function of alloy composition, temperature, partial pressure of oxygen, and elapsed time of reaction.

The oxidation kinetics show a protective behaviour. However, the overall oxidation can generally not be described in terms of ideal parabolic behaviour, although the oxidation in cases or over limited periods of time may be described as approximately parabolic. A common feature under many conditions is that the oxidation rate decreases faster than that of parabolic behaviour.

The protective behaviour clearly shows that the overall oxidation is solid state diffusion controlled. The marked deviation from ideal parabolic behaviour is in no way unexpected in view of changes in overall oxide composition and the parabolic occurrence of solid state reactions between the oxides during oxidation. In view of this complexity detailed interpretations of the kinetics and the oxidation mechanism do not appear justified at this stage. More general and qualitative considerations will be given in the following.

4.1 Temperature dependence.

A general feature of the temperature dependence of the alloys is that the oxidation goes through a maximum in the temperature range 900-1300 °C. This is a result of a gradual change in the oxidation mechanism which in its main feature involves an increasingly preferential and selective oxidation of the aluminium-content in the alloy with increasing temperature. This results in oxide scales increasingly enriched in α-Al_2O_3, and after extended oxidation at 1200 °C oxide scales generally consist of α-Al_2O_3. Due to the excellent protective properties of this oxide phase, the oxidation results in the observed irregular temperature dependence. These features are, for instance, illustrated in Fig. 10 (which shows microprobe scans and aluminium X-ray images on metallographic cross sections of Ni-9Cr-6Al specimens oxidized at 900, 1100, and 1200 °C).

4.2 Effects of aluminium and chromium contents.

Variations in the total amount of chromium and aluminium and the relative amounts of these greatly affect the oxidation behaviour. These effects are particularly marked at 900-1100 °C as at higher temperatures aluminium tends

to be selectively oxidized in all the alloys.

As described above the Ni-9Cr-6Al alloy exhibits the best overall oxidation resistance, and the primary reason for this is that the oxide on this alloy mainly consists of α-Al_2O_3 at all temperatures after extended oxidation.

As α-Al_2O_3 is the most stable oxide which may be formed in oxidation of the different alloy components, the preferential or selective oxidation of aluminium will inhibit or prevent internal oxidation of the alloy. In the Ni-9Cr-6Al alloy internal oxidation zones are also small or absent.

Alloys No. 2 (Ni-14Cr-6Al) and No. 6 (Ni-4Cr-6Al) contain the same amount of aluminium as No. 3, but the chromium-contents is either higher or lower. In oxidation of these alloys at 1200 °C for extended periods of time, formation of α-Al_2O_3 predominates, and there is no significant difference compared to the Ni-9Cr-6Al alloy. However, in oxidation at 900-1000 °C the oxide scales consist to a large extent of NiO and simultaneously internal oxidation of chromium and aluminium takes place.

Whether internal oxidation or selective oxidation of the least noble alloying elements take place is determined by transport properties through the oxide scale and the relative rates of diffusion of oxygen and the alloy components in the alloy phase. The tendency for a more selective oxidation of aluminium in the Ni-9Cr-6Al alloy compared to that of alloys No. 2 and 4 therefore probably means that the aluminium and/or oxygen diffusion in the alloy phase is a function of alloy composition, and that aluminium-diffusion in the Ni-9Cr-6Al alloy, for instance, is faster than in alloys with higher or lower chromium-content. A factor to be considered in this connection is that the Ni-9Cr-6Al alloy has an aluminium-content which exceed that for precipitations of Ni_3Al.[11] However, a detailed interpretation must await results of studies of diffusion rates in the alloy system.

Alloy No. 4 (Ni-8Cr-3Al) also exhibits internal oxidation, and in this the aluminium-concentration is probably not sufficiently high for selective oxidation of aluminium.

4.3 Composition of Oxide Scale as a Function of Time.

When one compares the composition of the surface oxide formed after an initial oxidation (~ 10 min) and after extended oxidation (~50-100 hrs.) it can be concluded that important changes take place in the composition as a function of time. An important difference is that after initial oxidation of the Ni-9Cr-6Al alloy at 1200 °C the oxide film consists of an outer NiO layer and spinel crystallites, while after extended oxidation the oxide scale predominantly consists of α-Al_2O_3. During the initial oxidation all the alloy components are thus oxidized, but gradually a compact protective layer of α-Al_2O_3 is built up. The outer NiO layer may possibly disappear through direct evaporation or through displacement reactions between aluminium and chromium and NiO.[12,13] The spinel crystallites may also decompose to Al_2O_3 by the same mechanism.

4.4 Effect of Oxygen Pressure.

The partial pressure of oxygen affects the oxidation behaviour of the Ni-9Cr-6Al alloy. The effect is most marked at 1200 °C, but the changes in oxidation rates do not show large differences.

One would generally expect an increasingly selective oxidation of aluminium decreasing partial pressure of oxygen and with that an increased oxidation resistance. The results indicate a larger relative amount of NiO and Cr_2O_3 in the scale after oxidation at 10 torr than at 1 atm. O_2. This result can not readily be explained. It could possibly reflect minor variations in the composition of the specimens, edge effects, or differences in pretreatment.

4.5 Concluding Remarks.

This study shows that excellent oxidation resistance at temperature may be achieved in nickel-chromium alloys with reduced chromium-content. When considering the possible use of an alloy such as Ni-9Cr-6Al as constructional material it must, however, be concluded from an oxidation point of view that a main disadvantage is the poor adherence of the oxide scale after cooling. As a further development it is therefore important to improve the adherence

of the scales without deleterious effects on the oxidation behaviour at temperature.

This may possibly be achieved through minor additions of such metals as manganese, titanium, yttrium and rare earth metals.

All in all, alloy oxidation theories suffer from a lack of basic understanding of properties of oxide scales and diffusion characteristics, knowledge of solid state reactions, and alloy chemistry. Such studies are needed in future development work.

PART II - EFFECT OF TITANIUM AND TITANIUM PLUS SAMARIUM ADDITIONS ON THE HIGH TEMPERATURE OXIDATION OF Ni-9Cr-5Al

1. INTRODUCTION

As discussed in Part I it is of interest to study the effect of small alloy additions on the oxidation behaviour of nickel-chromium-aluminium base alloys. In the following the oxidation of Ni-9Cr-5Al alloys with additions of 2 w/o titanium and 2 w/o titanium + 0.1 w/o samarium, respectively, is described.

2. MATERIALS AND METHODS

The composition of each alloy (Nos. 7 and 8) is given in Table I.

The alloys were prepared in argon atmosphere ($\sim$ 0.5 atm. pressure) in an induction furnace and cast. The cast alloys were cut directly to rectangular oxidation test specimens by means of spark errosion machining. Before oxidation the specimens were vacuum annealed at 1000 ^{o}C for about 1 hr. Methods for studying the oxidation behaviour are described in Part I.

3. EXPERIMENTAL RESULTS

3.1 Reaction Rate Measurements.

The oxidation was performed in flowing air (1 l/min) and oxygen at a pressure of 1 atm. Weight gain data obtained at 900, 1000, and 1200 ^{o}C are given in Fig. 22-24. The results are presented in linear plots.

It may be noted that the titanium-modified alloy oxidizes relatively rapidly at 900 ^{o}C and under this condition faster than at 1000 and 1200 ^{o}C.

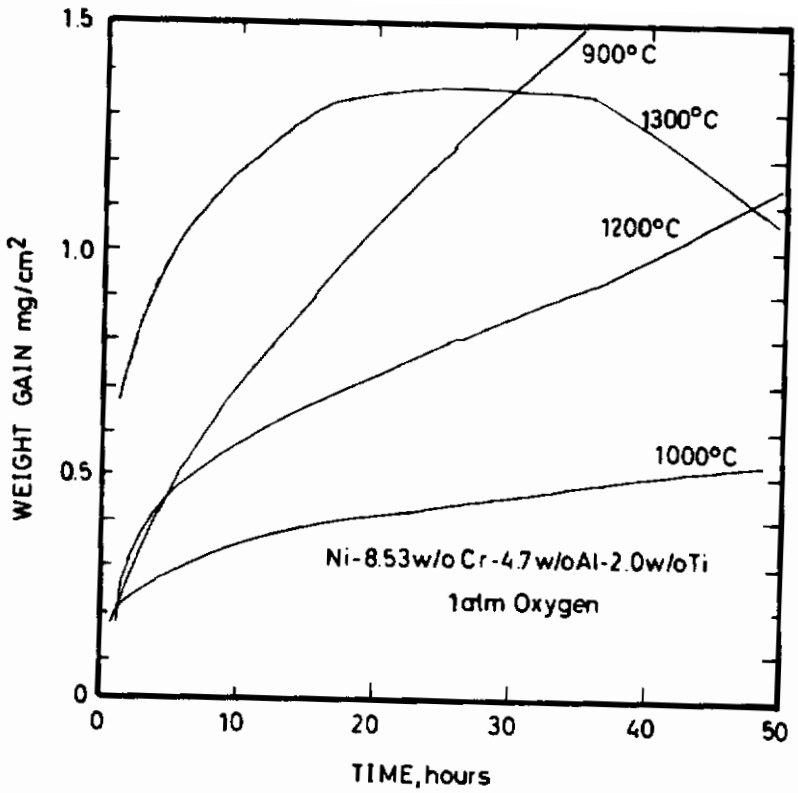

Fig. 22. Oxidation of alloy No. 7 (Ni-8.3Cr-4.7Al-2.0Ti). Linear plot.

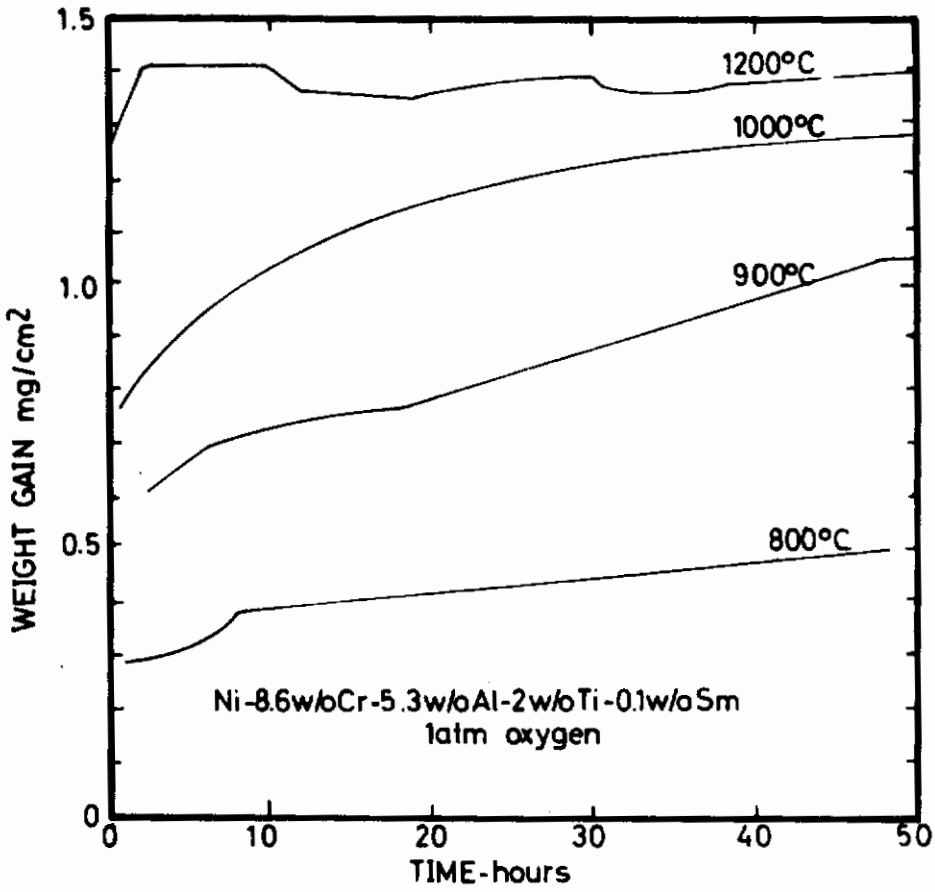

Fig. 23. Oxidation of alloy No. 8 (Ni-8.6Cr-5.3Al-2.0Ti-0.1Sm). Linear plot.

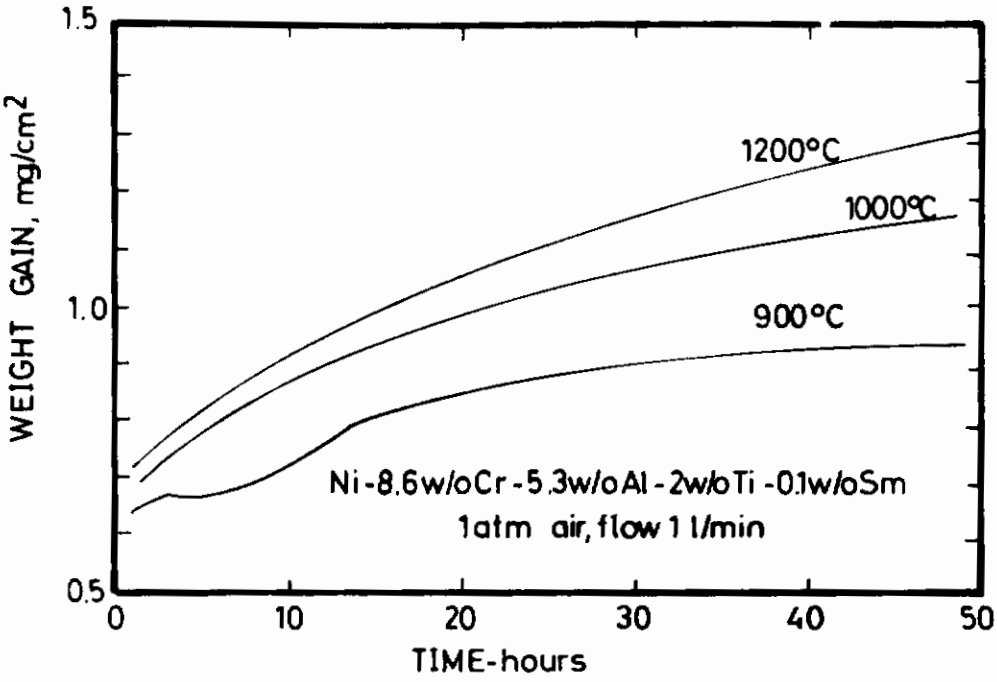

Fig. 24. Oxidation of alloy No. 8 (Ni-8.6Cr-5.3Al-2.0Ti-0.1Sm) in flowing air. Linear plot.

The weight gain results of the titanium + samarium modified alloy show a regular temperature dependence. The weight gain curves indicates a rapid oxidation during the initial stage, after which the reaction decreases rapidly with time.

Under some conditions, the oxidation of the modified alloys results in marked oxide spallation and evaporation of oxides. The former is for instance illustrated by the abrupt changes on the weight gain curve for 1200 °C in Fig. 23 for the titanium+samarium modified alloy. Evaporation of oxides is specifically observed for the titanium modified alloy after ~30 hrs. reaction at 1300 °C as illustrated in Fig. 22.

The kinetics are difficult to describe in terms of classical rate equations.

3.2 Examinations of Reacted Specimens.

The oxide scales on the titanium-modified alloy were generally loosely adherent and in most cases the scale exfoliated either during cooling or after taking the specimen out of the furnace. The exfoliated oxide from a specimen reacted at 1000 °C for 50 hrs. consisted mainly of α-Al_2O_3. NiO is found as the main oxide remaining on the alloy surface. After more extended reaction NiO and Cr_2O_3 became the predominant oxides. There were also traces of a spinel with an axis of 8.25 Å which may indicate the presence of $NiCr_2O_4$ with aluminium or titanium in solid solution. The exfoliated oxide at 1300 °C consisted mainly of α-Al_2O_3 and a spinel. The axis of the spinel was 8.04Å which suggests the presence of $NiAl_2O_4$.

Characteristic features of the alloy with addition of titanium + samarium are illustrated in the metallographic cross section shown in Fig. 25 a-b which refer to specimen reacted at 1000 °C in oxygen and flowing air at atmospheric pressure, respectively. No penetration of oxide along the grain boundary occurs in the alloy, but the precipitation free zone beneath the oxide/alloy interface may be noted. The thickness of the zone appears to be smaller on specimens reacted in flowing air. The scales adhered to the alloy substrate.

After extended oxidation in air or oxygen comparatively large amounts of NiO and Cr_2O_3 were identified in the outer layer.

(a) Reacted for 52.5 hrs. in 1 atm. oxygen at 1000 °C. 500 x.

(b) Reacted for 49.5 hrs. in 1 atm. flowing air (1 l/min at 1000 °C). 500 x.

Fig. 25. Metallographic cross section of alloy No. 8 (Ni-8.6Cr-5.3Al-2.0Ti-0.1Sm).

The distribution of the elements in the oxides is illustrated in the X-ray images shown in Fig. 26, which refer to a titanium + samarium modified specimen reacted for 52.3 hrs. at 1000 °C in oxygen. After the microprobe runs, the oxide scale on the specimen was partly ground down and rechecked by X-ray diffraction. The oxide phases TiO_2 and Al_2O_3 were identified. From these results the oxide scale appears to consist of different layers containing different elements. The surface layer is enriched in nickel, the layer beneath in chromium, then comes another nickel-enriched layer, which is followed by a layer enriched in titanium and aluminium to the alloy. The electron optical image is also included in Fig. 26.

The distribution of elements in the oxide scale for specimens reacted 53 hrs. at 1200 °C in air was the same as for 1000 °C.

4. DISCUSSION

The additions of titanium and of titanium + samarium result in a more complex oxidation behaviour than that observed in the nickel-chromium-aluminium base alloy. The number of oxide phases in the scale is increased and includes TiO_2. The tendency for selective oxidation of aluminium is also decreased.

Generally it may be concluded that the titanium addition does not improve the oxidation characteristics of the nickel-chromium-aluminium base alloy, and at 900 °C it even has a marked deleterious effect on the oxidation rate. The detailed reasons for this behaviour is not understood, but generally it is to be expected that the presence of TiO_2 will not add to the oxidation resistance of the scale.

It appears that the addition of Sm improves the oxide adherence, but the mechanism for this can not be ascertained. As to the effects of other rare earth metals, more detailed studies of the effects of yttrium on the oxidation behaviour are reported in Part IV of this report.

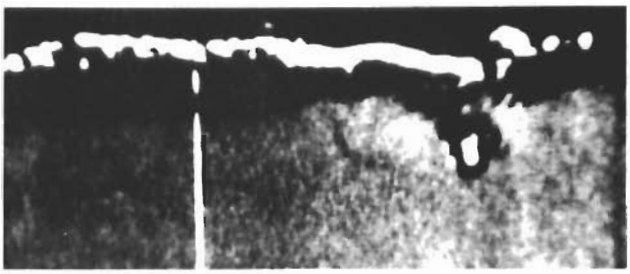

(a) Electron-optical image. 500 x.

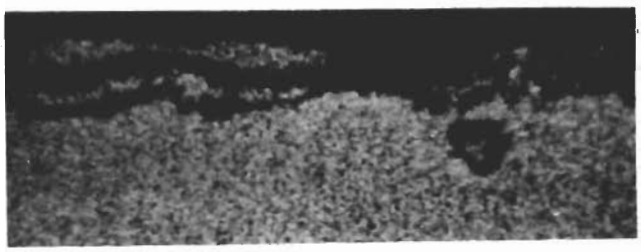

(b) X-ray image of Nickel. 500 x.

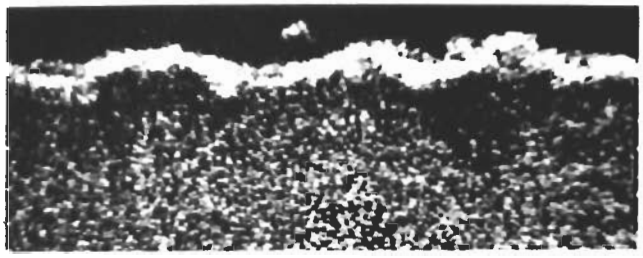

(c) X-ray image of Chromium. 500 x.

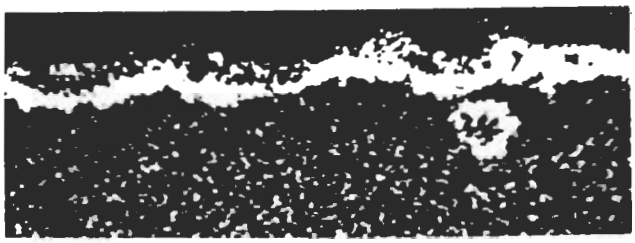

(d) X-ray image of Aluminium. 500 x.

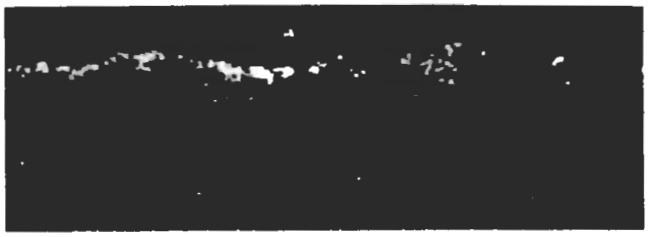

(e) X-ray image of Titanium. 500 x.

Fig. 26. Electron-optical and X-ray images of metallographic cross section of alloy No. 8 (Ni-8.6Cr-5.3Al-2.0Ti-0.1Sm). Reacted for 52.5 hrs. at 1000 °C in 1 atm. oxygen.

PART III - INFLUENCE OF MANGANESE-ADDITIONS ON HIGH TEMPERATURE OXIDATION OF SOME NICKEL-CHROMIUM AND NICKEL-CHROMIUM-ALUMINIUM BASE ALLOYS.

1. INTRODUCTION

As mentioned in the previous parts of this report, small alloy additions may significantly affect the oxidation behaviour of alloys. In the following are presented results of a few studies of oxidation of nickel-chromium and nickel-chromium-aluminium base alloys with minor additions of manganese.

2. PREVIOUS STUDIES

Gulbransen et al.[3, 15-17] studied the effect of manganese and silicon-additions on the oxidation behaviour of Ni-20Cr. They report that manganese has a deleterious effect on the oxidation resistance, while silicon improves the oxidation characteristics and service life of this type of alloys. Hessenbruch [18] similarly reports that a few tenths of a percent of manganese significantly lowers the heat resistance, but larger manganese-additions have less effect. Antill et el.[19] have recently shown that 0.65 w/o manganese addition to Fe-20Cr-25Ni-Nb stainless steel does not significantly influence the long term oxidation.

3. MATERIALS AND METHODS

3.1 Materials

Induction melted nickel-chromium-manganese and nickel-chromium-aluminium-manganese alloys were used in the studies. The chemical analyses of the alloys are given in Table I, (alloys Nos. 9-13).

The cast alloys were cut directly to oxidation test specimens by means of spark errosion machining. The total surface area was about 2.2 cm^2. Before oxidation the specimens were washed in acetone and vacuum annealed for 1 hr. at 1000 °C.

3.2 Methods.

The oxidation behaviour was studied through thermogravimetric measurements of oxidation rates and characterization of oxidized specimens by means of metallographic techniques, X-ray diffraction, electron microscopy and diffraction, and electron microprobe analysis. The methods have been described in more detail in Part I.

4. EXPERIMENTAL RESULTS

4.1 Thermogravimetric Measurements.

The specimens were oxidized for 50 hrs. in 1 atm. O_2 in the temperature range 800-1200 °C. The results are presented in Figs. 27-31.

Generally the alloys show protective behaviour. The oxidation can as a rule not be described in terms of an ideal parabolic behaviour. It may be noted that alloy No. 12 (Ni-5.6Cr-5.5Al-1.2Mn) exhibited weight loss after more extended reaction at 1200 °C. This may be due to oxide evaporation.

The two nickel-chromium-manganese alloys (Nos. 9 and 11) show very rapid oxidation rates compared to nickel-chromium-aluminium-manganese alloys.

4.1.1 Effect of oxygen pressure on oxidation rate. Oxidation of alloy No. 11 (Ni-8.5Cr-6Al-1.1Mn) was also studied at 10 and 1 torr O_2. The results at 1 atm., 10 and 1 torr O_2 at 1000 and 1200 °C are shown in Fig. 32. At both temperatures the amount of oxidation decreases with decreasing oxygen pressure.

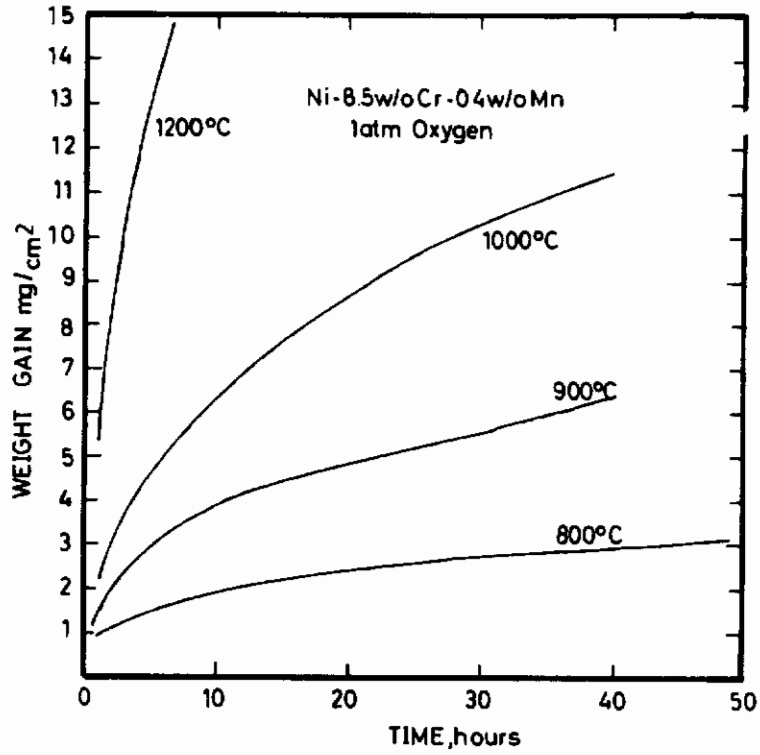

Fig. 27. Oxidation of alloy No. 9 (Ni-8.5Cr-0.4Mn).

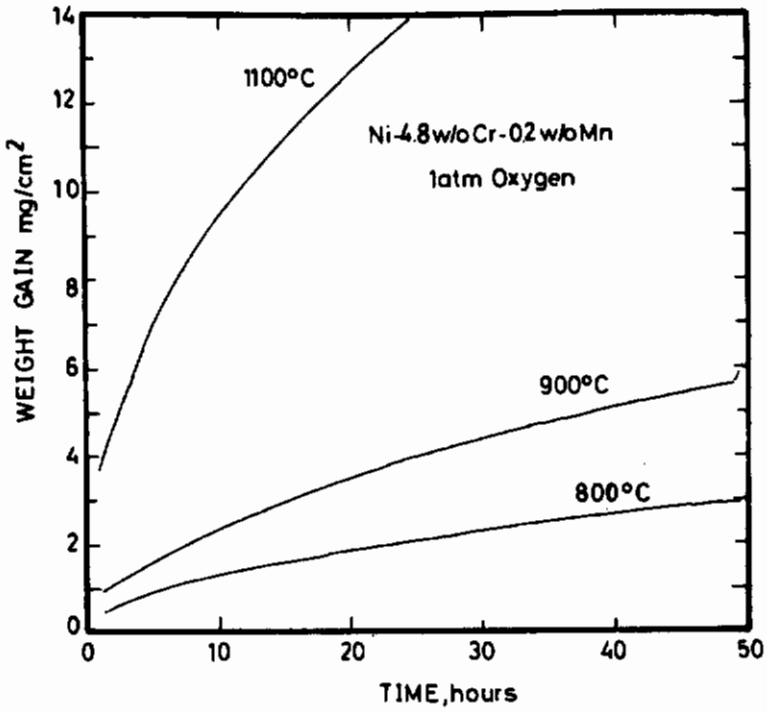

Fig. 28. Oxidation of alloy No. 10 (Ni-4.8Cr-0.2Mn).

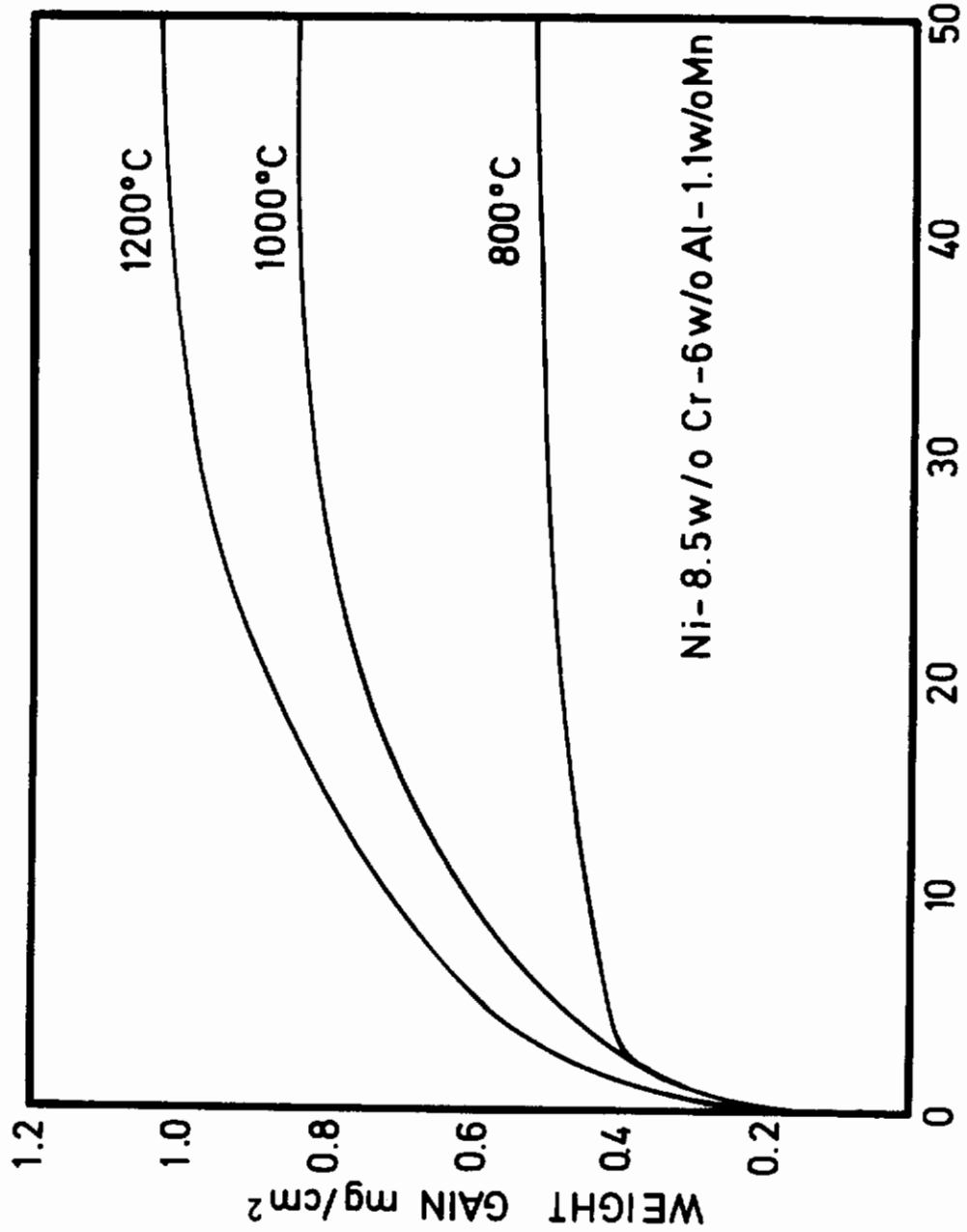

Fig. 29. Oxidation of alloy No. 11 (Ni-8.5Cr-6Al-1.1Mn).

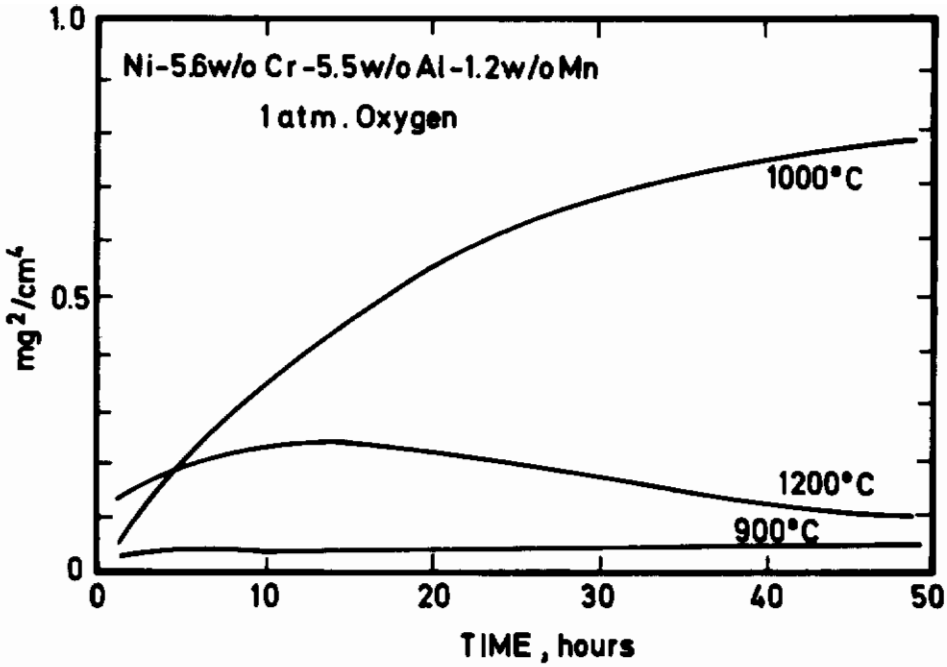

Fig. 30. Oxidation of alloy No. 12 (Ni-5.6Cr-5.5Al-1.2Mn).

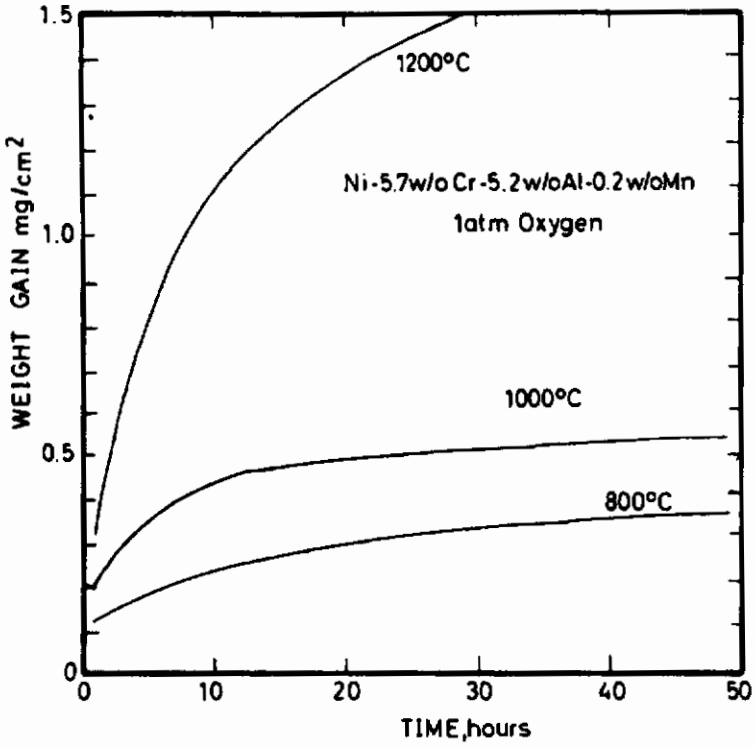

Fig. 31. Oxidation of alloy No. 13 (Ni-5.7Cr-5.2Al-0.2Mn).

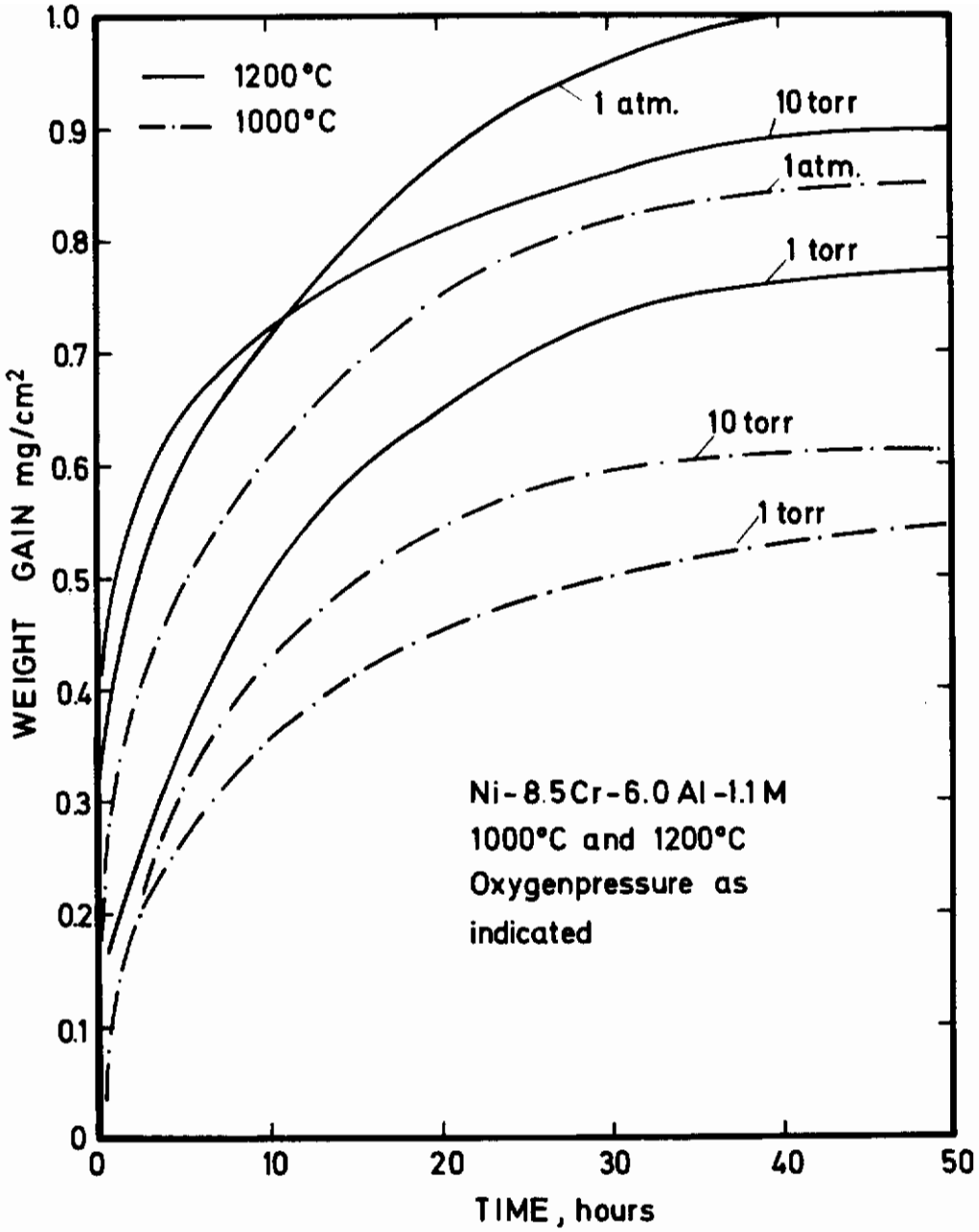

Fig. 32. Oxidation of alloy No. 11 (Ni-8.5Cr-6Al-1.1Mn) at 1 atm., 10 and 1 torr O_2 at 1000 and 1200 °C.

4.2 Characterization of Oxidized Specimens.

Nickel-chromium-manganese alloys. The oxide scales on the two nickel-chromium-manganese alloys (Nos. 9 and 10) have similar composition and appearance. The scales are double-layered: an outer layer mainly consists of NiO and an inner layer of NiO with embedded particles of $NiCr_2O_4$. In addition an internal oxidation zone is formed with particles of Cr_2O_3 in a nickel-matrix. No manganese-oxides are detected. Manganese is probably substitutionally dissolved in the nickel-oxides.

These features are illustrated in Figs. 33-37, which show metallographic cross sections, electron optical and X-ray images of the cross sections, and microprobe scans on oxidized specimens of the two alloys. Manganese is uniformly distributed in both the scales and alloy substrates, except with a tendency toward enrichment at the alloy/scale interface of alloy No. 9.

Nickel-Chromium-Aluminium-Manganese alloys. These alloys show the same main features as for the nickel-chromium-aluminium alloys described in Part I. Aluminium and chromium are enriched in the scale, and preferential oxidation of aluminium to Al_2O_3 increases with increasing temperature and decreasing oxygen pressure. Internal oxidation is either absent or present in small amounts.

The distribution of the alloying elements as determined by electron microprobe scan in the scale and alloy substrate after oxidation of alloy No. 11 (Ni-8.5Cr-6Al-1.1Mn) in 1 torr O_2 at 800, 1000, 1200 ^{o}C is shown in Fig. 38. From these studies and supporting X-ray diffraction and metallographic studies it is concluded that an outer layer mainly consists of NiO after oxidation at 800 and 1000 ^{o}C, while an inner layer is enriched in aluminium and chromium, probably as Al_2O_3, Cr_2O_3 and corresponding spinels. At 800 and 1200 ^{o}C the manganese content is distributed homogeneously throughout the scale and alloy.

Fig. 39, which shows a metallographic cross section and electron optical and X-ray images of the same for a specimen of alloy No. 13 (Ni-5.7Cr-5.2Al-0.2Mn) oxidized at 1200 ^{o}C, illustrates the same features in the oxidation behaviour. A comparison between alloys Nos. 12 and 13 (containing 0.2 and 1.2 % manganese) does not reveal any significant difference.

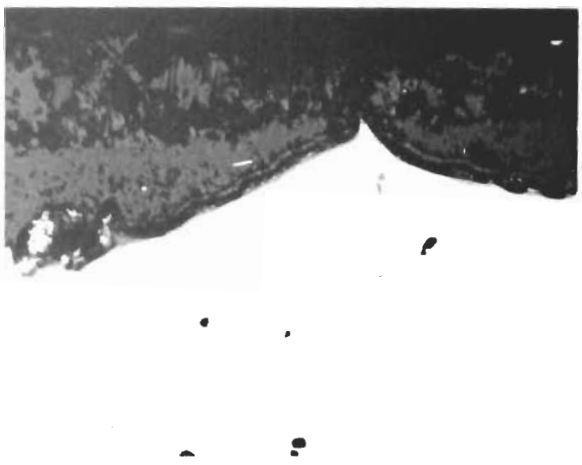

(a) Reacted for 41 hrs. at 1000 °C. 500 x.

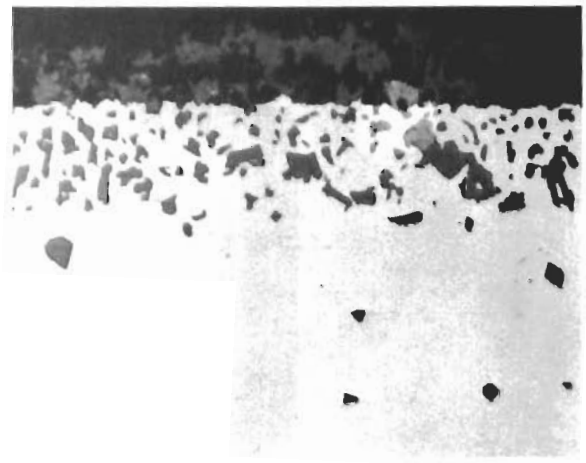

(b) Reacted for 6.5 hrs. at 1200 °C. 500 x.

Fig. 33. Metallographic cross section of alloy No. 9 (Ni-8.5Cr-0.4Mn) reacted in 1 atm. oxygen.

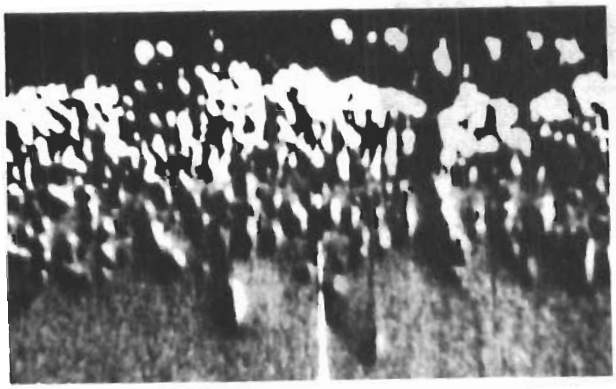

(a) Electron optical image. 500 x.

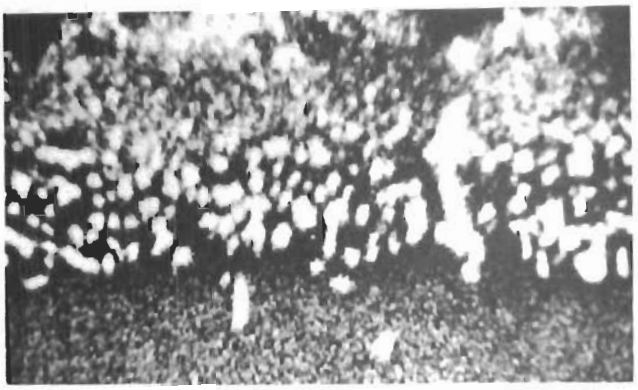

(b) X-ray image of Chromium. 500 x.

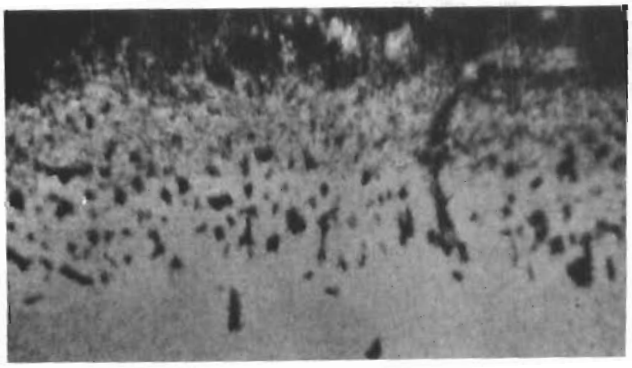

(c) X-ray image of Nickel. 500 x.

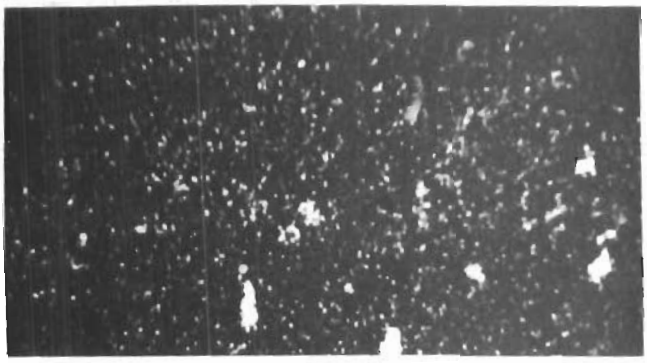

(d) X-ray image of Manganese. 500 x.

Fig. 34. Electron optical and X-ray images of metallographic cross section of alloy No. 9 (Ni-8.5Cr-0.4Mn) reacted for 6.5 hrs. at 1200 °C at 1 atm. oxygen.

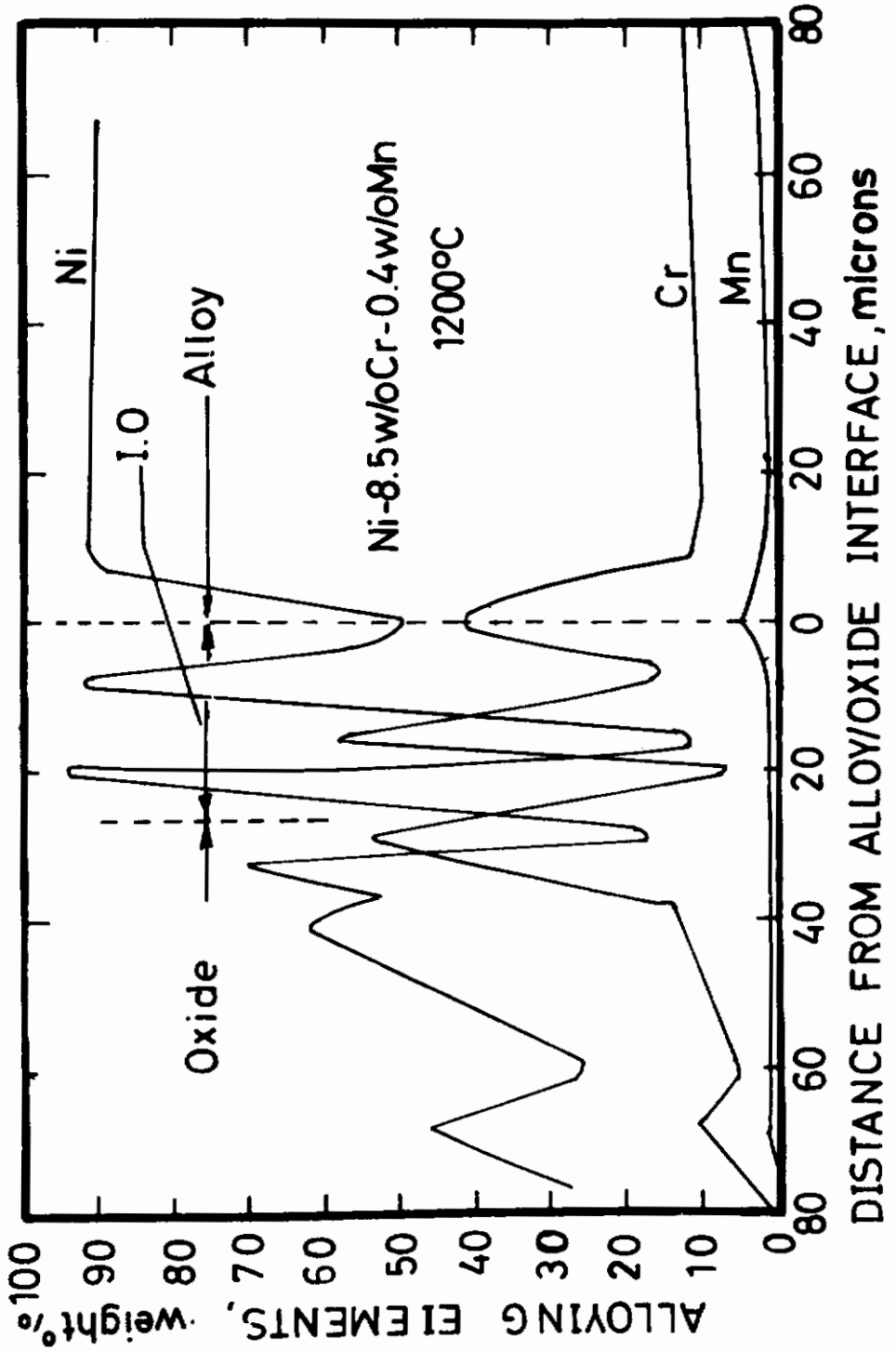

Fig. 35. Results of microprobe scans on cross section of alloy No. 9 (Ni-8.5Cr-0.4Mn) specimen oxidized for ~ 6.5 hrs. at 1200 °C and 1 atm. oxygen.

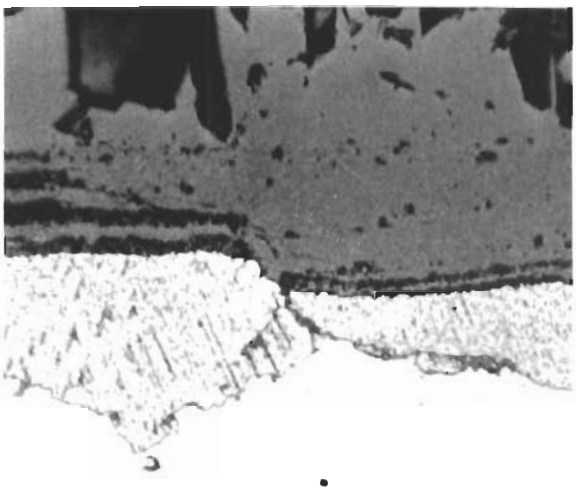

Fig. 36. Metallographic cross section of alloy No. 11 (Ni-4.8Cr-0.2Mn), reacted for 45 hrs. at 1000 °C in 1 atm. oxygen. 500 x.

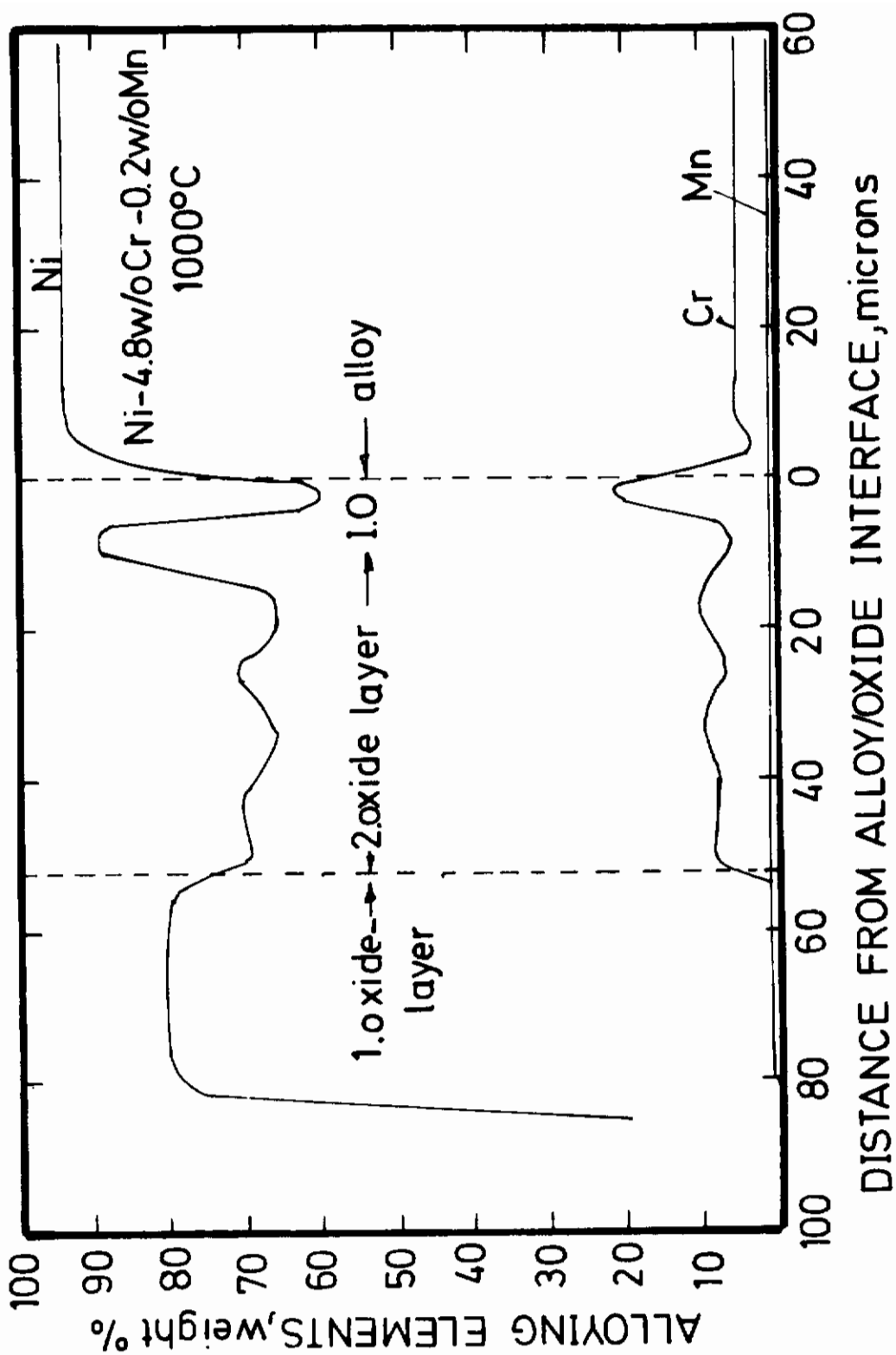

Fig. 37. Results of microprobe scans on cross section of alloy No. 11 (Ni-4.8Cr-0.2Mn) specimen oxidized for ~ 45 hrs. at 1000 °C and 1 atm. oxygen.

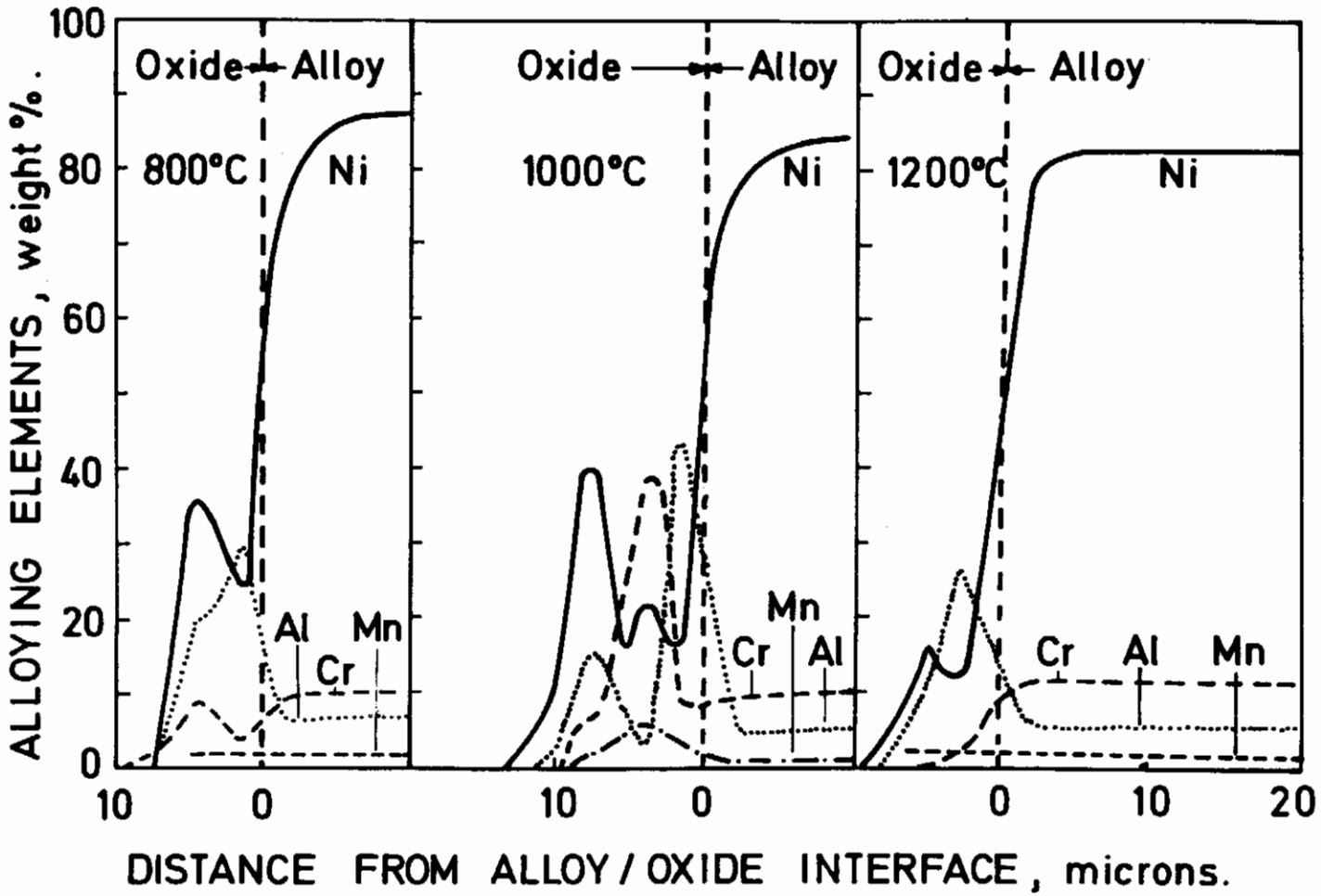

Fig. 38. Electron microprobe scans on cross-sections of specimens of alloy No. 11 (Ni-8.5Cr-6.0Al-1.1Mn) oxidized in 1 torr oxygen at 800, 1000, and 1200 °C.

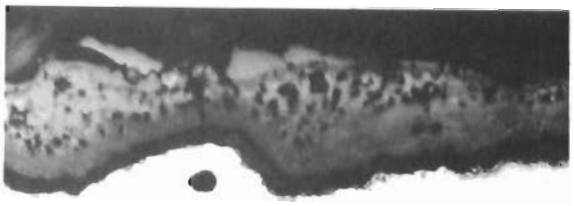

(a) Metallographic cross section. 500 x.

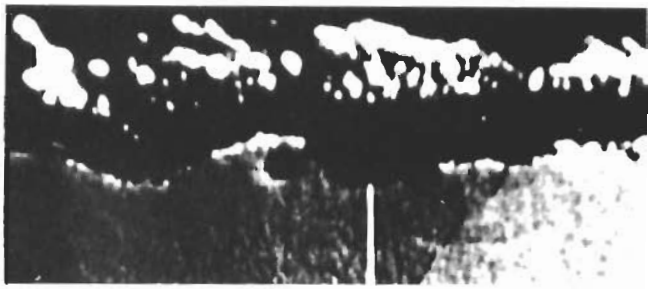

(b) Electron-optical image. 500 x.

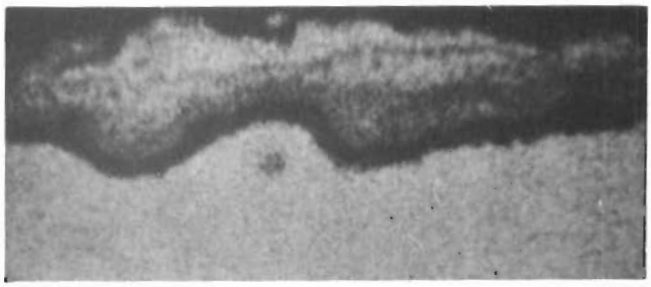

(c) X-ray image of Nickel. 500 x.

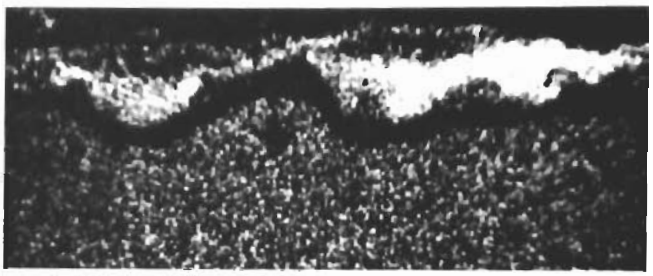

(d) X-ray image of Chromium. 500 x.

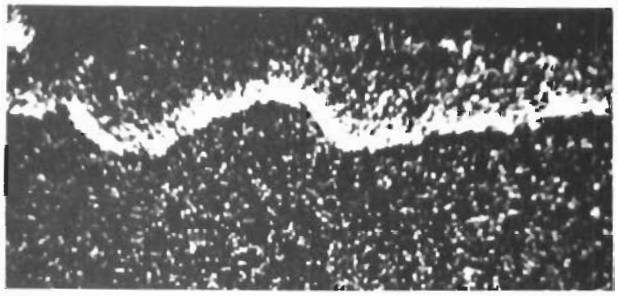

(e) X-ray image of Aluminium. 500 x.

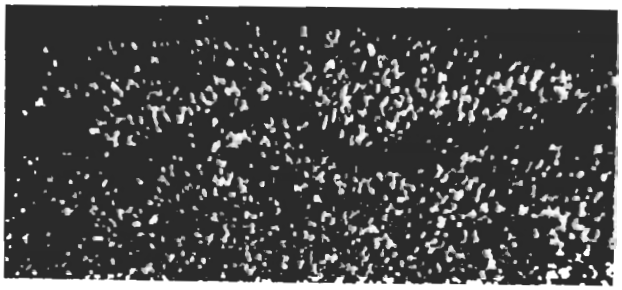

(f) X-ray image of Manganese. 500 x.

Fig. 39. Metallographic cross section (a), electron-optical (b), and X-ray images (c-f) of specimen of alloy No. 13 (Ni-5.7Cr-5.2Al-0.2Mn) reacted for 47 hrs. at 1200 °C in 1 atm. oxygen.

4.3 Initial Oxide Film on Alloy No. 10 (Ni-8.5Cr-6.0Al-1.1Mn). A specimen of this alloy was oxidized for 15 min. at 1200 °C in 1 atm. O_2, and the oxide film was stripped and examined by means of electron microscopy and diffraction.

The oxide film is similar to that formed on Ni-9Cr-6Al alloys oxidized under the same conditions. It consists of two main layers. An inner layer consists of grains of the order 1 μ in diameter which has a tetragonal structure (see Part I). The outer layer has a non-uniform appearance. It consists of NiO, smaller amounts of $NiAl_2O_4$, a spinel with lattice parameter a = 8.23Å which may possibly reflect the presence of $MnAl_2O_4$, and traces of Cr_2O_3. The studies are still being evaluated and will be reported in more detail in a later report.

5. DISCUSSION

The studies on the manganese-modified alloys have not as yet been completed, and only the main aspects will be summarized.

The oxidation behaviour of the manganese-modified nickel-chromium-aluminium alloys is not significantly different from that of the nickel-chromium-aluminium alloys (Part I). The Ni-8.5Cr-6Al base composition exhibits the best oxidation resistance. Partial spallation of the oxide occurs during cooling, and from this point of view the manganese-additions are not expected to increase the service life of the alloys.

PART IV - EFFECTS OF YTTRIUM ADDITIONS ON THE OXIDATION BEHAVIOUR OF NICKEL-CHROMIUM-ALUMINIUM BASE ALLOYS AT HIGH TEMPERATURES

1. INTRODUCTION

It has been known for many years that minor additions of the rate earth metals (cerium, yttrium), calcium, and others improve the oxidation resistance of iron and nickel base alloys.[8,16,20-27] There is a general agreement that one of the main advantages of addition of reactive elements is to improve the oxide scale adherence. However, there is no unequivocal explanation for this effect. Wenderott[20] has discussed most of the various hypotheses presented. Seybolt[21] has later proposed that internally dispersed oxides act as sinks for vacancies, and thus prevent void formation at the alloys/oxide interface. Some of the mechanisms proposed can be generalized and listed as follows:

1. "Blocking" of diffusion within the oxide scale due to the high ionic volume of the rare earth metal ions.

2. Formation of an oxide of the reactive metal at the oxide metal interface.

3. Higher diffusion of desirable elements by changing the properties of the base metal (alloy) as for example by expanding the lattice by addition of elements with large atomic volume.

4. Increase irregularity at the interface between the alloy and its protective scale resulting in a "key-on" of the oxide layer.

5. The ability of internal oxide particles on the alloy itself to absorb inwardly flowing vacancies, and then prevent void formation at the alloy/oxide interface.

The specific effects of yttrium or Y_2O_3 on nickel[20], chromium[21], and nickel-base super alloys oxidation[8] have been described. One of the main beneficial effects of yttrium-addition to nickel-base alloys is to improve scale adherence.[8] It may be noted that yttrium-additions to unalloyed nickel does not improve the oxidation characteristics of nickel.[28]

Yttrium-additions to chromium did not result in any change in the parabolic rate constant up to 1100 °C, but improved scale adherence was observed.[29] It has been proposed that additions of Y_2O_3 to chromium will decrease the oxidation rate through formation of a double oxide ($YCrO_3$) layer, which decreases the diffusion through the growing scale.[2]

As part of this study of the oxidation behaviour of nickel-chromium-aluminium alloys, effects of small additions of yttrium were studied in the temperature range 800-1200 °C.

2. EXPERIMENTAL METHODS

2.1 Materials.

The alloys were melted in a sintered alumina crucible in an induction furnace and casted. Prior to the melting process, the furnace was evacuated to 10^{-5} torr and filled with purified argon to 0.5 atm. The compositions of the alloys are summarized in Table I, (alloy Nos. 14-17,20).

The test specimens were cut by means of spark errosion machining from the cast alloys. Prior to oxidation the specimens were cleaned in acetone and vacuum annealed for 1 hr. at 1000 °C.

The distribution of yttrium in some of the alloys was checked with autoradiographic techniques. Yttrium was homogeneously distributed in the cross section normal to the cast bars, but showed a slight concentration gradient from the top to the bottom of the bars.

2.2 Methods.

Rates of oxidation were studied by thermogravimetry and the oxidized specimens were identified and characterized by means of metallographic techniques, X-ray diffraction, electron microscopy and diffraction, and electron probe microanalysis. A more detailed description of the methods is given in Part I.

3. EXPERIMENTAL RESULTS

3.1 Thermogravimetric Studies.

Oxidation of yttrium modified nickel-chromium-aluminium alloys was studied over the temperature range of 800-1200 °C.

Results of the thermogravimetric rate measurements in 1 atm. O_2 are presented in Figs. 40-44, where the weight gains of the specimens in mg/cm^2 are plotted as a function of time in hrs. The weight gains were evaluated from the geometrical surfaces of the unoxidized samples. All the alloys show protective behaviour, but the kinetics can not be interpreted in terms of ideal rate equations.

Figs. 45 and 46 show the effect of oxygen pressure on the oxidation of alloys No. 15 and 16 at 1000 °C. Both alloys show an unusual behaviour in that the oxidation is faster at 10 torr than at 1 atm. and 1 torr O_2.

3.2 Examinations of Oxidized Specimens.

3.2.1 Distribution of alloy components in unreacted specimens. For comparative purposes the distribution of the alloy components was examined in unreacted specimens. In the alloys with yttrium-content less than 0.1 % (alloys Nos. 14 and 20) the yttrium-distribution could not be determined by means of microprobe measurements. But in the alloys with yttrium-content $\geq$ 0.3 % the distribution was clearly revealed. An example of this is shown in Fig. 47, which shows a light microscope cross section and X-ray images of alloy No. 17 (Ni-8.7Cr-6.3Al-0.75Y) in the as cast condition. The results show that yttrium is enriched in the grain boundaries. Similar results were found for alloys Nos. 15 and 16.

3.2.2 Composition of oxide scales. Table II summarizes the oxide phases identified in the scales on the different alloys oxidized for periods longer than 20 hrs. Generally all the alloys show the same general tendency as observed in oxidation of the nickel-chromium-aluminium alloys (Part I) in that NiO is an important reaction product at 800 °C and that selective oxidation of aluminium to Al_2O_3 becomes increasingly important with increasing temperature.

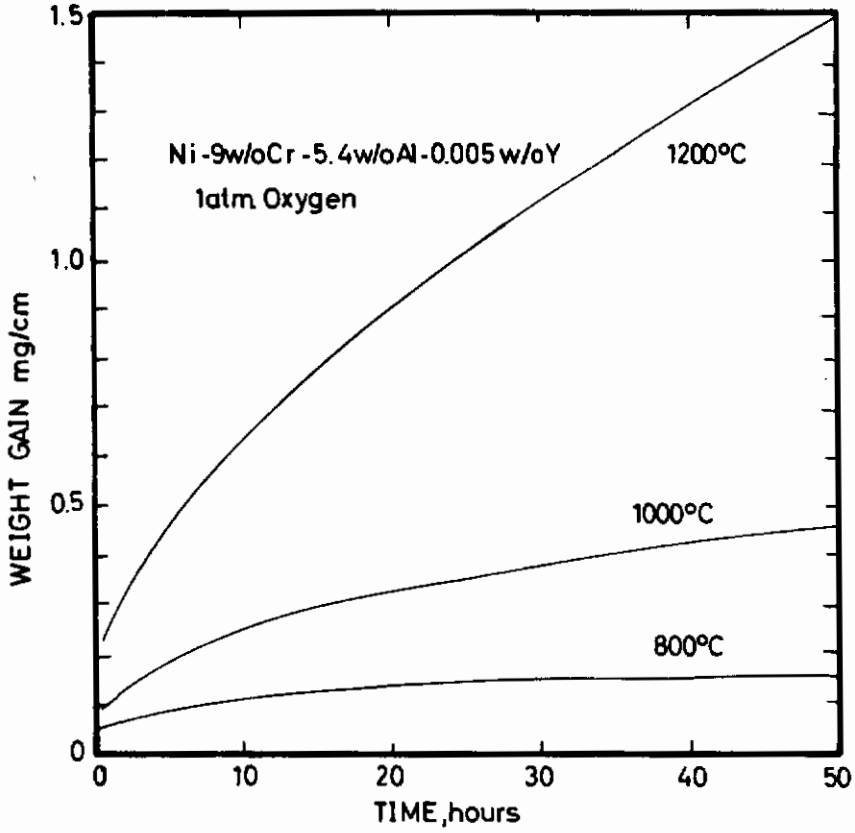

Fig. 40. Oxidation of alloy No. 14 (Ni-9Cr-5.4Al-0.005Y).

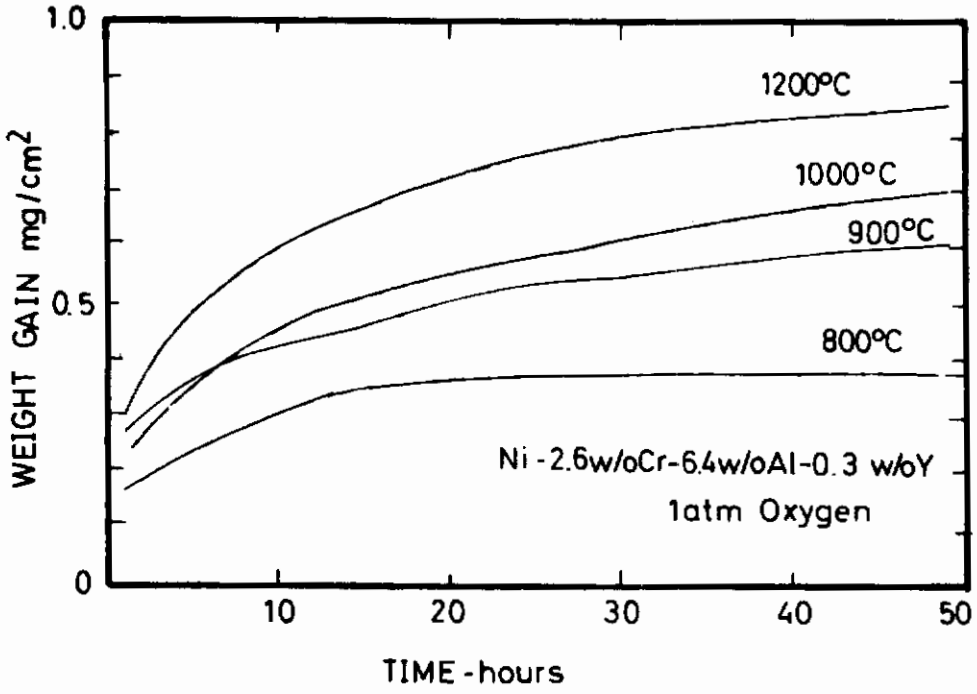

Fig. 41. Oxidation of alloy No. 15 (Ni-2.6Cr-6.4Al-0.3Y).

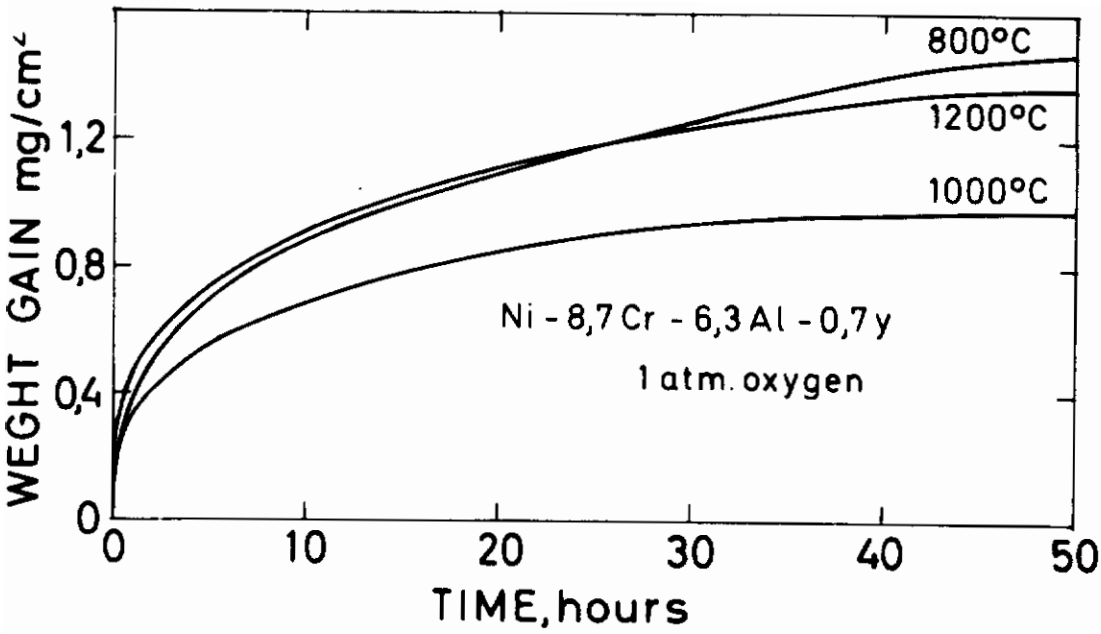

Fig. 42. Oxidation of alloy No. 17 (Ni-8.7Cr-6.3Al-0.7Y).

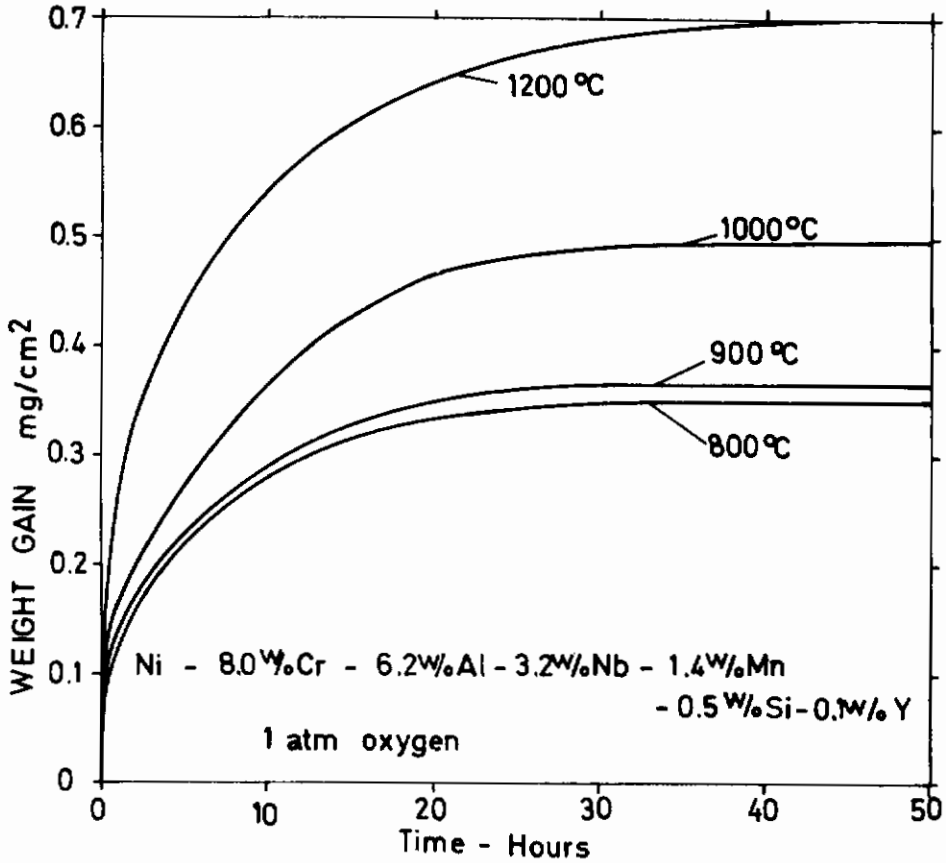

Fig. 43. Oxidation of alloy No. 20 (Ni-8Cr-6.2Al-0.1Y-3.2Nb-1.4Mn-0.5Si).

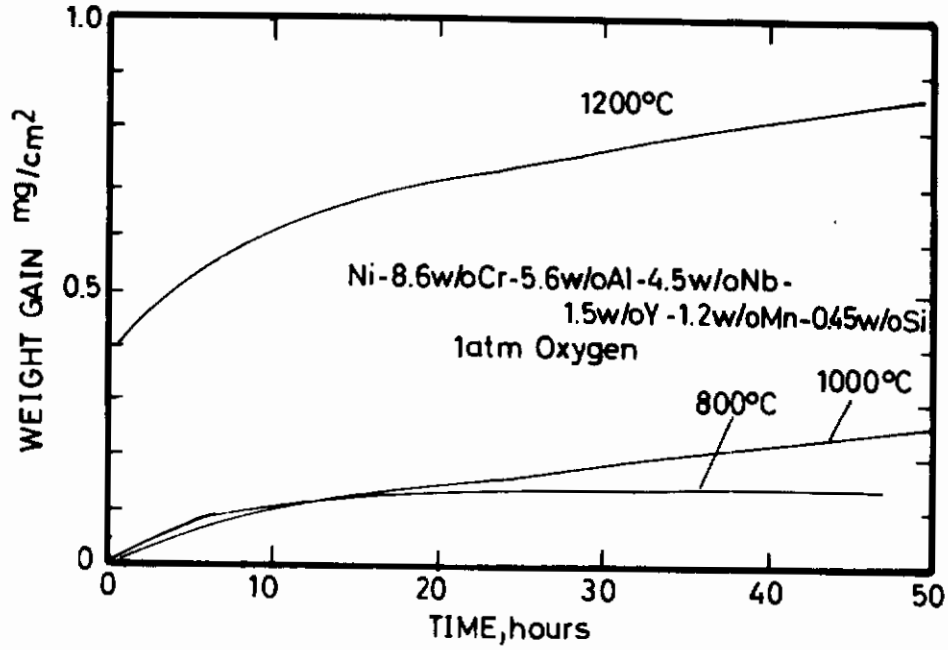

Fig. 44. Oxidation of alloy No. 16 (Ni-8.6Cr-5.6Al-4.5Nb-1.5Y-1.2Mn-0.45Si).

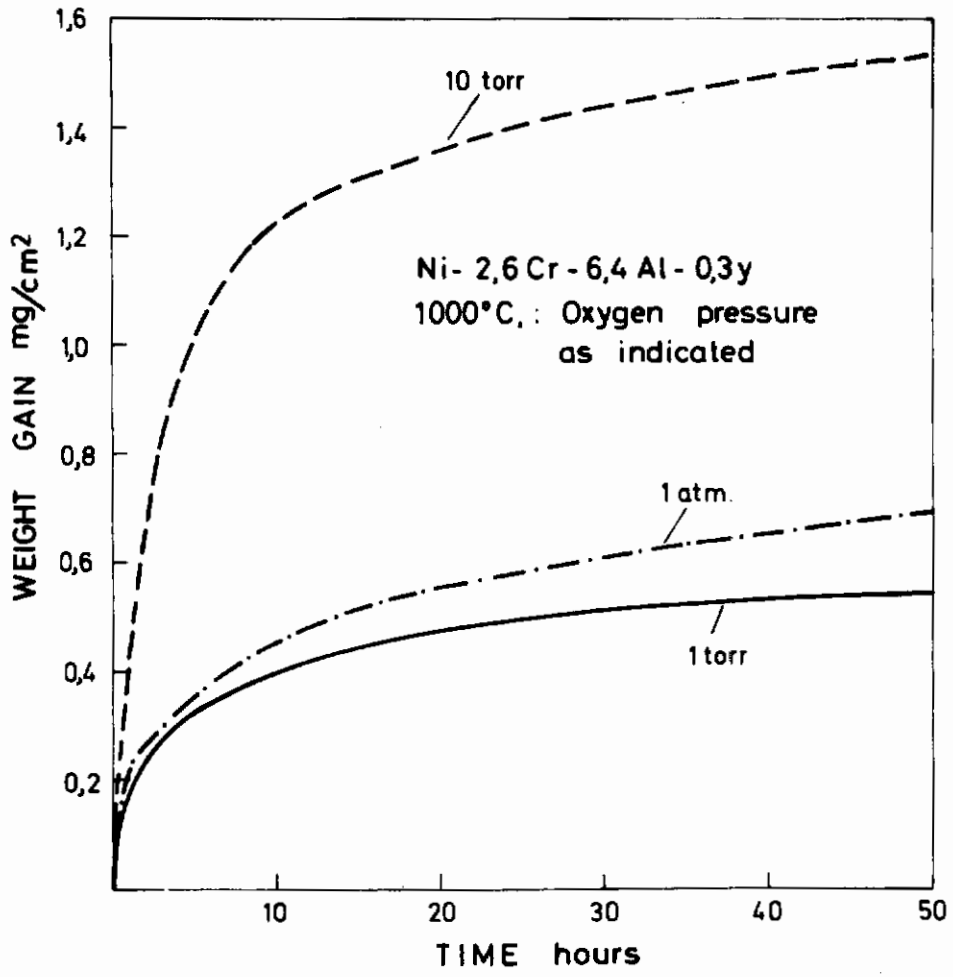

Fig. 45. The effect of oxygen pressure on oxidation of alloy No. 15 (Ni-2.6Cr-6.4Al-0.3Y) at 1000 °C.

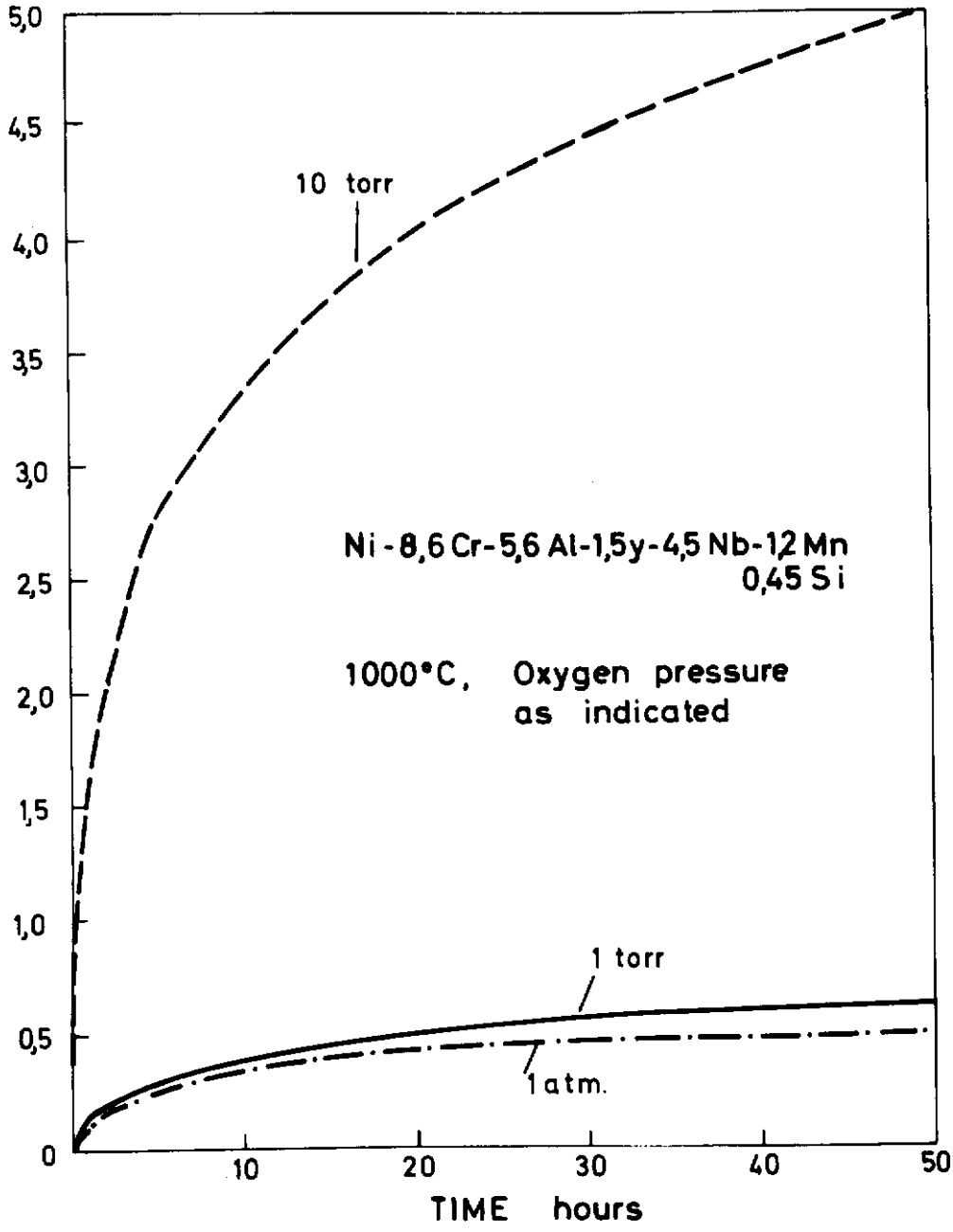

Fig. 46. The effect of oxygen pressure on oxidation of alloy No. 16 (Ni-8.6Cr-5.6Al-5.1Y-4.5Nb-1.2Mn-0.45Si) at 1000 °C.

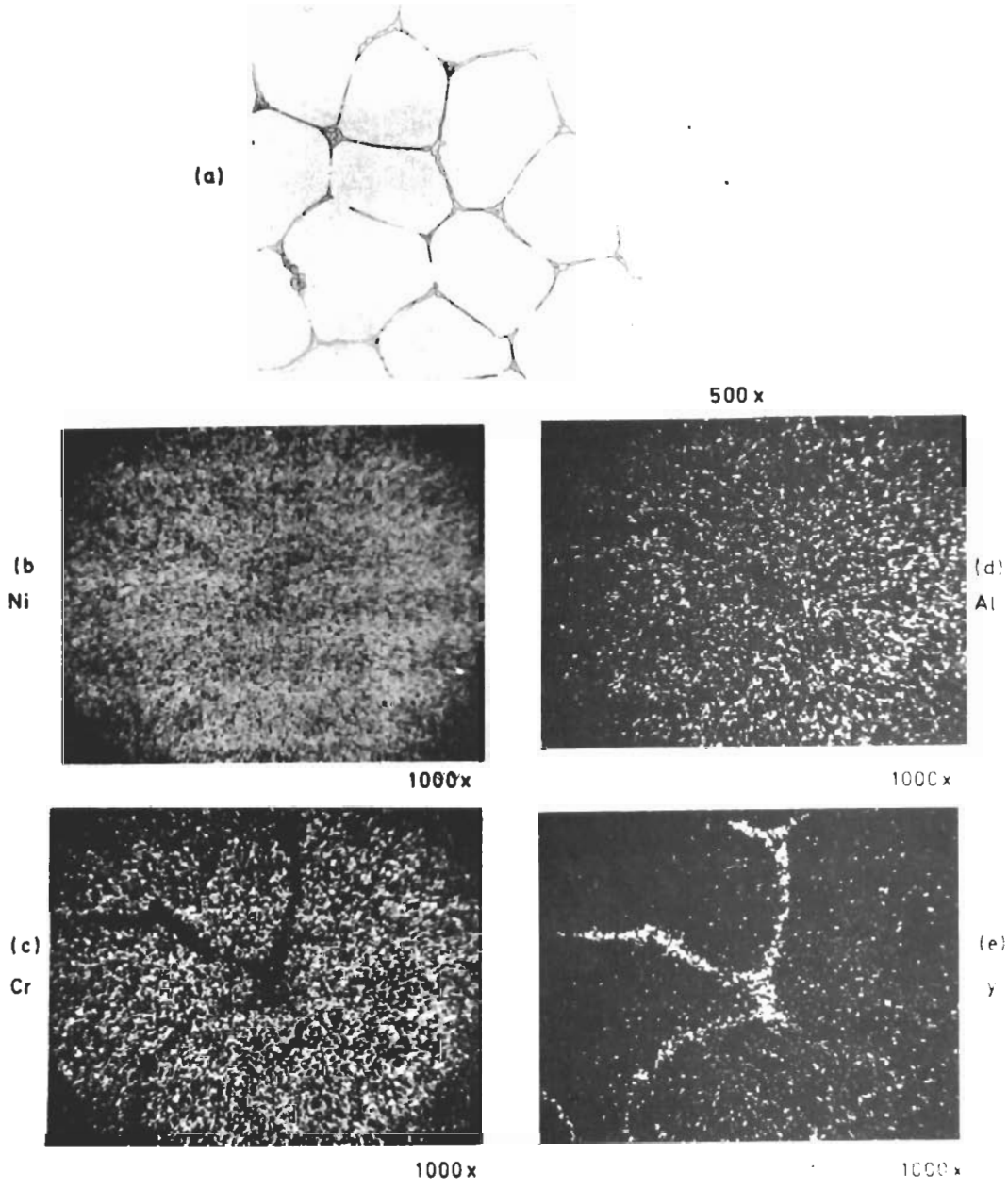

Fig. 47. Light microscope (a), and X-ray images (b-e) of alloy No. 17 (Ni-8.7Cr-6.3Al-0.75Y), as cast.

TABLE II

THE OBSERVED OXIDES

ALLOY		800 °C		1000 °C		1200 °C	
	PRESSURE	TIME hrs.	OXIDES FOUND	TIME hrs.	OXIDES FOUND	TIME hrs.	OXIDES FOUND
Ni-9.0Cr-5.4Al-0.005Y No. 14	1 atm.	50	NiO, α-Al_2O_3 traces Cr_2O_3	70	α-Al_2O_3	51 49	α-Al_2O_3, NiO α-Al_2O_3, NiO, spalled powder: α-Al_2O_3, NiO, $NiAl_2O_4$.
Ni-2.6Cr-6.4Al-0.3Y	1 atm.	48	No oxide detected	51 90	NiO NiO, α-Al_2O_3	52 100	NiO, α-Al_2O_3, $NiAl_2O_4$ α-Al_2O_3, $NiAl_2O_4$
	10 torr	70	NiO	52	NiO	46	α-Al_2O_3, NiO
No. 15	1 torr			24	NiO, α-Al_2O_3		
Ni-8.7Cr-6.3Al-0.7Y No. 17	1 atm.	47	NiO	31	NiO	47	α-Al_2O_3, $NiAl_2O_4$
	10 torr	64	NiO	21	NiO traces, α-Al_2O_3	46	α-Al_2O_3, NiO and probably γ-Al_2O_3, spinel struct., a=7.94Å
Ni-8.6Cr-5.6Al-1.5Y-4.5Nb-1.2Mn-0.45Si	1 atm.	47	No oxide detected	211 90	α-Al_2O_3, NiO, $NiAl_2O_4$ spinel a=8.3Å NiO traces, spinel and Cr_2O_3	47 20 48	α-Al_2O_3, $NiAl_2O_4$ α-Al_2O_3, a comp.a=3.56Å α-Al_2O_3, NiO, $NiAl_2O_4$
	10 torr			44	NiO, α-Al_2O_3	48	$NiAl_2O_4$, α-Al_2O_3
No. 16	1 torr	52	NiO	46	NiO, $NiAl_2O_4$, α-Al_2O_3	48	α-Al_2O_3
Ni-8.0Cr-6.2Al-0.1Y - 3.2Nb-1.4Mn-0.5Si	1 atm.	45	No oxide detected	42	α-Al_2O_3	45	α-Al_2O_3 traces Cr_2O_3

3.2.3 Microstructure of oxidized specimens. The alloys with yttrium-content ≥ 0.1 % (alloys Nos. 14 and 20) did not show significant differences in appearance after oxidation compared to nickel-chromium-aluminium alloys. X-ray images from cross sections of alloy No. 20 showed a homogeneous distribution of yttrium.

In the 3 other alloys with yttrium-content ≥ 0.3 % yttrium is enriched in the grain boundaries similar to that found in the as cast specimens. Various examples of this feature are shown in the following illustrations.

Fig. 48 shows a light microscope picture and X-ray images of a metallographic cross section of a specimen of alloy No. 15 (Ni-2.6Cr-6.4Al-0.3Y) oxidized for 51 hrs. at 1000 °C in 10 torr O_2. The thin oxide layer mainly consists of α-Al_2O_3 and marked preferential oxidation of the grain boundary is observed. Fig. 49 shows an electron microprobe scan on a metallographic cross section of a specimen from the same alloy oxidized for 24 hrs. at 1 torr O_2. The preferential oxidation of aluminium is clearly illustrated. The scan shows the composition of the grain boundary areas of the alloys. Yttrium and nickel are enriched in the middle part of the grain boundary region, while aluminium is enriched in neighbouring areas. This suggests that yttrium and nickel form an intermetallic compound.

A light microscope picture and X-ray images of a metallographic cross section of a specimen of alloy No. 17 (Ni-8.7Cr-6.3Al-0.75Y) reacted for 20.5 hrs. at 1000 °C in 10 torr O_2 are shown in Fig. 50. The same general features are observed as for alloy No. 15: aluminium is preferentially oxidized and marked attack of grain boundaries near the alloy substrate surface is observed. Yttrium is concentrated at grain boundaries in the alloy.

Corresponding light microscope and X-ray images of a specimen of alloy No. 16 (Ni-8.6Cr-5.6Al-1.5Y-4.5Nb-1.2Mn-0.45Si) oxidized for 47.5 hrs. at 1200 °C in 10 torr O_2 are given in Fig. 51. Again yttrium is concentrated at grain boundaries; aluminium is preferentially oxidized particularly in grain areas next to the alloy substrate surface. This alloy also contains silicon, and it is noteworthy that this alloy component is concentrated next to the alloy surface where it is probably preferentially oxidized.

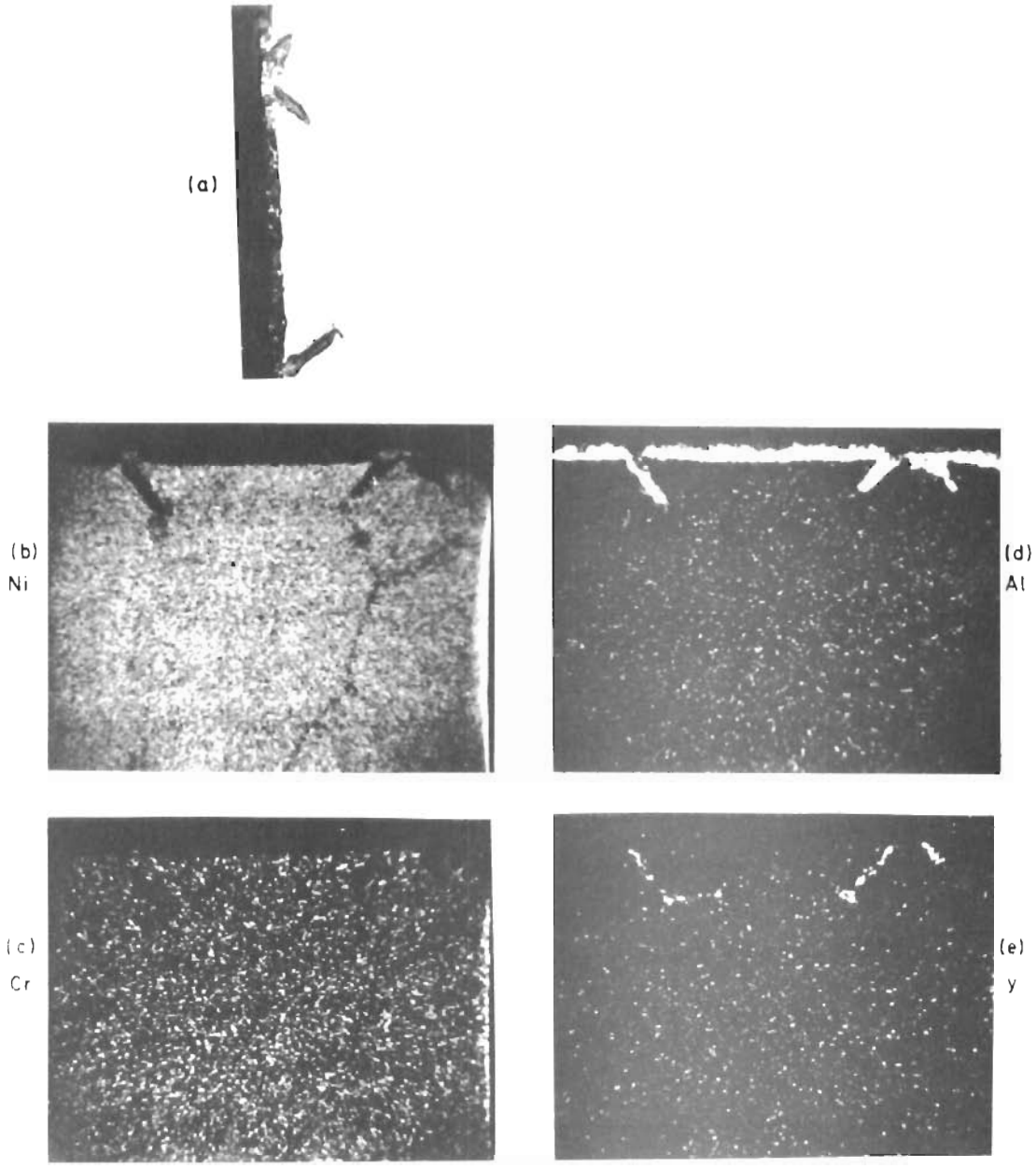

Fig. 48. Light microscope picture (a) and X-ray (b-e) images of metallographic cross section of alloy No. 5 (Ni-2.6Cr-6.4Al-0.3Y) reacted for 51 hrs. at 1000 °C in 10 torr oxygen.
500 x.

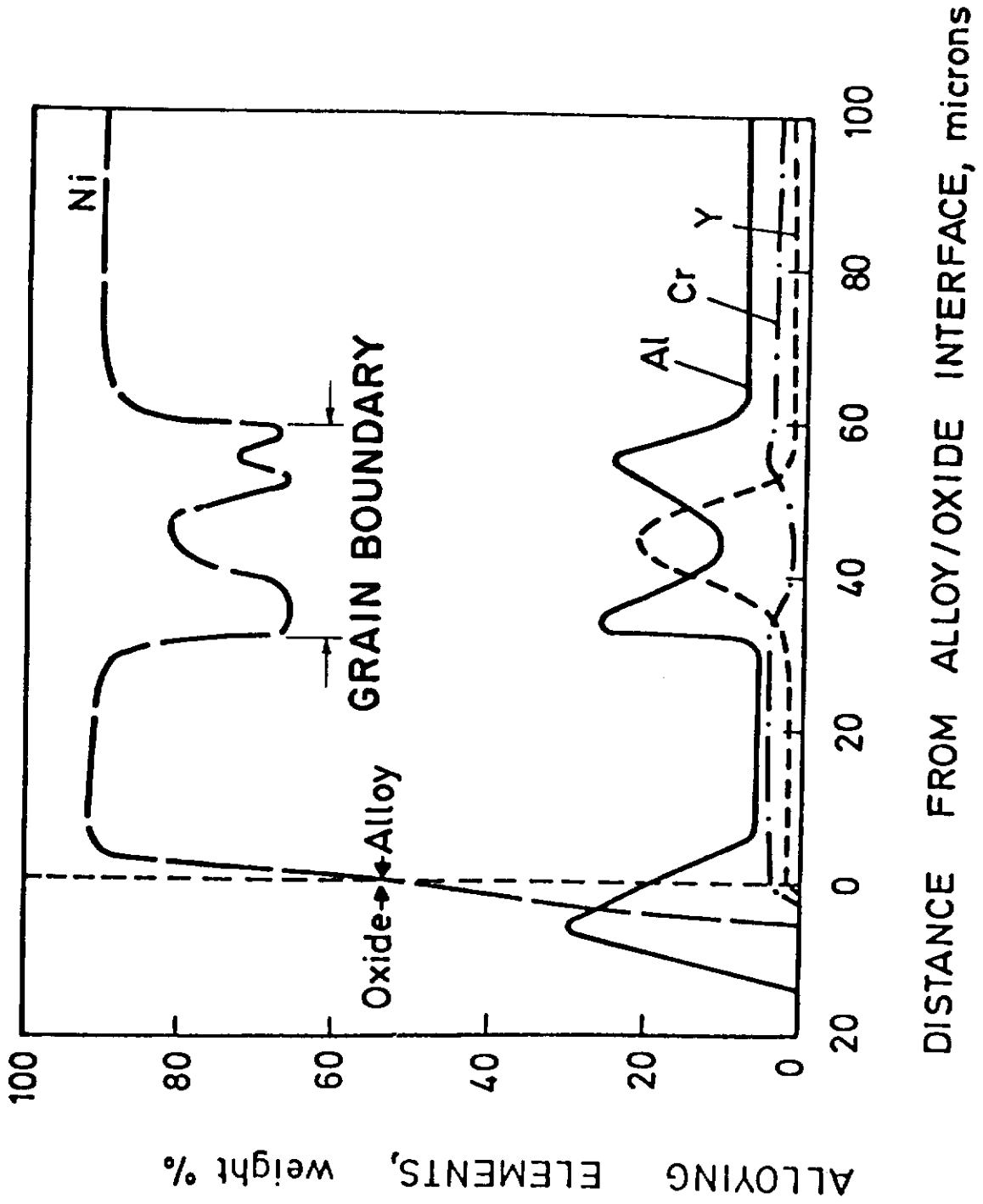

Fig. 49. Electron microprobe scan on metallographic cross section of alloy No. 15 (Ni-2.6Cr-6.4Al-0.3Y) reacted for 24 hrs. at 1000 °C in 1 torr oxygen.

(a)

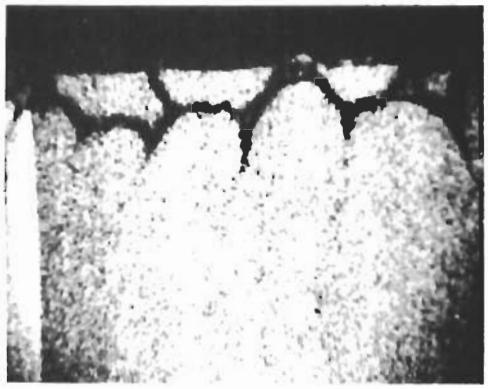

(b)
Ni

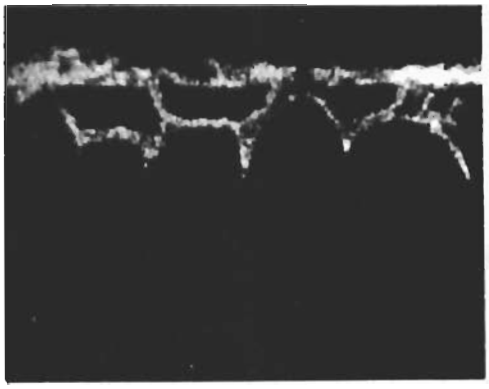

(d)
Al

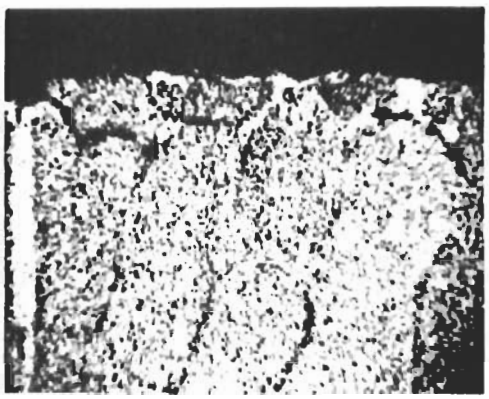

(c)
Cr

(e)
y

Fig. 50. Light microprobe picture (a) and X-ray images (b-e) of metallographic cross section of alloy No. 17 (Ni-8.7Cr-6.3Al-0.75Y) reacted for 20 1/2 hrs. at 1000 °C in 10 torr oxygen. 500 x.

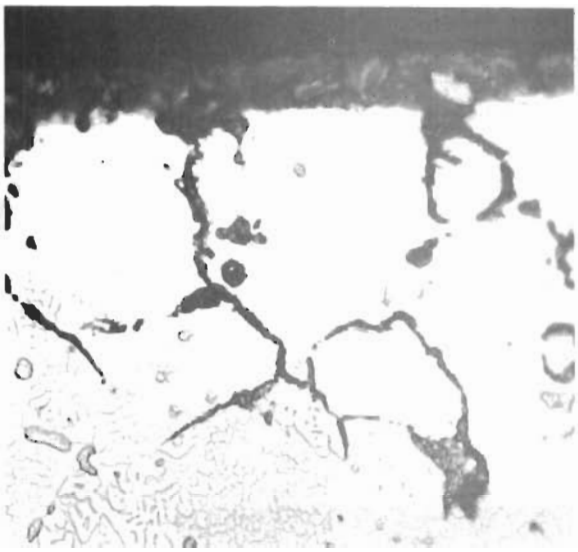

(a) Metallographic cross section. 500 x.

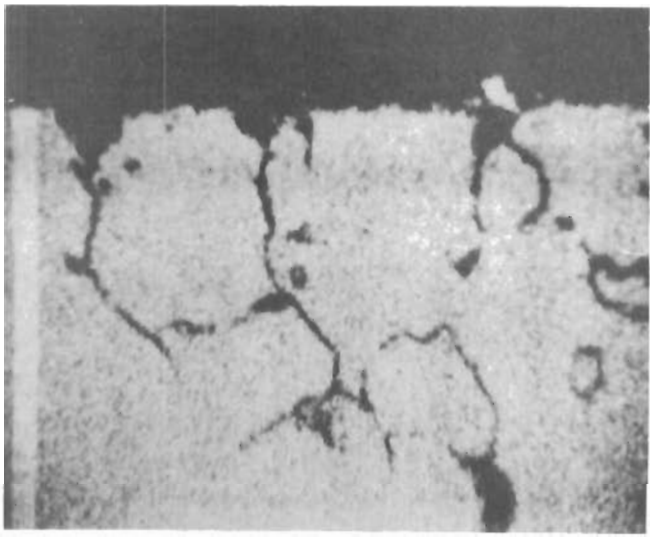

(b) X-ray image of Nickel. 500 x.

(c) X-ray image of Aluminium. 500 x.

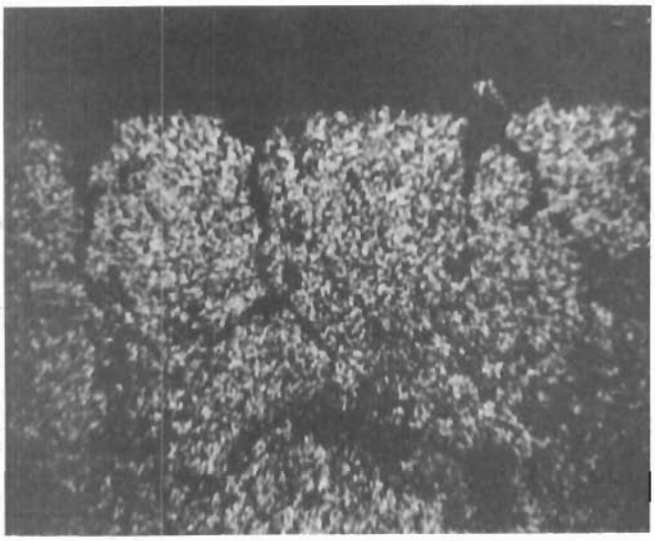

(d) X-ray image of Chromium. 500 x.

Fig. 51. Light microscope picture and X-ray images of metallographic cross section of specimen of alloy No. 16 (Ni-8.6Cr-5.6Al-1.5Y-4.5Nb-1.2Mn-0.45Si) oxidized for 47.5 hrs. at 1200 °C in 10 torr O_2.

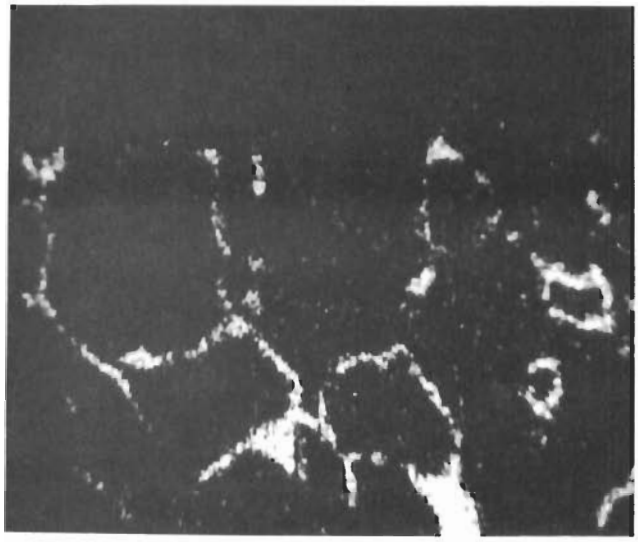

(e) X-ray image of Yttrium. 500 x.

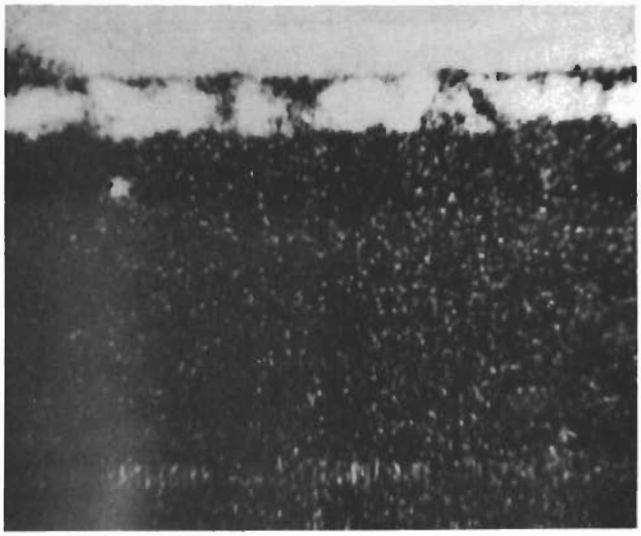

(f) X-ray image of Silicon. 500 x.

(g) X-ray image of Manganese. 500 x.

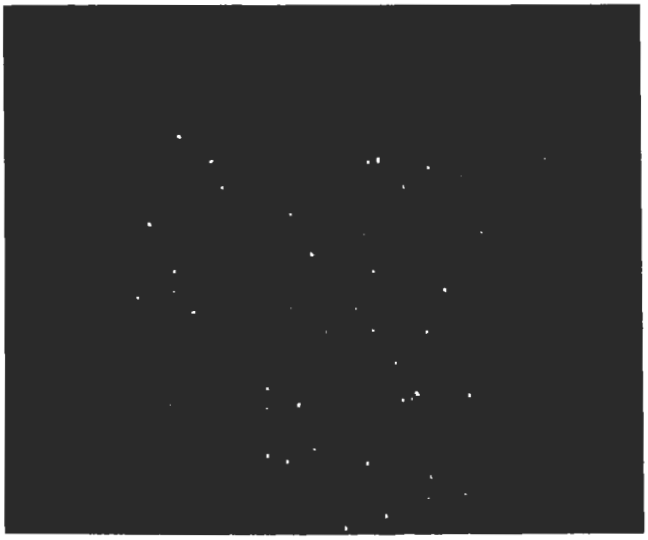

(h) X-ray image of Niobium. 500 x.

Fig. 51. Light microscope picture and X-ray images of metallographic cross section of specimen of alloy No. 16 (Ni-8.6Cr-5.6Al-1.5Y-4.5Nb-1.2Mn-0.45Si) oxidized for 47.5 hrs. at 1200 °C in 10 torr O_2.

3.2.4 Electron diffraction and transmission electron microscope studies.

Such studies were made on thin oxide layers formed on alloys Nos. 15 and 20.

The studies on alloy No. 15 were made on the oxide scale formed on a specimen oxidized for 15 min. at 900 °C in 1 atm. O_2. The results are illustrated on Fig. 52 and suggest that the scale consists of two layers separated by a middle zone. The inner layer (marked A) has a thickness of about 3000Å and consists of the spinel $NiAl_2O_4$ and traces of γ-Al_2O_3. The outer layer (C) is of the order 1000Å and consists of NiO. The middle zone consists of thin plates (B) of an unidentified phase which was only found in the scale of the yttrium modified alloys. α-Al_2O_3 particles were also found in the middle zone and Cr_2O_3 is also probably present in this zone.

The studies on alloy No. 20 were made on a specimen oxidized for 46 hrs at 800 °C in 1 atm. O_2. An electron transmission picture of the scale is shown in Fig. 53. An outer layer consists of NiO (A-polycrystalline NiO; B-ordered NiO-layer), an inner layer (D) consists of $NiAl_2O_4$ and traces of γ-Al_2O_3, and a thin (< 1000Å) middle zone consists of the same unidentified oxide phase as described in Fig. 52. No oxides of chromium, niobium, silicon, and magnanese could be identified in the scale.

4. DISCUSSION AND SUMMARY

The Y-modified nickel-chromium-aluminium alloys generally show many of the same general features as that of the nickel-chromium-aluminium alloys: the oxidation is protective and the main reaction products are the same. However, as regards the details of the reaction behaviour differences are observed and generally the oxide scales on yttrium-modified alloys have a better oxide adherence on cooling to room temperature.

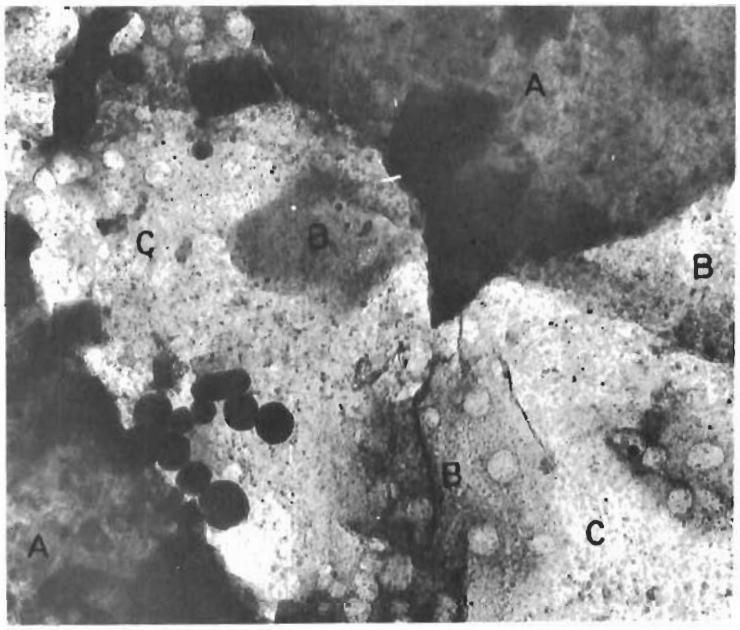

Fig. 52a. Transmission electron microscope picture of oxide layer formed on alloy No. 15 (Ni-2.6Cr-6.4Al-0.3Y) oxidized for 15 min. at 900 °C in 1 atm. O_2. 36000 x.

A. $NiAl_2O_3$
B. Unidentified oxide phase
C. NiO

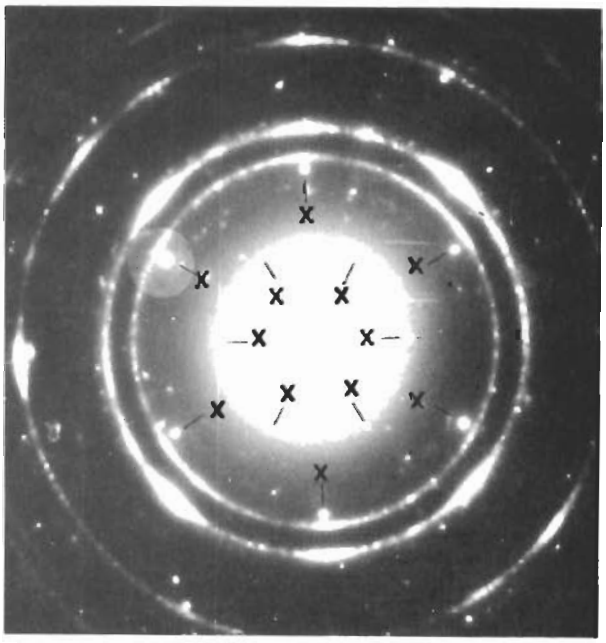

Fig. 52 b. Electron diffraction pattern of the unidentified phase B on Fig. 52 a. The reflections from B are marked x.

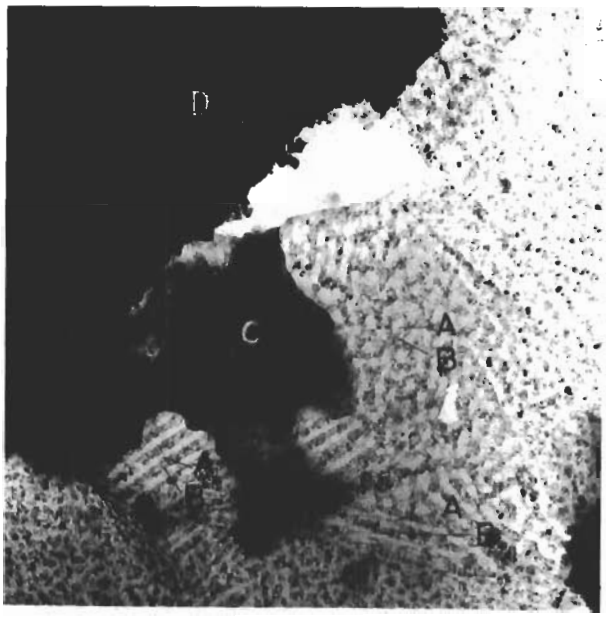

Fig. 53. Transmission electron microscope picture of oxide scale formed on specimen of alloy No. 20 (Ni-8.0Cr-6.2Al-0.1Y-3.2Nb-1.4Mn-0.5Si) oxidized for 15 min. at 900 °C in 1 atm. O_2. 36000 x.

A. Polycrystalline NiO
B. Ordered NiO
C. Unidentified oxide phase
D. Ni-Al_2O_4.

Any specific effects of small yttrium-additions ($\leq$ 0.1 %) are difficult to ascertain because of the experimental difficulty in analyzing and detecting yttrium at these concentration levels. Larger yttrium-additions, however, have a marked effect on the microstructure of the alloy and the detailed reaction characteristics. Yttrium is at these levels enriched at grain boundaries most probably through the formation of a nickel-yttrium intermetallic compound. These alloys further show a marked and preferential oxidation of the grain boundaries next to the alloy substrate surface. The preferential grain boundary oxidation involves preferential oxidation of aluminium and in all probability also yttrium. This reaction behaviour leads to a surface scale and preferential grain boundary attack beneath the scale (Figs. 49-51). Judging from these results a not improbable interpretation for the increased adherence of the scale is a "key-on" effect due to the irregularity in the interface between the oxide and alloy. This effect may also possibly extend to low concentration of yttrium, but this must be confirmed by additional studies.

A notable result of these studies is the excellent oxidation resistance of alloy No. 15 which only contains 2.6 % chromium. Further studies of such alloys with low chromium-content would be of interest.

It may also be noticed that in alloy No. 16 there is a marked selective oxidation of silicon in addition to that of aluminium.

The detailed oxidation mechanism of these types of alloys is complicated and involves selective oxidation of one or more of the alloying components, and in addition solid state reactions take place between oxide phases in the scale. For this reason the composition and the oxide phases present in the scale may as a rule change with temperature, oxygen pressure, and elapsed time of oxidation. Considerable further studies are needed to optimize the compositions of superalloys to yield the best combination of properties both as to mechanical and oxidation properties.

REFERENCES

1. O. Kubaschewski and B.E. Hopkins, "Oxidation of Metals and Alloys", Butterworths, London, 1962.

2. K. Hauffe, "Oxydation von Metallen und Metallegierungen", Springer, Berlin, 1957.

3. J. Bénard, "Oxydation des Métaux", Gauthier-Villars et Cie., Paris,1962.

4. P. Kofstad, "High-Temperature Oxidation of Metals", Wiley, New York, 1966.

5. H. Pfeiffer and H. Thomas, "Zunderfeste Legierungen", Berlin, Springer 1963.

6. E.D.V. Ignatov and R.D. Shambunova, Technical Translation, NASA, f 59, March 1969.

7. E.A. Gulbransen and K.F. Andrew, J. Electrochem.Soc., 106 (1959) 941.

8. G.E. Wasilewski, "Nickel-Base Superalloy Oxidation", Technical Report AFML, Contract AF33(615)2861, January 1967.

9. Philibert, (1962), Symp. on X-ray Optics and X-ray Microanalysis, Stanford, Calif., 1962, p. 379.

10. P.B. Hirsch, A. Howie, R.B. Nicholson, D.W. Pashley, and M.J. Whelan, "Electron Microscopy of Thin Crystals, Butterworth, London, 1965.

11. E. Hornbogen, Z.f. Metallkunde, 6 (1964) 293.

12. C. Wagner, Gordon Conference on Corrosion 1962, to be published in Corrosion Science.

13. I. Pfeiffer, Z.f. Metallkunde, 53 (1962) 309.

14. J. Gjönnes and Chr.J. Simensen, to be published in Acta Met.

15. J.W. Hickman and E.A. Gulbransen, Trans. AIME 120 (1949) 519.

16. E.A. Gulbransen and W.R. McMillan, Ind.Eng.Chem., 45 (1953) 1734.

17. E.A. Gulbransen and K.F. Andrew, J. Electrochem.Soc., 101 (1954) 163.

18. W. Hessenbruch, Metalle und Legierungen für hohe Temperaturen, Berlin 1940.

19. Antill et al., Corrosion Science, 9 (1969) 431.

20. B. Wenderott, Z. Metallkde. 56 (1965) 63.

REFERENCES

21. A.H. Seybolt, Corrosion Science, 6 (1966) 263.

22. H. Pfeiffer and G. Sommer, Z. Metallkde., 57 (1966) 326.

23. J.W. Hickman and E.A. Gulbransen, Trans.AIME, 180 (1949) 519.

24. B. Lustman, J. of Metals, 188 (1950) 995.

25. N.S. Kreschanowskii and J.E. Zabludovskii, Metallov.Term.Obra.Met., 3 (1959) 33, Brutcher Translation No. 4542.

26. H.O. Beaver, Metal Progress, 66 (1954) 115.

27. J.E. Antill and K.A. Peakall, J. the Iron and Steel Inst. (1967) 1136.

28. R.M. Doerr et al., Bureau of Mines, Report of Investigations, 6800 (1966).

29. W.C. Hagel, Trans.Am.Soc.Metals, 56 (1963) 583.

UNCLASSIFIED
Security Classification

DOCUMENT CONTROL DATA - R & D
(Security classification of title, body of abstract and indexing annotation must be entered when the overall report is classified)

1. ORIGINATING ACTIVITY (Corporate author)	2a. REPORT SECURITY CLASSIFICATION
Central Institute for Industrial Research Blindern, Oslo 3, Norway	UNCLASSIFIED
	2b. GROUP

3. REPORT TITLE

Studies on the Behavior of Nickel-Base Superalloys at High Temperatures

4. DESCRIPTIVE NOTES (Type of report and inclusive dates)

Final Scientific Report 1 November 1967 - 31 October 1969

5. AUTHOR(S) (First name, middle initial, last name)

Ingard Kvernes
Per Kofstad

6. REPORT DATE	7a. TOTAL NO. OF PAGES	7b. NO. OF REFS
July 1970	81	29

8a. CONTRACT OR GRANT NO.	9a. ORIGINATOR'S REPORT NUMBER(S)
F61052-67-C-0057 b. PROJECT NO. 7312 cTask No. 731202 d.	9b. OTHER REPORT NO(S) (Any other numbers that may be assigned this report) AFML-TR-70-103

10. DISTRIBUTION STATEMENT This document is subject to special export controls and each transmittal to foreign governments or foreign nationals may be made only with prior approval of the Metals and Ceramics Division (MAM), Air Force Materials Laboratory, Wright-Patterson Air Force Base, Ohio 45433.

11. SUPPLEMENTARY NOTES	12. SPONSORING MILITARY ACTIVITY
	Air Force Materials Laboratory Air Force Systems Command Wright-Patterson AFB, Ohio 45433

13. ABSTRACT

The work covers studies of the oxidation behavior of a number of Nickel-Chromium-Aluminum base alloys at high temperatures:

I. High Temperature Oxidation of Some Nickel-Chromium-Aluminum Alloys containing different Chromium/Aluminum Ratio.

II. Effect of Titanium and Titanium puls Samarium Additions on the High Temperature Oxidation of Ni-9Cr-5Al.

III. Influence of Manganese-Additions on High Temperature Oxidation of Some Nickel-Chromium-and Nickel-Chromium-Aluminum Base Alloys.

IV. Effects of Yttrium Additions on the Oxidation Behavior of Nickel-Chromium-Aluminum Base Alloys at High Temperatures.

Most of the studies cover the temperature range 800-1200°C. The experimental methods included thermogravimetric measurements of oxidation rates and studies on reacted specimens by means of X-ray diffraction, metallographic techniques, electron micorprobe analysis, and electron diffraction and microscopy.

"This abstract is subject to special export controls and each transmittal to foreign governments or foreign nationals may be made only with prior approval of the Metals and Ceramics Division (MAM), Air Force Materials Laboratory, Wright-Patterson AFB, OHio 45433."

DD FORM 1 NOV 68 1473

UNCLASSIFIED
Security Classification

14. KEY WORDS	LINK A		LINK B		LINK C	
	ROLE	WT	ROLE	WT	ROLE	WT
High temperature oxidation of alloys.						
Nickel-Chromium-Aluminum alloys.						
Nickel-Chromium-Aluminum alloys with small additions of Titanium and Titanium plus Samarium.						
Nickel-Chromium-Aluminum alloys with small additions of Yttrium.						
Nickel-Chromium-Aluminum alloys with small additions of Manganese.						